CFRP Strengthening of RC Beams with Corroded Lap Spliced Steel bars

by

Ayman Shihata

A thesis
presented to the University of Waterloo
in fulfillment of the
thesis requirement for the degree of
Master of Applied Science
in
Civil Engineering

Waterloo, Ontario, Canada, 2011

AUTHOR'S DECLARATION

I hereby declare that I am the sole author of this thesis. This is a true copy of the thesis, including any required final revisions, as accepted by my examiners.

I understand that my thesis may be made electronically available to the public.

Abstract

Corrosion is the number one deterioration mechanism that decreases the service life of the concrete structures. Many structures in severe environments have experienced an unacceptable loss in serviceability earlier than anticipated due to corrosion.

Advanced composite materials in the form of externally bonded fiber reinforcing polymer (FRP) sheets have been successfully used for rehabilitation and strengthening of infrastructure in lieu of traditional repair techniques such as steel plates bonding. FRPs are used because of their light weight, ease of application, non-corrosiveness material, and high strength.

The current study comprised of testing eighteen reinforced concrete beams to investigate the confinement provided by carbon fiber-reinforced polymer (CFRP) sheets on the bond strength of corroded tension lap splices under static loading. The beams were 200mm wide by 300mm high by 2000mm. Each beam was reinforced on the tension side with two steel bars (2 M 15 or 2 M20 steel bars) spliced at mid span in the constant moment region. The nominal concrete strength was 43 MPa and the yield stress of the steel reinforcement was 400MPa. The test variables were the concrete cover to bar diameter ratio (c/d) which varied from 1.5 to 2.67, the level of corrosion (0% and 2.5% mass loss), and the presence or absence of transverse CFRP wrapping. The corrosion in the steel bars was induced by means of accelerated technique withan impressed current density of 150mA/cm2. The specimens were instrumented by strain gauges on the steel reinforcement, concrete, and CFRP sheets. Linear variable differential transformer (LVDT) was used to measure mid span deflection. The specimens were tested to failure in four point bending.

The test results showed that all beams failed by bond splitting. The reduction in the ultimate bond strength due to a 2.5% corrosion level ranged between 16% and 25% depending on the c/d ratio. The reduction in the ultimate bond strength due to a 5.0% corrosion level ranged between 20% and 45% depending on the c/d ratio. FRP wraps were effective in confining the tension splice region. The failure in the FRP repaired beams was more ductile and more gradual although the final mode of failure was splitting of the concrete cover. A new, (Ktr,f,) accounting for the presence and amount of FRP confining tension lap-splice was proposed.

Acknowledgements

The preparation of this work has been done under the supervision and guidance of professor Khaled Soudki of the department of Civil Engineering to whom I deeply indebted for his brotherly kindness, and relentless encouragement throughout all the course of this work.

I would like to express my sincere thanks and gratitude to my parents, family and friends who encouraged and supported me during the completion of this work. I doubt that I will ever be able to convey my appreciation fully, but I owe them my endless gratitude. Mum and Dad without your love, guidance, encouragement and influence on my life, I would not have made it that far. My sister Nahla, I am blessed to have you in my life

Part of this acknowledgment goes to the all technicians who have supported me in the laboratory work specifically Ken, Richard, Douglas, and Andy

I am very grateful to my fellow graduate student, Adham, Rizwan, Noran, and Rania for their help and helpful discussion.

I greatly appreciate the Saudi Cultural Bureau for their spiritual and financial support.

Table of Contents

List of Figures

List of Tables

Chapter 1
Introduction

1.1 General

The service life of reinforced concrete structures depends on how durable is the concrete structure and what is the environmental exposure. Durability depends on several factors, including the concrete quality, type of aggregate and concrete permeability. Environmental exposures include de-icing chemicals, high relative humidity, chloride attack, and carbonation attack. Lack of durability and severe environmental exposures leads to concrete deterioration. Corrosion is the number one deterioration mechanism that rapidly decreases the service life of reinforced concrete structures. Many structures in severe environments have experienced an unacceptable loss in serviceability earlier than anticipated due to corrosion of their steel reinforcement. Corrosion causes deterioration in reinforced concrete structure by two mechanisms. Firstly, as steel corrodes, there is a corresponding drop in the cross sectional area and load carrying capacity of the reinforcing steel. Secondly, the corrosion products occupy a larger volume than the original steel, exerting substantial tensile expansive stresses on the surrounding concrete that can cause cracking and spalling of the concrete, and hence a loss of structural bond between the reinforcement and concrete (ACI Committee 222, 1996).

To increase the service life of existing concrete structures, fiber reinforced polymers (FRP) reinforcement is being used as repaired and strengthening measure. FRPs are being applied in lieu of traditional repair techniques such as steel plates bonding. FRP laminated composites, constituting of carbon, glass, and armid fibers, presents significant advantages over comparable steel products in retrofitting and strengthening applications. These advantages include high strength/weight ratio, light weight, ease of handling and application, elimination of false work

and heavy equipment, faster construction rate and non-corrosiveness. This retrofit technique has been the subject of numerous experimental and analytical investigations and has been recently used for strengthening and rehabilitation of bridges and structure in many areas in the world. Most of the research work has focused on flexural, shear, and bond strengthening of beams of columns. Some research has been undertaken to investigate the repair of

corroded concrete members. To the researcher's knowledge, no study was found in the literature that investigated the effect of FRP repair on corroded tension lap-spliced RC beam.

1.2 Research objectives and scope

The main objective of the study is to examine the effect of Carbon FRP (CFRP) repair on the behavior of corroded tension lap-spliced reinforced concrete beams.

Specific objectives of the current study are:

- Investigate the effect of corrosion on tension lap spliced RC beams.
- Assess the use of fiber reinforced polymer (FRP) wraps in improving the serviceability and ultimate response of corroded tension lap-spliced RC.
- Develop a model to account for the contribution of FRP wrap in enhancing the bond behavior of corroded tension lap-spliced RC beams.

To meet these objectives, 18 full scale lap-spliced beam specimens were tested. The beams were divided into two groups of nine beams (un- wrapped and wrapped with CFRP). Each group was further divided into three series based on the concrete cover to diameter ratio (c/d) ratio (1.5, 2.0, and 2.67) and the corrosion levels (0%, 2.5%, and 5.0%).

The beams were tested in four point bending. Analysis of the test results was based on evaluating the modes of failure, load-deflection curves and bond strengths of the specimens.

1.3 Theses organization

The thesis is divided into five chapters as follows:

Chapter-1: This chapter describes the problem statement, objectives of the research program, scope of work and organization of the thesis.

Chapter-2: This chapter presents the background and literature review on bond strength of RC beams corrosion in reinforced concrete and effect of corrosion on bond strength of reinforced concrete beams.

Chapter-3: This chapter describes the experimental program including the fabrication of test specimens, instrumentation, accelerated corrosion and test setup.

Chapter-4: This chapter presents the experimental results including accelerated corrosion results, static test results.

Chapter-5: This chapter presents the new FRP confinement index Ktr,f and the prediction bond strength model.

Chapter-6: This chapter presents the main conclusions from this study and recommendation for future research.

Chapter 2

Background and Literature Review

2.1 Review of bond

2.1.1 Introduction

Bond is the interaction of two materials, concrete and steel. Bond is the most important factor that maintains the integrity in the composite material known as reinforced concrete. In reinforced concrete structures, the external applied load is carried by the concrete and the internal steel reinforcement. Forces are transferred to the steel reinforcement through the surrounding concrete by shear stresses along the concrete to steel interface. Inherent in the analysis of a reinforced concrete section is the assumption of strain compatibility which means that the strains in the concrete and steel are equal at the location of the steel. This implies perfect bond between the concrete and the steel. The bond stresses transfer from the concrete to the steel by:

1- Chemical adhesion between the concrete and steel bar.
2- Friction due to small indentation on the surface of the steel bar
3- Mechanical interaction between the ribs of the bar and the surrounding concrete.

Figure 2.1 shows the bond mechanisms for the steel rebar and the concrete. Bond for plain bars depends mainly on the chemical adhesion and friction although; there is some mechanical interlock due to the roughness of the surface of the bar. For deformed rebar, the bond mainly depends primarily on the mechanical interlock for superior bond properties and secondary on the chemical adhesion and the friction. The bearing of the rebar ribs against the concrete is the primary bond mechanism restraining the relative slip between the rebar and the surrounding concrete. It has been well established that the bond strength of deformed bars is affected by: concrete cover, bar spacing, amount of confining transverse reinforcement, splice and development length, concrete compressive strength, bar size, and relative rib area. The effects of splice length, concrete cover and the bar size are the principal factors studied in this thesis

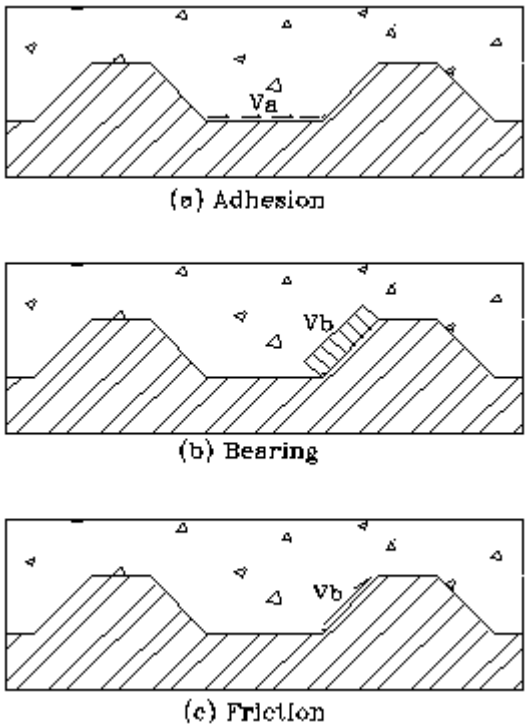

Figure 2-1 Bond mechanisms for the deformed steel rebar and the concrete

2.1.2 Factor affecting bond

2.1.2.1 Concrete cover and bar spacing

Concrete cover is the clear distance between the bar and the concrete surface. Cover is typically defined in terms of side cover (cover to the side of the beam) and bottom cover (cover to the tension face of the beam). When determining the required development or splice length, the smallest cover is assumed to control, since that is where the concrete will experience splitting failure first. Increasing the concrete cover can increase the bond force at failure by increasing the confining force on the bar prior to failure. If the cover is high enough, bond failure due to splitting may not occur, and the member may fail in flexure or in bond due to pullout instead. Because splitting cracks can propagate between the bars as well as to the concrete surface, closely spaced bars can exhibit reduced bond strength. To help prevent this, bars are typically spaced one or two bar diameters apart (ACI Committee 408 2003).

2.1.2.2 Transverse reinforcement

Transverse reinforcement helps limit the growth of splitting cracks and provides additional clamping force. Confinements by transverse reinforcement reduce the required development and splice length, increase the bond strength, and increase the ductility of the splice. The effectiveness of the confining transverse reinforcement depends on the total cross-sectional area of the transverse steel per deformed bar being developed or spliced (ACI Committee 408 2003).

2.1.2.3 Development / splice length

Development length is the distance required for the reinforcing bar to yield before bond failure. If the development length is inadequate, the member may fail in bond before the steel yields. Where lap splices are necessary, the required lap length is the development length needed to fully transfer the tensile force from a bar to the adjoining bar (ACI Committee 408 2003).

2.1.2.4 Bar size

Larger reinforcing bars are capable of reaching higher bond forces per unit length than smaller bars for the same cover to the center of the bar or the same confining transverse reinforcement. The increase in bond force in larger bars, however, is not proportional to the increase in bar area. Thus, using a greater number of smaller bars may be more effective than using fewer large bars if the available development length is limited. This will be true until closer bar spacing becomes detrimental to the member (ACI Committee 408 2003).

2.1.3 Bond test specimens

A variety of test specimen configurations have been used to study the bond between the reinforcing bars and concrete. The most four common configurations are a pullout test specimen, beam end specimen, beam anchorage specimen, and splice specimen (ACI Committee 408 2003).

2.1.3.1 Pullout specimen

Pullout tests are one of the simplest bond tests to perform and are outlined in ASTM standard C900-01. The pullout tests consist of either a block or cylinder of concrete with an embedded bar located at the center of the sample. Figure 2.2 shows a typical pullout test. The bar is pulled in tension while the concrete is restrained in the opposite direction. Several researchers have argued about the inaccuracies of this test and that it does not represent a realistic bond situation. Ferguson (1966), mentioned that the pullout test places the concrete in compression with no other outside forces acting on the members. The concrete in compression around the specimen eliminates the development of any tension cracks in the specimen. In addition, the compression forces increase the confinement around the bar, resulting in higher bond stresses than those generated in a beam. In a realistic situation, the concrete in the bond zones is typically in tension. The bond zone is also subjected to additional stresses due to shear and moment, and the confinement by transverse reinforcement. All of these influences cannot be replicated in the pullout test. However, pullout tests are still used since they are relatively inexpensive and simple to set-up and provide quick comparative bond test results.

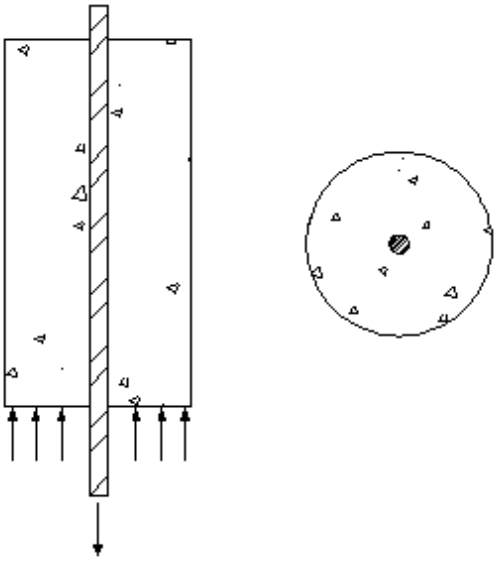

Figure 2-2 Pullout test specimen

2.1.3.2 Beam-end specimen

The procedure for beam-end tests is specified in ASTM Standard A944-99. The beam-end test is a simplification of the RILEM test, essentially only using half the specimen (Figure 2.3). The test frame applies a tension force directly to the reinforcing bar to generate bond forces. The advantage of this test over the pullout test is in the way the specimens are mounted in the test frame. Bearing points on the sample are placed in a similar fashion to the reaction forces at the end of a beam, thus inducing tension in the concrete around the bar and moment and shear forces into the member.

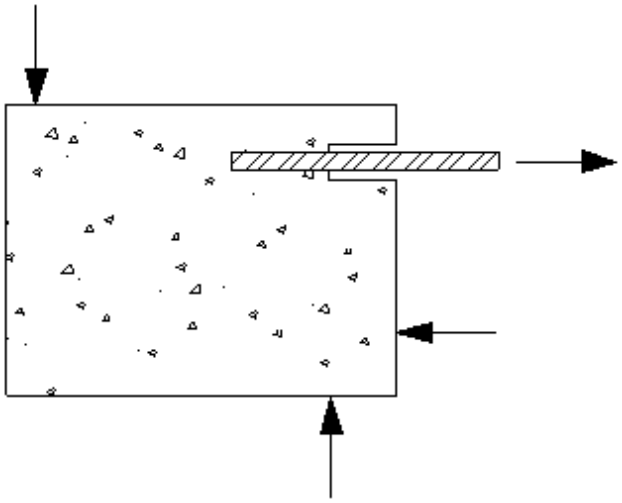

Figure 2-3 Beam-end specimen

2.1.3.3 Beam anchorage specimen

The simplest method to incorporate the effects of tension concrete, shear and transverse reinforcement into a bond test, is by testing flexural beams. In the case of standard beams, a reinforcing bar may be extended beyond the ends of the beam to monitor free end slip. A modification to the standard beam test is to incorporate pockets (voids with beam) to allow for internal slip measurements on the reinforcing steel. The pockets would exist outside the bond area in the beam and would be useful to monitor the loaded end slip and the tensile stresses in the steel bar (Figure 2.4). The reinforcing bar maybe de-bonded by using plastic sleeves around the bar to control bond length of the bar. The set-up is simple since it uses a standard simply supported beam test.

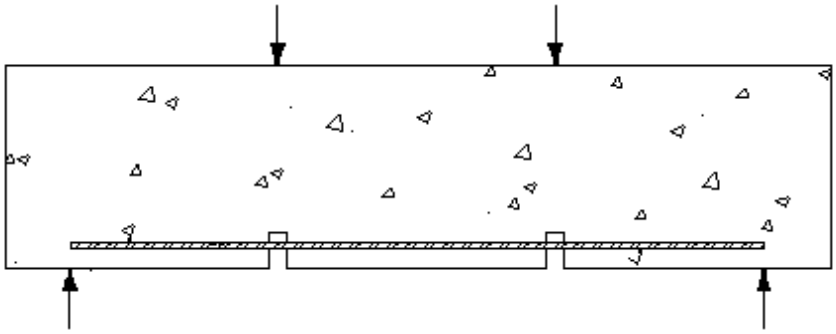

Figure 2-4 Beam anchorage specimen

2.1.3.4 Splice beam specimen

The splice specimens represent larger-scale specimens designed to measure the bond in lap-spliced bars (Figure 2.5). A splice specimen is normally fabricated with the lap splice in constant moment region, is easier to fabricate and produces similar bond strength to those obtained with beam anchorage specimens. The splice specimens simulate a member with flexural cracks and known bonded length. Both beam anchorage specimen and splice beam specimen provide more realistic measures of the bond strength in actual structure.

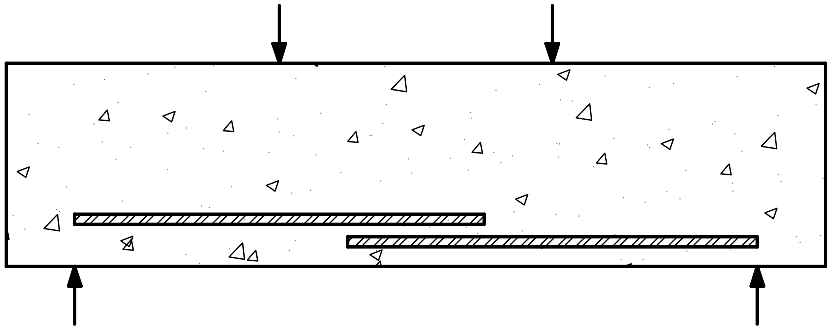

Figure 2-5 Splice beam specimen

2.1.4 Bond failure modes

Bond failure can occur through splitting or pullout. A splitting failure occurs when the relative movement between the reinforcing steel and the concrete becomes high enough that the deformations on the bar begin to act as wedges, putting the surrounding concrete in transverse tension and causing the formation of splitting cracks parallel to the bar. Splitting cracks typically radiate outward from the bar and tend to form first where there is the least amount of concrete cover. If the bottom concrete cover is bigger than the side concrete cover, a horizontal split develops at the level of the bars and is termed as "side-splitting failure". With the side clear cover bigger than the clear bottom concrete cover, longitudinal cracks develop through the bottom cover followed by splitting along the plan of the rebar. Figure 2.6 shows these splitting type bond failures. With continued loading, splitting cracks grow in width and radiate outward to the face of the specimen or between adjacent bars or splices. As they continue along the development length of the bar, the cracks can cause the delamination of a concrete layer unless confining transverse reinforcement is provided.

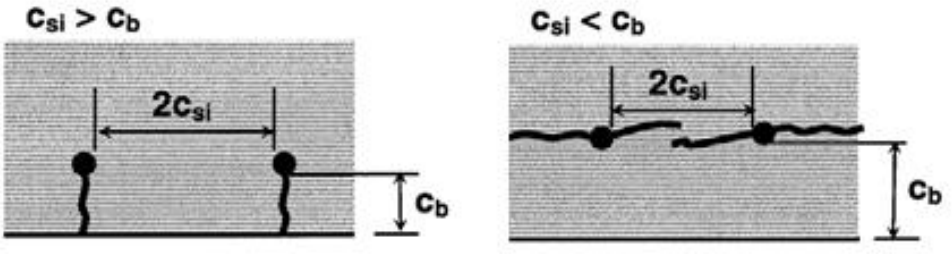

Figure 2-6 Splitting type bond failure (El Maaddawy, 2004)

A pullout failure occurs when the concrete between the deformations on the bar fails in shear or compression. A pullout failure tends to occur only when the concrete cover is high or when the bar is confined by transverse reinforcement that limits the propagation of splitting cracks.

2.2 Corrosion of steel reinforcement in concrete structure

The corrosion mechanism in reinforced concrete members is an electrochemical process. Embedded steel in reinforced concrete is normally protected from corrosion by a passive film of iron oxide on the steel resulting. Passivation of the steel rebar is destroyed by carbonation or chloride attack. The corrosion mechanism in reinforced concrete can be described as a galvanic corrosion cell with four essential components which are *anode, cathode, electrolyte*, and *electrical conductor* (ACI committee 222R-01).

- An anode, where iron, Fe^{2+}, is removed from the steel (iron oxidation).
- A cathode, where hydroxyl ions , OH^-, are produced (oxygen reduction)
- An electrical conductor, for charge (electrons) transfer to occur, and
- An electrolyte (aqueous medium), for ion transfer to occur and thus complete the corrosion cell.

In reinforced concrete structures, the cathode and the anode can be on the same reinforcing bar or on different bars. Dissimilarity in the material properties along the steel bar causes a potential difference. The anode is located on the reinforcing steel where the corrosion occurs and the metal loses mass. The pore water in the concrete acts as an electrolyte solution when concrete is exposed to a salted, moist environment that leads to increase conductivity and decrease concrete resistance. In addition, oxygen which is usually available in the atmosphere should be present at the cathode as a polarizing agent.

During the corrosion of steel in concrete, chemical reactions occur on the steel surface in the cathodic and anodic regions. At the anode, iron is oxidized and two electrons are released at the anodic region and transfer to the cathodic region where oxygen is reduced by the electrons and hydroxyl ions. The hydroxyl ions, OH^-, move to the anode by diffusion through the water in the concrete which acts as the electrolyte to complete the corrosion cell. Figure 2.7 shows a corrosion cell in concrete. The anodic and cathodic reactions are given in equations 2.1 and 2.2

$$Fe \rightarrow Fe^{2+} + 2e^- \quad \text{(Anodic reaction)} \tag{2.1}$$

$$2e^- + H_2O + \frac{1}{2} O_2 \rightarrow 2(OH)^- \quad \text{(Cathodic reaction)} \tag{2.2}$$

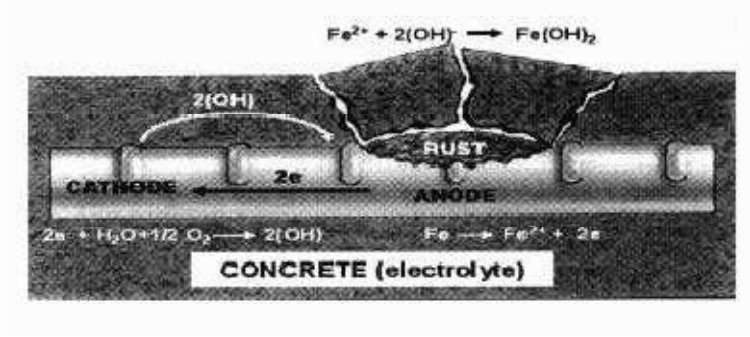

Figure 2-7 Corrosion cell in concrete (El Maaddawy, 2004)

Following the anodic and cathodic reactions, a variety of secondary reactions occur to form the expansive corrosion products. These secondary reactions are given in equation 2.3 to 2.10 (West, 1999).With absence of oxygen, one or both of the following reactions occur to form ferrous oxides or hydroxide as follow:

$$Fe^{2+} + 2(OH)^- \rightarrow Fe(OH)_2 \tag{2.3}$$

$$Fe^{2+} + 2(OH)^- \rightarrow FeO + H_2O \tag{2.4}$$

With Oxygen, ferric oxide and/or hydroxides form according to the following reaction:

$$2Fe(OH)_2 + \frac{1}{2} O_2 \rightarrow Fe_2O_3.H_2O + H_2O \tag{2.5}$$

$$2Fe(OH)_2 + \frac{1}{2} O_2 + H_2O \rightarrow 2Fe(OH)_3 \tag{2.6}$$

$$3Fe(OH)_2 + \frac{1}{2} O_2 \rightarrow 2Fe_3O_4 + 3H_2O \tag{2.7}$$

$$2FeO + \frac{1}{2} O_2 + H_2O \rightarrow Fe_2O_3.H_2O \tag{2.8}$$

$$2FeO + \frac{1}{2} O_2 + H_2O \rightarrow 2Fe(OH)_3 \tag{2.9}$$

$$3FeO + \frac{1}{2} O_2 \rightarrow Fe_3O_4 \tag{2.10}$$

The volume increase at the steel to concrete interface depends on the type of corrosion product formed. Different kinds of rust products have different densities and volume expansions. Figure 2.8 shows the volume of different corrosion product versus the volume of

iron from which they are formed. Expansive corrosion products create tensile stresses in the surrounding concrete. Tensile stresses lead to the cracking and spalling of the concrete cover.

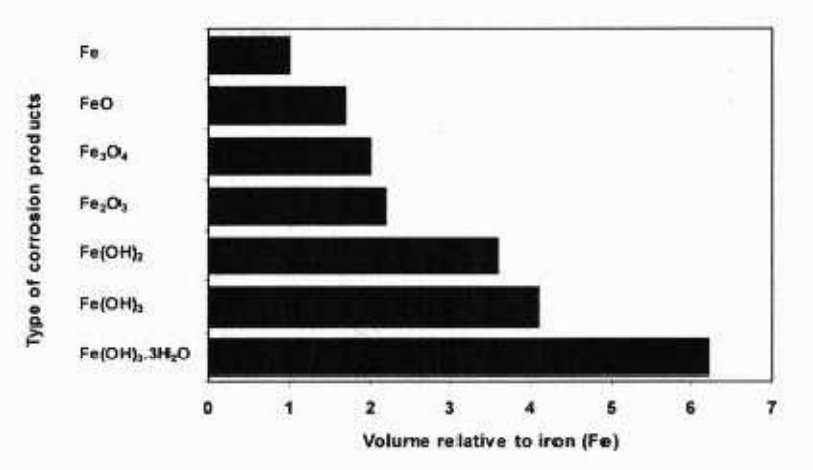

Figure 2-8 Relative volumes of irons and different corrosion products (Liu, and Weyers, 1998)

2.2.1 Types of corrosion in reinforced concrete structure

There are two types of corrosion that occur in a reinforced concrete member. The first type is macrocell corrosion that occurs when the cathode and anode are separated by some distance (Benture, 1997). Microcell or pitting corrosion occurs when the cathode and anode are located next to each other on the same bar. Figure 2.9 shows the Macrocell and Microcell corrosion (Benture 1997).

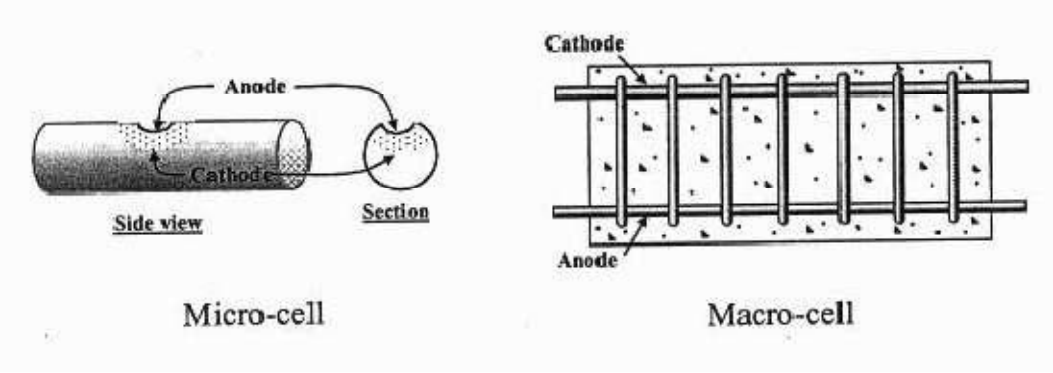

Figure 2-9 Macro-cell and Microcell (Badawi, 2003)

2.2.1.1 Macro-cell corrosion

Macro-cells normally occur in the case of chloride-induced corrosion. They consist of anodically acting areas, normally where the critical chloride content is reached and large cathodes which vary in location from being next to anodes or being at a distance of a few meters (Raupach, .1996).

2.2.1.2 Microcell (pitting) corrosion

Uniform corrosion is generally caused by carbonation of the concrete over a wide area. This leads to the formation of microcells, consisting of pairs of immediately adjacent anodes and cathodes. These cells are microscopic in size, so that externally they appear to produce uniform removal of the steel.

2.2.2 Impressed corrosion in the laboratory

The average current density in actively corroding reinforced concrete structure ranges from 1 to 10 $\mu A/cm^2$. At these current density levels, corrosion requires a long time frame for use in laboratory simulation. Therefore, a corrosion current density less up to 200 μA/cm2 which has been shown not to affect the structural behavior of corroded concrete is recommended (EL Maaddawy and Soudki, 2003). As shown in Figure 2.10, impressing a high current density level will not change the damage due to the concrete strain versus mass loss behavior if the current density levels are less than 200 $\mu A/cm^2$ (El Maaddawy and Soudki, 2003). Craig (2002) used a current density of 105 $\mu A/cm^2$; Al-Hammoud (2006) used a current density of 150 $\mu A/cm^2$. Using these current densities, there was a reasonable agreement between mass loss predicted using Faraday's law and the measured mass loss.

2.2.3 Effect of corrosion on bond strength

2.2.3.1 Al-musallam, and Al-gahtani, 1995

Al-musallam et al. (1995) investigated the effect of reinforcement corrosion on the bond strength of steel in concrete. The test specimen was an end-beam specimen measuring 152×254x279 mm with a 12 mm diameter tension steel bar. The embedment length of the tension bar was 102 mm to avoid yielding of the reinforcement under the pullout force. The

remaining length of the reinforcement was debonding using 89 mm long PVC sleeves in both ends of the specimen. Open legged, U-shaped stirrups with spacing of 76 mm were used to avoid possible shear failure. Compression reinforcement was also used. Figure 2.10 shows the design details of the pullout test specimen.

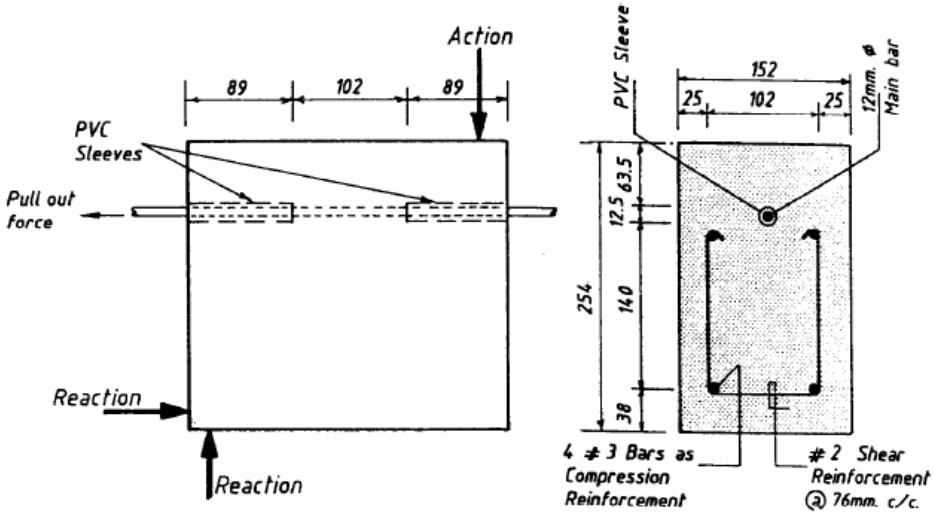

Figure 2-10 Design details of the pullout test specimen

To accelerate the reinforcement corrosion, a constant current of 0.4 A was impressed into the tension steel bar in the pullout specimen. After corroding the tension bar, the pullout tests were conducted using a specially designed loading frame which was fixed to the base of an Instron universal testing machine. Figure 2.11 shows the effect corrosion on bond strength.

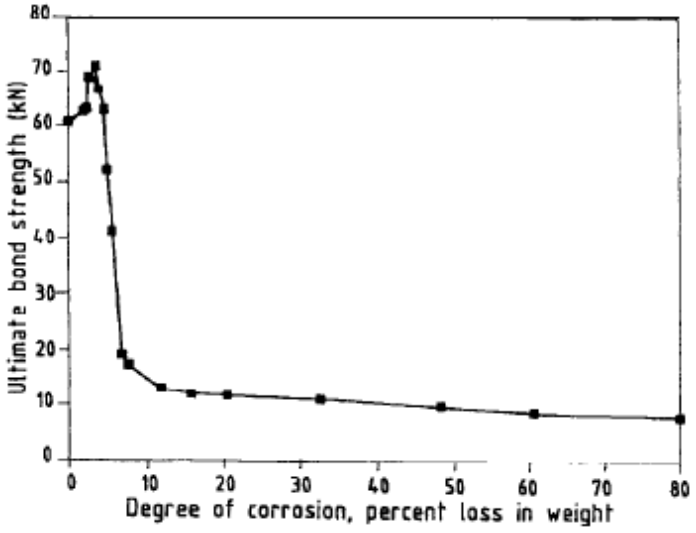

Figure 2-11 Relationship between the ultimate bond strength and different corrosion levels (Al-musallam, 1995).

Based on the analysis of the test results, the following conclusions were made:

- Up to 4% corrosion, the ultimate bond strength increases by about 17 % and rebar slip decreases. The reason why of the bond strength increases at this level is attributed to the fact that the corrosion product increases the rebar roughness and the confinement of the concrete.
- At about 5% corrosion, corrosion cracking is observed and the bond strength decreases gradually for an additional 1% corrosion level and thereafter decreases rapidly.
- Corrosion levels between 5% and 7% are observed to cause significant increase in the crack width as well as loss of the rib profile.
- At a corrosion level of about 12 %, the failure mode changes from splitting to continuous slippage of the bar.

2.2.3.2 Stanish and Hooton (1999)

Stanish et al. (1999) assessed the effect of corrosion product on bond strength. A total of ten one-way slab specimens were cast having cross section of 350 mm (width) by 150 mm (height) and 1300 mm span. Three 10M longitudinal reinforcing bars were used in each specimen at 125 mm lateral spacing and concrete clear cover was 20 mm. Figure 2.12 shows the slab details. The test variable was the degree of corrosion (0%, 2.0%, 5.0%, 8.0%, and 10%). The slabs were subjected to accelerated corrosion. They were immersed in a 3% NaCl solution up to mid-depth of the bars and subjected to the constant current of 100 mA.

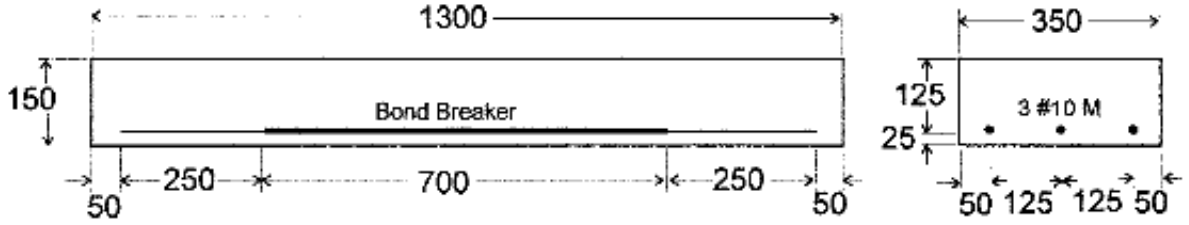

Figure 2-12 Slab details (Stanish, 1999)

Stanish et al. (1999) observed that all the corroded slabs were partly cracked as a result of corrosion before loading. The extent of this damage ranged from small surface cracks to large section spalling off the slab. This damage was restricted to the ends of the slab where the corrosion occurred. Figure 2.13 shows a typical damage pattern of corroded specimens.

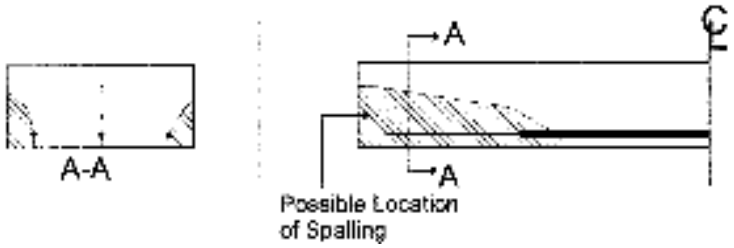

Figure 2-13 Typical damage pattern of corroded specimen (Stanish, 1999)

The test result illustrated that bond resistance was adversely affected by corrosion. The corrosion products led to cracking that relieved the internal pressure and weakened the anchorage of the reinforcing steel; creating a weak layer of corrosion product that will break off under low stress levels.

2.2.3.3 Craig and Soudki (2002)

Craig and Soudki (2002) reported on an experimental study designed to investigate the effect of corrosion on the bond strength of the steel reinforcement in concrete. Five pullout specimens measuring 150 x 150 x 150 mm were constructed and tested. A 15M deformed bar was placed at the corner of each specimen with a clear concrete cover of 30 mm. Debonding sleeves were used to maintain a bond length of 80 mm. All specimens were cast with concrete contaminated with 2.3% chloride by mass of cement. A 6.3 mm stainless steel bar was placed in the center of each specimen to act as the cathode during the accelerated corrosion process. The variable was the corrosion level (0%, 2.0%, 5.0%, 10%, and 15%). Accelerated corrosion was induced with specimen wired by means of an impressed current in series of 9.0 mA current power supply.

Craig observed that the corrosion cracks radiated from the bar towards the sides of the specimen with least amount of cover. The crack width increased with the level of corrosion. After testing, the mode of failure of all corroded specimens was the bond splitting failure. The maximum bond strength vs. Corrosion level is shown in Figure 2.14.

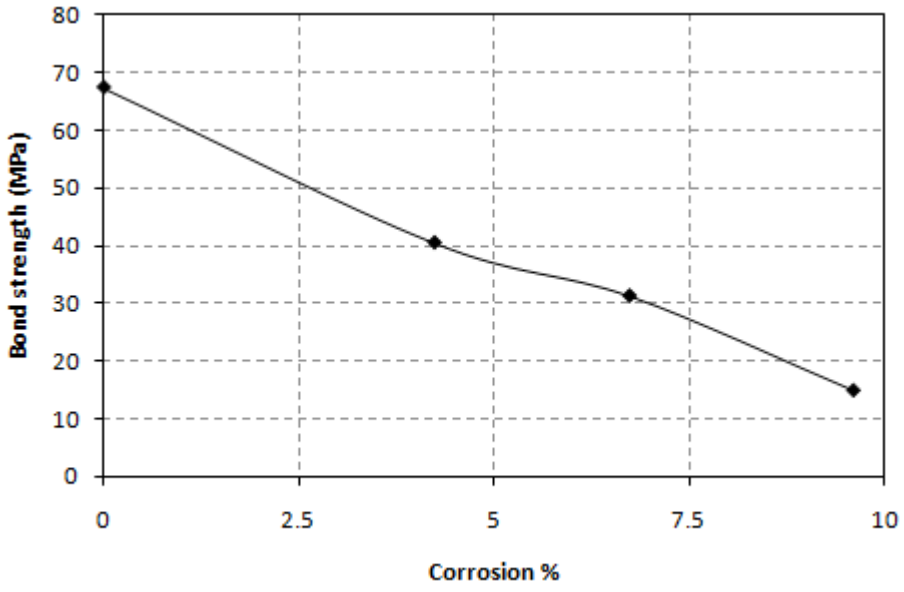

Figure 2-14 Bond strength vs. Degree of corrosion % (Craig and Soudki (2002)

As the level of the corrosion increased the bond strength of the steel reinforcement decreased. The bond strength reduced by 40%, 53%, and 77% for (5.0%, 10%, and 15% corrosion level), respectively in comparison to specimen with 0% corrosion.

2.2.3.4 Soudki and Sherwood (2003)

Soudki and Sherwood (2003) studied the effect of different corrosion levels on the bond strength of steel bars in concrete. Sixteen pullout specimens were tested and they consisted of a concrete prism measuring 150 x 150 x 200 mm with a 10M reinforcing bar placed in the corner of the specimen. A 6.3 mm stainless steel bar was placed in the specimen to serve as the cathode for the accelerated corrosion process. Figure 2.15 shows the pullout specimen configuration. The test variables included the clear concrete cover (15, 30, and 60 mm), and the corrosion level (0, 1, 5, 7, and 10% mass loss). Accelerated corrosion was induced by means of an impressed current with the specimen wired in series. The current density used was 140 $\mu A/cm^2$ which corresponds to an applied current of 7.4 mA.

It was observed that the corrosion cracks were similar in the 15 and 30 mm clear cover specimens. The corrosion cracks were in the corner with the reinforcing bar. The corrosion cracks appeared at 1% corrosion level and the width of the cracks increased as the corrosion level increased. For the specimens with 60 mm clear cover, no corrosion cracks appeared on the concrete surface up to 7% corrosion. The corrosion cracks were evident in specimens corroded to 7% and 10%. The modes of failure of all corroded specimens were bond splitting and bar rupture. Table 2.1 gives the maximum bond strength and the modes of failure for all specimens. As evident in Table 2.1 show that the ultimate bond strength increases slightly in the early stages of reinforcement corrosion. As corrosion increases the ultimate bond strength decreases.

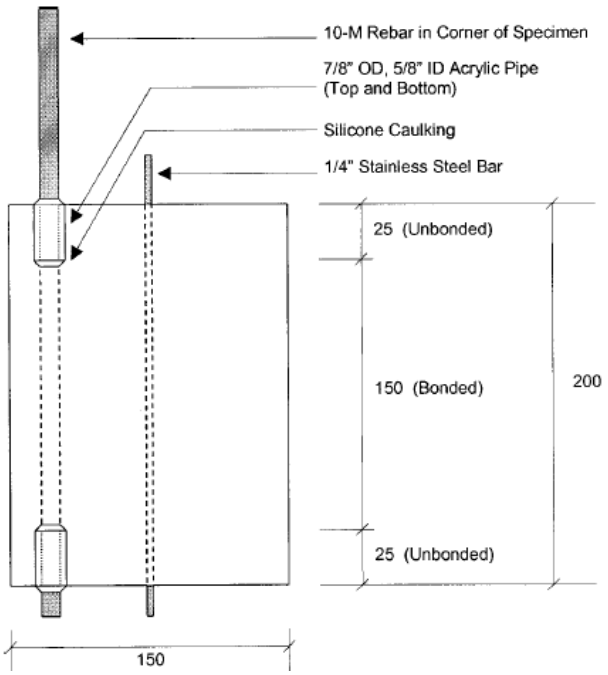

Figure 2-15 Pullout specimen configurations (Soudki and Sherwood, 2003)

Table 2-1 Summery of test results (Soudki and Sherwood, 2003)

Specimen	Corrosion %	Maximum bond strength (kN)	Failure mode
15-U-0	0	46.2	Splitting
15-U-1	1	30.6	Splitting
15-U-5	5	52	Splitting
15-U-10	10	29.8	Splitting
30-U-0	0	62.2	Splitting
30-U-1	1	65.3	bar
30-U-3	3	59.1	Splitting
30-U-5	5	64.3	bar
30-U-7	7	48.6	Splitting
30-U-10	10	22.5	Splitting
60-U-0	0	66.9	Pullout
60-U-1	1	68	bar
60-U-3	3	68	bar
60-U-5	5	67.1	bar
60-U-7	7	63.5	Splitting
60-U-10	10	42.8	Splitting

2.2.3.5 Summary

Based on the literature, the effect of corrosion on the bond strength of the steel reinforcement in concrete can be summarized as follows:

- The corrosion crack width depends on the concrete clear cover to the bar diameter ratio (c/d) and the level of corrosion. The corrosion crack width increased as the corrosion level increased. As the (c/d) ratio increased the corrosion crack width decreased.
- Ultimate bond strength increases slightly at low levels of corrosion. As corrosion increases, the ultimate bond strength decreases. Figure 2.16 shows a schematic of the bond strength versus corrosion level.

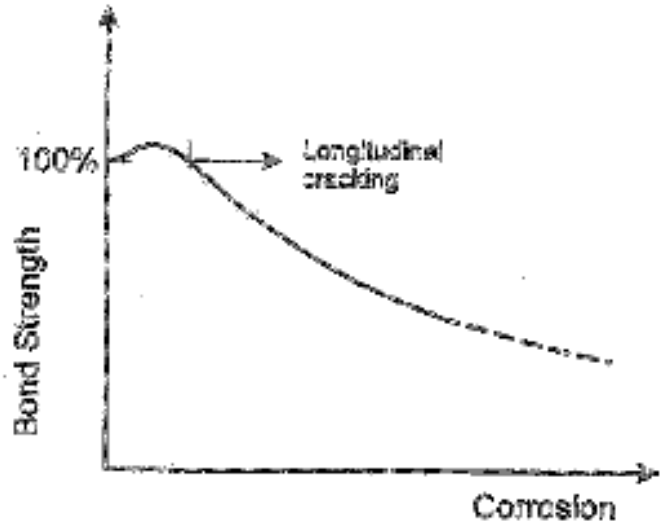

Figure 2-16 Effect of corrosion on bond strength (fib, 2000)

2.3 Fiber reinforced polymers

Fiber reinforced polymers (FRP) are composite materials made of high strength fibers embedded in a resin matrix. The combination of two or more constitutes produces a synergistic effect with the properties of the composite being superior to those of its components (Badawi, 2003).

2.3.1 Resins

A wide range of polymeric resins including primers, putty fillers, and adhesives are used with FRP system. Commonly used resin types include epoxies, vinyl- esters and polyesters. The main function of the matrix (resin) is to support, protect, and separate the fibers. The currently available resins have been formulated to optimize their structural behavior in a wide range of environmental conditions. The resins allow for easy application by qualified installers. The FRP resin is characterized by the following properties (ACI committee 440):

- Low density which gives the composite materials their high strength to weight ratio; one of their most attractive characteristic.
- Resistance to environmental effects including moisture, salt water, temperature extreme, and other chemicals normally associated with concrete exposure.
- Filing ability.
- Compatibility with bond strength to substrate.
- Compatibility with and adhesion to the reinforcing fiber.

2.3.2 Fibers

Continuous fibers like glass, aramid, and carbon are common reinforcements used with FRP systems (Soudki, 1997). The fibers can be unidirectional, bi-directional, and pseudo-isotropic as shown in Figure 2.17. They typically have a linear elastic stress-strain relation up to rupture as illustrated in Figure 2.18.

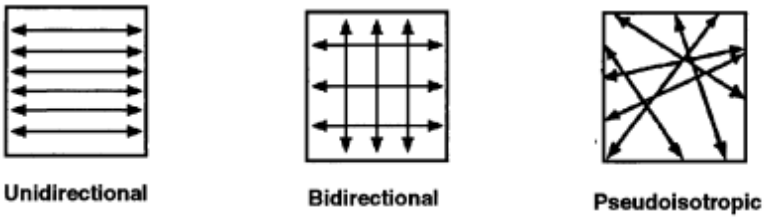

Figure 2-17 Various fiber orientations of FRP laminates (ACI 440, 2002)

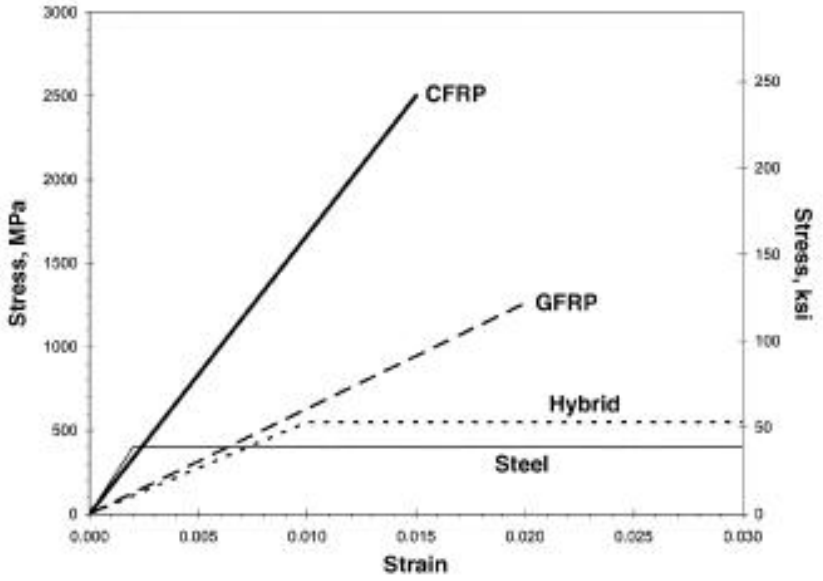

Figure 2-18 Stress-strain behavior of FRP (ACI 440, 2007)

Glass Fibers

Different types of Glass fibers are found in the market with E- glass being the mostly used fiber. Advantages of glass fiber include their low production costs, high tensile strength, excellent heat resistance and low electrical conductivity. However, glass fibers are characterized by their low stiffness and low specific strength due to the low Young's modulus and high specific gravity for glass fiber.

Carbon fibers

Carbon fibers are more attractive for structural use because of their high tensile strength, excellent corrosion resistance, and high strength to weight ratio, excellent fatigue behavior, low coefficient of thermal expansion, and high stiffness. However, they are expensive to produce. And they suffer from low inter-laminar shear strength that leads to low ductility.

Aramid Fibers

Aramid is generic name for aromatic polyamide. Armid fibers are stiffer than glass fiber and cheaper than carbon fibers. They possess low density, high strength and fatigue and corrosion resistance.

2.3.3 Use of FRP for repair and strengthening

FRPs have been used in the repair and strengthening of concrete structure to increase their flexural, shear or for confinement. North American codes were developed to provide design rules and specifications for the use FRP strengthening (ACI 440,2R-2005 , ISIS manual 4, 2010).

1) Flexure – flexural strengthening involves applying FRP sheets in the tensile zone of a member which leads to improvement of its flexural capacity. In addition the internal reinforcement exhibit stress relief as a result of adding FRP, which leads to strength increase ranges from 20 to 100%, has been reported, smaller deflections, reduced fatigue effects and finer crack distribution in a flexural member. Numerous research studies and the development work on the use flexural strengthening techniques in the last decade (ACI 440, 2007)

2) Shear - shear strengthening is achieved by bonding the FRP sheets to the sides of the beam in the high shear zones. Research on this topic indicated an increase in ultimate strength between 60 to 150 percent when using FRP sheets. Issues still that need resolution relate to the debonding of the sheets. (ACI 440, 2007)

3) Corrosion repair – FRPs have been used to protect concrete members against corrosion in severe environments such as coastal areas and where de-icing chemicals are used. Few researchers have investigated the use of FRPs to mitigate corrosion damage. This includes

the work by Craig and Soudki (2002), Sherwood and Soudki (2003), Hammad, Rteil, and Soudki (2004), and Wang, et al (2011). FRP improved the performance of these damaged structures by one of the following mechanisms:

- Confinement of the concrete section, thus capturing any cracks due to corrosion
- Increasing the flexural and shear capacity of the corroded concrete member

2.3.4 Effect of the FRP wraps on bond strength

2.3.4.1 Craig and Soudki (2002)

Craig and Soudki (2002) investigated the confining effect of carbon and glass fibre reinforced polymer (CFRP, GFRP) wrap on the bond behaviour of corroded reinforcing bars. Fifteen pullout specimens were constructed and tested. The specimens consisted of concrete cube measured 150 x 150 x 150 mm with a 15M deformed bar was placed at the corner of each specimen at a clear concrete cover of 30 mm. Debonding sleeves were used to maintain a bond length of the steel bar 80 mm. All specimens were cast with concrete contaminated with 2.3% chloride by mass of cement. A 6.3 mm stainless steel bar was placed in the center of each specimen to act as the cathode during the accelerated corrosion process. A single ply of FRP sheet measuring 150 by 700 mm was placed on the specimen such that the direction of the fibres was oriented perpendicular to the direction of the bar. The test variables included the corrosion level (0%, 2.0%, 5.0%, 10%, and 15%) and presence or absence of transverse FRP wrapping. Accelerated corrosion was induced by means of an impressed current of 9.0 mA with specimen wired in series.

It was reported that, the corrosion cracks radiated from the bar towards the sides of the specimen with the least amount of cover. For specimen with no wrap, severe corrosion cracks occurred along the length of the specimen. For the wrapped specimens, minor cracks were observed on the top and bottom face. These results demonstrate that the FRP wrapping was able to effectively reduce and confine cracking. The mode of failure of all unwrapped corroded specimens was bond splitting failure and bar pullout failure for the wrapped specimen. The maximum bond strength of all specimens is listed in Table 2.3.

The results in Table 2.2 show that FRP repair was quite effective in maintaining the bond strength of severely corroded concrete members. Wrapped specimens were able to retain at

least 60% of their maximum bond strength after failure. In addition, FRP laminates were able to change the failure mode from a brittle bond splitting failure to that of bar pullout failure.

Table 2-2 Summary of the test results (Craig and Soudki, 2002)

Specimen	Corrosion %	Maximum bond strength (kN)	Failure mode
U0	0	67.4	Splitting
U2	NA	NA	Splitting
U5	4.24	40.5	Splitting
U10	6.74	31.3	Splitting
U15	9.61	14.9	Splitting
G0	0	79.7	Bar Pullout
G2	2.73	92.8	Bar Pullout
G5	5.36	92	Bar Pullout
G10	7.95	88.2	Bar Pullout
G15	10.25	87.3	Bar Pullout
C0	0	90.1	Bar Pullout
C2	1.83	87.5	Bar Pullout
C5	4.22	84.5	Bar Pullout
C10	7.46	75.1	Bar Pullout
C15	8.96	62.7	Bar Pullout

2.3.4.2 Soudki and Sherwood (2003)

Soudki and Sherwood (2003) examined the ability of carbon fibre reinforced polymer (CFRP) wrapping to enhance the bond of corroded reinforcing steel bars in concrete. Thirty-two bond pullout specimens were tested. The specimens consisted of a concrete prism measuring 150 x 150 x 200 mm with a 10M reinforcing bar placed in the corner of the specimen. A 6.3 mm stainless steel bar was placed in the specimen to serve as the cathode for the accelerated corrosion process. The strengthening scheme consisted of a single ply of CFRP laminate measuring 150 mm wide by 300 mm long. The test variables included the clear concrete cover (15, 30, and 60 mm), corrosion level (0, 1, 5, 7, and 10% mass loss), and presence or absence of transverse CFRP wrapping. Accelerated corrosion was induced by means of an impressed current with the specimens wired in series. The current density used was 140 $\mu A/cm^2$ which correspond to an applied current of 7.4 mA. Figure 2.19 shows the wrapped pullout specimen configuration.

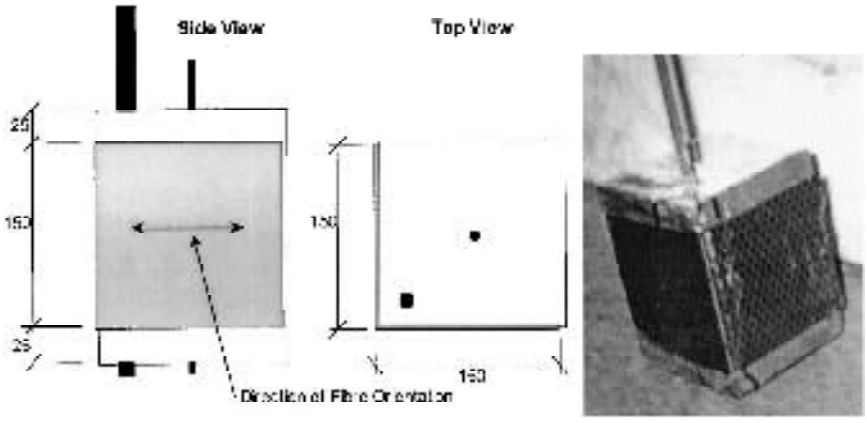

Figure 2-19 Bond pullout specimen-CFRP repair (Sherwood and Soudki, 2003)

The corrosion products were evident on the top and bottom surface but no corrosion cracks were observed. FRP repair of corroded members helped by confining the corrosion crack and increased the bond strength. The bond strength for all specimens is listed in Table 2.3.

The bond strength results reveal that the CFRP wrapped specimens exhibited a higher ultimate bond strength that was more than double in the case of severely corroded (higher than 7% corrosion) in case of 15 and 30 mm wrapped versus unwrapped specimens. CFRP wrapping was not as effective in the 60 mm cover specimens due to the higher clear cover. The specimens failed in three modes: bar pullout, bar rupture, and bar bond splitting. The

failure modes were affected by the concrete cover of reinforcing bar, the corrosion level, and the CFRP wrapping. Wrapped specimens failed due to bar pullout or bar rupture, while the unwrapped specimen failed due to bond splitting or bar rupture.

Table 2-3 Summery of test results (Soudki and Sherwood, 2003)

Specimen	Corrosion %	Maximum bond strength (kN)	Failure mode
15-U-0	0	46.2	Splitting
15-U-1	1	30.6	Splitting
15-U-5	5	52	Splitting
15-U-10	10	29.8	Splitting
15-W-0	0	56	pullout
15-W-1	1	65.8	pullout
15-W-5	5	64.4	pullout
15-W-10	10	67.3	pullout
30-U-0	0	62.2	Splitting
30-U-1	1	65.3	bar
30-U-3	3	59.1	Splitting
30-U-5	5	64.3	bar
30-U-7	7	48.6	Splitting
30-U-10	10	22.5	Splitting
30-W-0	0	64.3	Pullout
30-W-1	1	66	Bar
30-W-3	3	66.2	Bar
30-W-5	5	61.4	pullout
30-W-7	7	60.3	pullout
30-W-10	10	57.4	bar

2.3.4.3 Hammad, Rteil, and Soudki, (2004)

Hammad, Rteil, and Soudki (2004) examined the effectiveness of FRP sheets to confine bond in lap-spliced un-corroded RC beams. The study included seven beams made with normal concrete and ten beams made with high strength concrete. Figure 2.20 shows the details of the test specimen. One beam had no GFRP wraps and acted as a reference and the rest of the beams were tested in two series of three beams each. The variables used for the normal concrete beams were the configuration of the GFRP in the splice region (none, one strip, two strips, or continuous strip) and the area of the GFRP (one layer or two layers). The variables used for the high strength beams in the investigation were the type of the FRP wrap (glass or carbon), the configuration of the FRP sheets in the splice region (one strip, two strip, continuous strip), and the number of layer (one layer or two layers). Figure 2.20 shows the details of test specimen of the GFRP configurations are shown in Figures 2.21

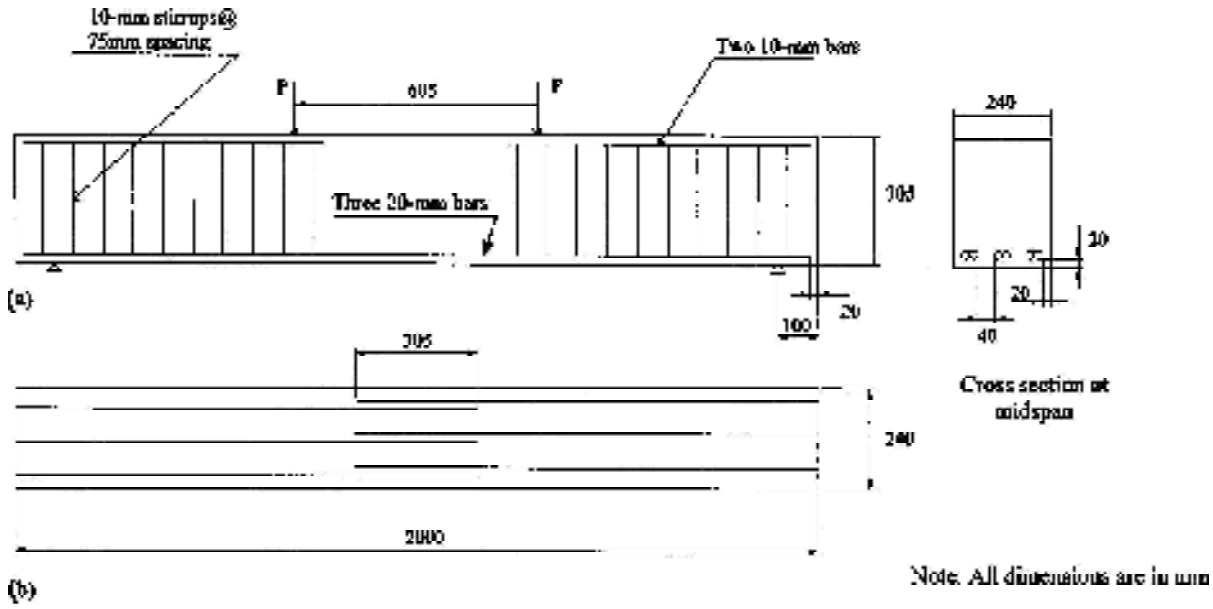

Figure 2-20 Longitudinal and cross- sectional details for beam specimens (a) side view; (b) bottom view (Hammad et al, 2004).

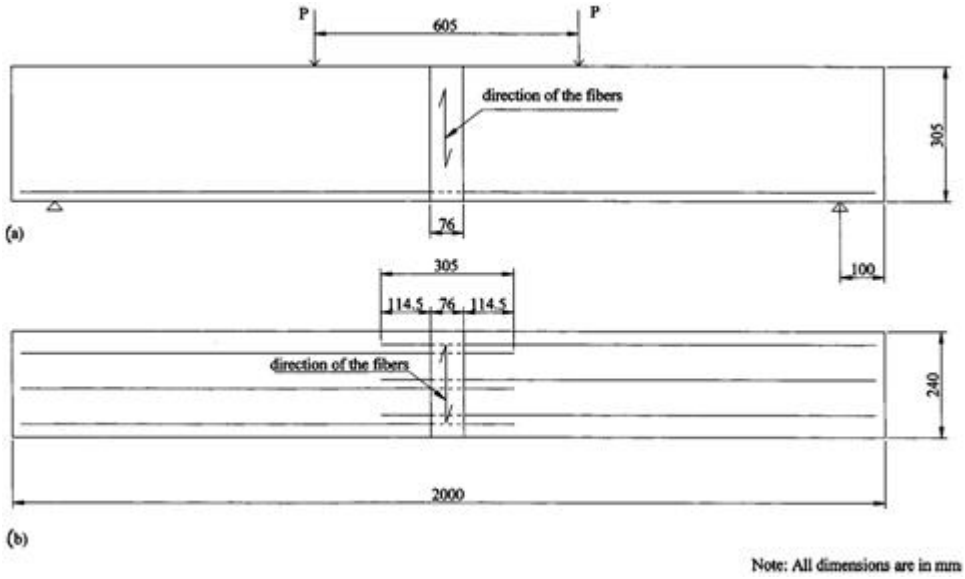

Scheme 1 : (a) bottom view; (b) side view

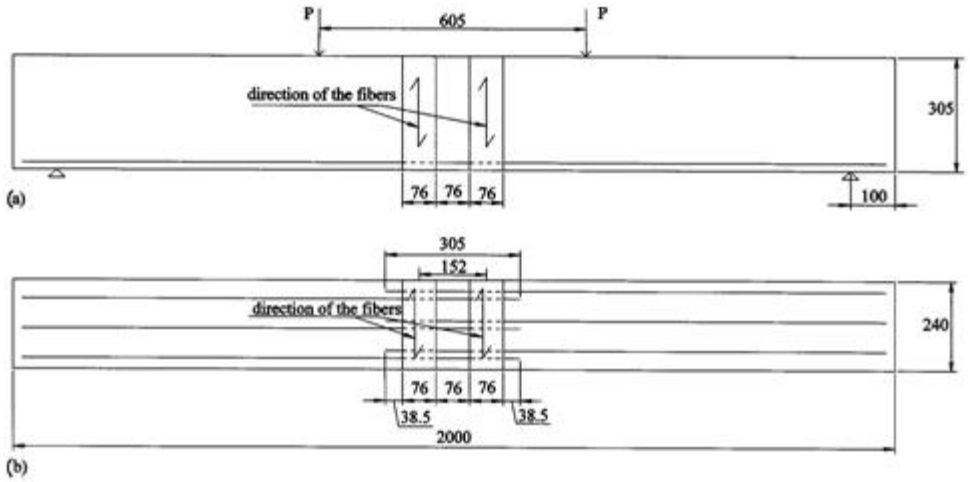

Scheme 2 : (a) bottom view; (b) side view

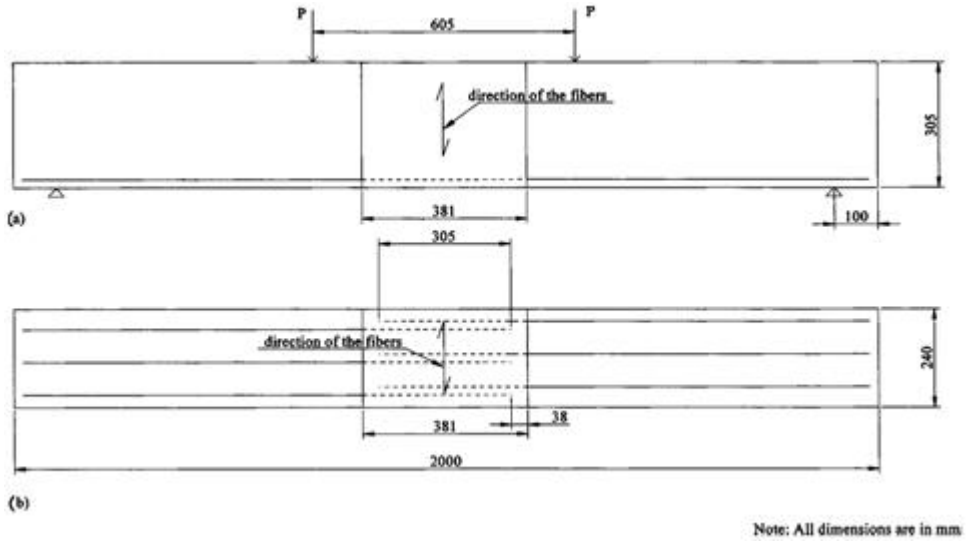

Scheme 3: (a) bottom view; (b) side view

Figure 2-21 GFRP wrap configuration (Hammad et al, 2004)

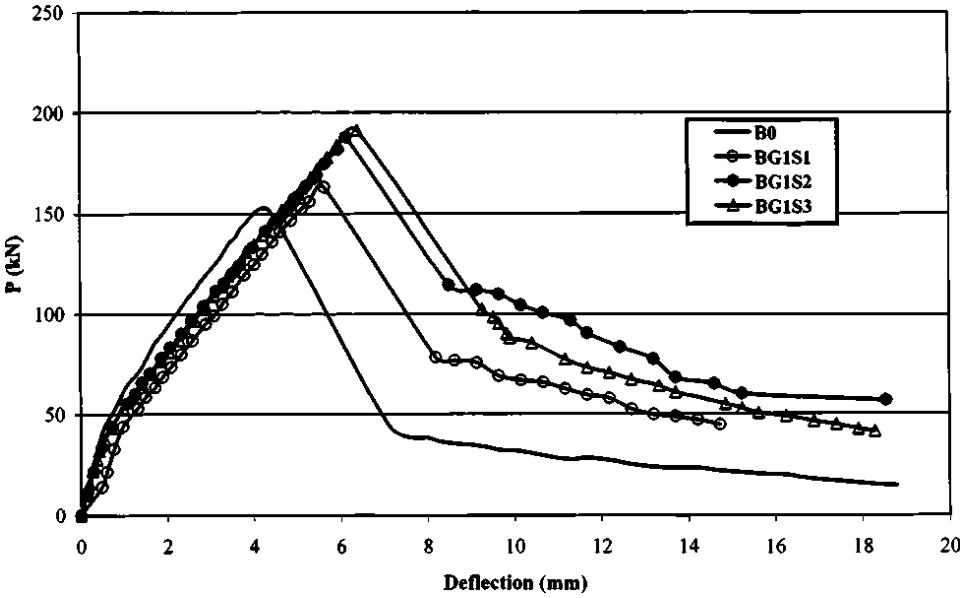

Figure 2-22 Comparisons of the load-deflections curves (Hammad et al, 2004)

Figure 2.22 shows a comparison of the load-deflection of control and FRP strengthened beams. The increase in strength and ductility is evident when using FRP sheets. The mode of failure in all beams was face-and side splitting failure. The splitting mode of failure indicated that the splice reached its maximum capacity. For the beam without FRP wrap, the failure

occurred after longitudinal splitting cracks formed in the bottom cover on the tension side directly below the splice region. Beams with FRP sheets exhibited, a more ductile and more gradual mode of failure than the control beam. The bond strength could be determined directly from the stress developed in the steel. The stress in the steel (f_s) was calculated based on an elastic cracked section analysis, and was determined from the maximum load measured for each beam. The average bond stress (U_t), was determined using the following equation:

$$U_t = \frac{A_b f_s}{\pi d_b l_s} \tag{2.11}$$

Where A_b = bar area; f_s= steel stress; d_b= bar diameter; and l_s= splice length. In Table 2.4 the test result are presented

Table 2-4 Test variables and test results (Hammad et al. 2004)

series number	Type of FRP	specimens notations	number of FRP sheets	configurations	Ultimate load (kN)	Steel stress (Mpa)	Bond stress (Mpa)
control	-	B0	0	-	137.7	392.9	6.4
One	Glass	BG1S1	1	1 strip	157	423.8	6.9
		BG1S2	1	2 strip	174.5	487.6	8
		BG1S3	1	Continuous	178.5	496	8.1
Two	Glass	BG2S1	2	1 strip	156.3	436.1	7.1
		BG2S2	2	2 strip	179.7	505.4	8.3
		BG2S3	2	Continuous	186.8	522.6	8.6
three	Carbon	BC1S1	1	1 strip	157.3	417.2	6.84
		BC1S2	1	2 strip	166.7	452.2	7.41
		BC1S3	1	Continuous	182.3	499.5	8.19

A new parameter $K_{tr,f}$ was introduced similar to the transverse reinforcement parameter K_{tr} proposed by Orangun ,Jirsa ,and Breen (1975) to account for the bond strength contribution provided by the FRP wraps confining steel reinforcement in the lap splice region.

$$K_{tr,f} = \frac{U_{tf}}{\sqrt{f'_c}} = \frac{C_1 \times A_{tr,f} \times f_{fe}}{s_f \times d_b \times n_b} \; ; \; C_1 = \frac{1}{200} \tag{2.13}$$

Where $A_{tr,f}$ = total cross sectional area of FRP; f_{fe}= effective stress in the FRP laminate; s_f= centre – to –centre spacing between FRP sheets; and d_b= bar diameter. The prediction of the bond stress using the new confinement index ($K_{tr,f}$) are presented in Table 2.5

Table 2-5 Measured and predicted bond strength contribution due to FRP (Hammad et al.2004)

series number	Type of FRP	U_t psi	Uc psi	Utr,f psi	Ktr,f
control	-	934	934	0	0
One	Glass	1008	934	74	0.61
		1159	934	225	1.23
		1179	934	245	2.45
Two	Glass	1037	934	103	1.23
		1202	934	268	2.45
		1243	934	309	3
three	Carbon	991.6	934	57.6	0.62
		1075	934	141	1.24
		1188	934	254	2.48

Based on the test results, the following conclusions were reached:

- For the beam without FRP wraps in the splice region, failure occurred just after longitudinal splitting cracks formed in the bottom and side covers adjacent to the location of the bars. The final mode of failure was a face-and-side split failure. The failure was sudden, brittle, and noisy.
- FRP wraps were effective in confining the tension splice region. The mode of failure was more ductile and more gradual, although the final mode of failure was splitting of the concrete cover.
- The bond strength of tension lap splices increased as the amount of FRP confining the splice region increased. The increase relative to the control beam without FRP ranged from 8% for the Beam with one layer, one strip in the middle of the splice length to 33% for the beam with two layers, continuous strip over the splice length.
- FRP sheets had positive effect on the ultimate strength and ductility of the load-deflection. Bond strength of the tension lap splices increased as the amount of FRP confining the splice region increased.
- The type of FRP sheets confining the splice region carbon or glass – had no significant on the mode of failure, or bond strength.

2.3.4.4 Summary

Based on the literature, the effect of FRP confinement on the bond strength of the steel reinforcement can be summarized in following points:

- Corroded and strengthened specimens exhibit much higher ultimate bond strength as compared to similar but un-strengthened specimen.
- Concrete cover to bar diameter ratio has a significant effect on the FRP confinement. As the c/d ratio increased, the confining effect of FRP strengthening decreased.
- For beams without FRP wraps in the splice region, failure occurred just after longitudinal splitting cracks formed in the bottom and side covers adjacent to the location of the bars. The final mode of failure was a face-and-side split failure and it was sudden, brittle, and noisy.
- FRP wraps were effective in confining the tension splice region. The mode of failure was more ductile and more gradual, although the final mode of failure was splitting of the concrete cover.
- The bond strength of tension lap splices increased as the amount of FRP confining the splice region increased. The increase relative to the control beam without FRP ranged from 8% for the Beam with one layer, one strip in the middle of the splice length to 33% for the Beam with two layers, continuous strip over the splice length.
- FRP sheets had positive effect on the ultimate strength and the ductility of the load-deflection. Bond strength of the tension lap splices increased as the amount of the FRP confining the splice region increased.
- The type of FRP sheets confining the splice region carbon or glass – had no significant effect on mode of failure, or bond strength.

2.4 Concluding remarks

The bond strength of steel reinforcing in concrete has been investigated using different types of specimens ranging from pullout specimens to bond beam specimens. The use of lap-spliced beams specimens has been found to produce the bond stresses that closely replicate those found in flexural members (ACI 408, 2003).

To the author's knowledge, no study has been reported in the literature on the effects of corrosion on tension lap-spliced RC beams. Also, based on the literature and according to the researcher knowledge, no study was found in the literature that investigated the effect of CFRP confinement on the bond strength of corroded tension lap-spliced RC beam.

Therefore, this research study was carried out to fill this gap in the state of the art to provide a better understanding to the effects of corrosion on bond strength and the use of FRP confinement to enhance the bond strength.

Chapter 3

Experimental program

3.1 Introduction

The experimental program included eighteen lap-spliced reinforced concrete (RC) beams. The study aimed to investigate the effect of corrosion of the lap spliced reinforcement in RC beams and to determine the viability of carbon fibre reinforced polymer (CFRP) repair for enhancing the bond strength and ductility of corroded tension lap splices.

This chapter describes the test specimen configuration, the materials and fabrication of the beams, the accelerated corrosion process, the mass loss measurements, the CFRP repair, and the load test setup and procedure.

3.2 Test matrix

The test program comprised of eighteen lap-spliced reinforced concrete beams (200 wide × 300 deep × 2000 long mm). The beams were divided into three series based on their concrete cover to bar diameter (c /d) ratio of 1.5, 2.0, and 2.67. Each group consisted of six beams: two beams in each group were not corroded (control beams); two beams were corroded to a 2.5% mass loss (low corrosion level), and two beams were corroded to a 5% mass loss (medium corrosion level). At the end of the corrosion phase, two beams, one control and one corroded, were tested without repair and the other three beams were repaired with CFRP laminates (wrapped) and then tested in flexure. The test matrix is given in Figure 3.1 and the details of the specimen configuration are given in Table 3.1

Table 3-1 Details of the specimen configuration

		Notations	Main reinforcement	Clear Concrete Cover	Transverse reinforcement
Corrosion	Un-Wrapped	N-1.5	2-20M	30 mm	10M@100 mm
		L-1.5			
		M-1.5			
		N-2.0	2-15M	30 mm	10M@100 mm
		L-2.0			
		M-2.0			
		N-2.67	2-15M	40 mm	10M@100 mm
		L-2.67			
		M-2.67			
	Wrapped	WN-1.5	2-20M	30 mm	10M@100 mm
		WL-1.5			
		WM-1.5			
		WN-2.0	2-15M	30 mm	10M@100 mm
		WL-2.0			
		WM-2.0			
		WN-2.67	2-15M	40 mm	10M@100 mm
		WL-2.67			
		WM-2.67			

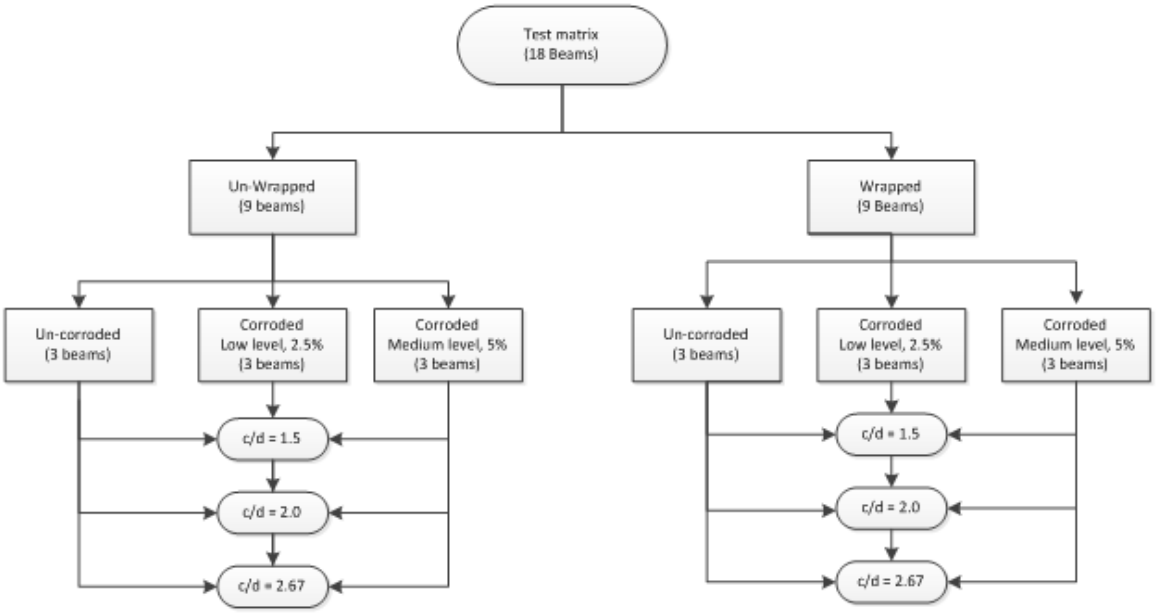

Figure 3-1 Test matrix

3.3 Description of the test specimen

The beams were divided into three groups according to their concrete cover to bar diameter (c/d) ratio. The beam geometry and reinforcement details are shown in Figures Figures 3.2, 3.3 3.4 for beams with c/d ratio of 1.5, 2.0 and 2.67, respectively. The overall geometry for all the beams was the same. The beam cross-section was 200 mm wide x 300 mm deep. The beam length was 2000 mm with a span of 1800 mm between the supports. The length of the constant moment region or the distance between the two applied loads was 600mm.The tensile reinforcement consisted of deformed bars spliced at mid span. The splice length for the bars was 300mm to develop a steel stress in the tensile reinforcement less than its yield strength to ensure a bond splitting mode of failure in all beam specimens. . In the first group with c/d ratio equal 1.5, two 20M reinforcing bars were used and the clear concrete cover was 30 mm. The clear spacing between the lap-splices was 40 mm. For the second group with a c/d ratio of 2.0, the main reinforcement was two 15M bars and the concrete clear cover was 30 mm. The clear spacing between the lap-splices was 60 mm. In the third group with a c/d ratio of 2.67, the main reinforcement was two 15M bars and the clear cover was 40 mm. The clear spacing between the lap-splices was 40 mm. The transverse reinforcement in the shear spans of all the beams consisted of 10M stirrups at a spacing of 100 mm. There were no transverse reinforcements in the splice region to examine the bond behaviour of the corroded steel reinforcement in concrete without the contribution of transverse reinforcement. The compression steel was 2-10M in the shear span.

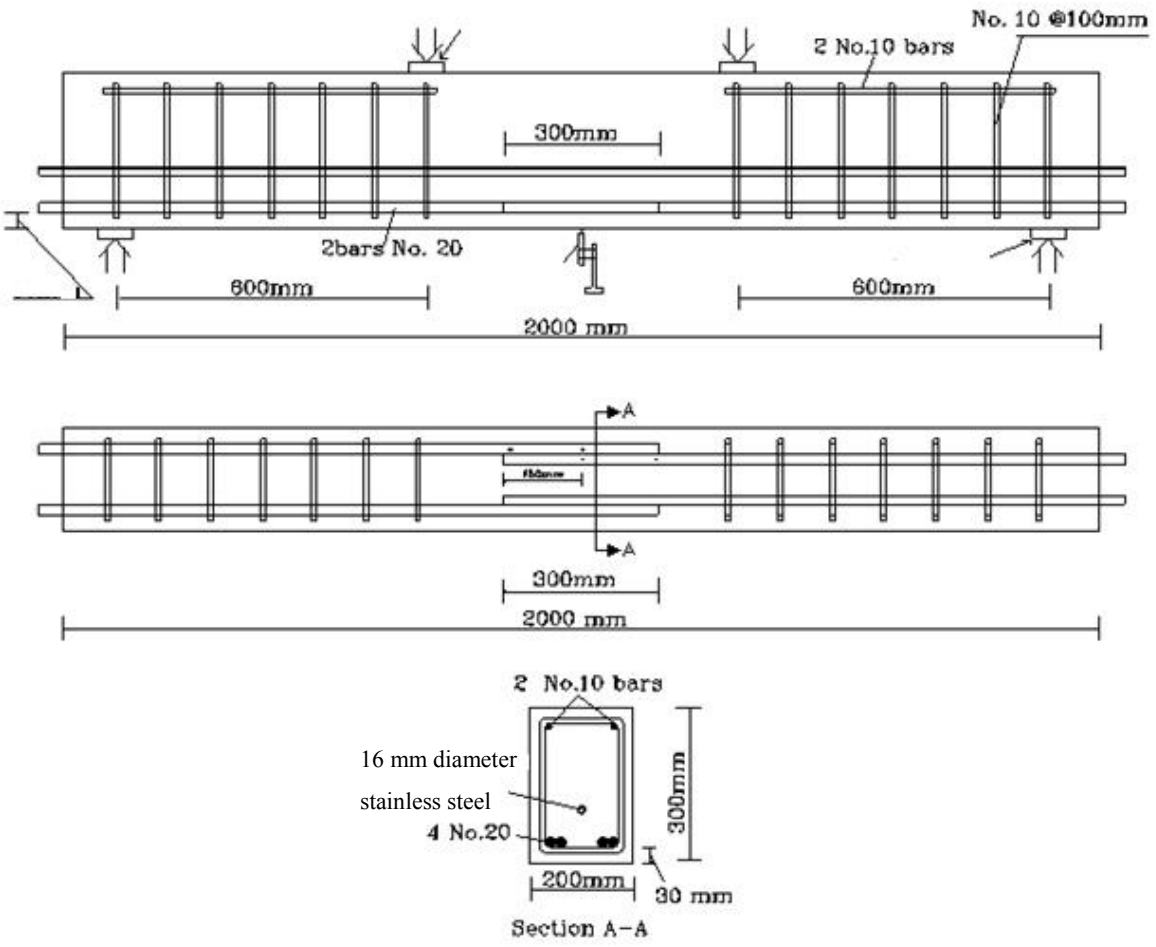

Figure 3-2 Beam configuration and reinforcement details (c/d = 1.5)

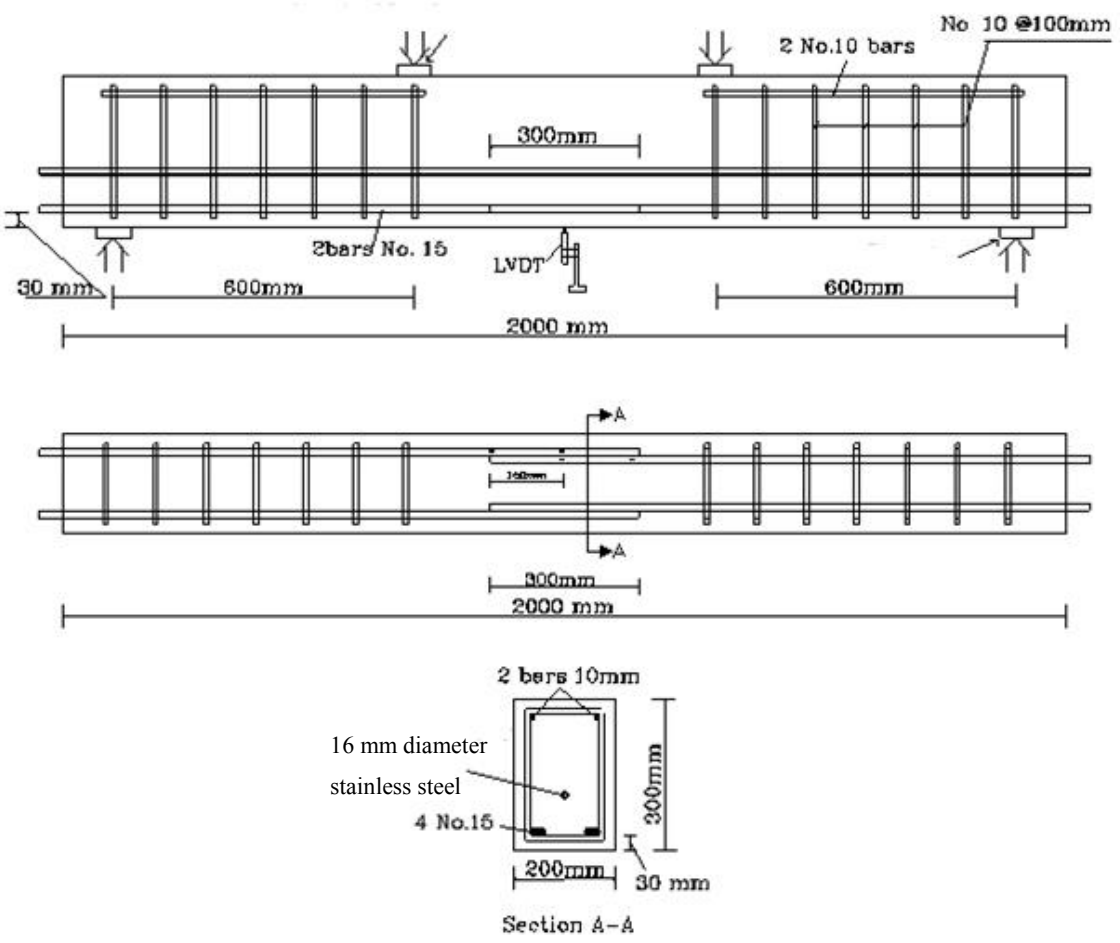

Figure 3-3 Beam configuration and reinforcement details (c/d = 2.0)

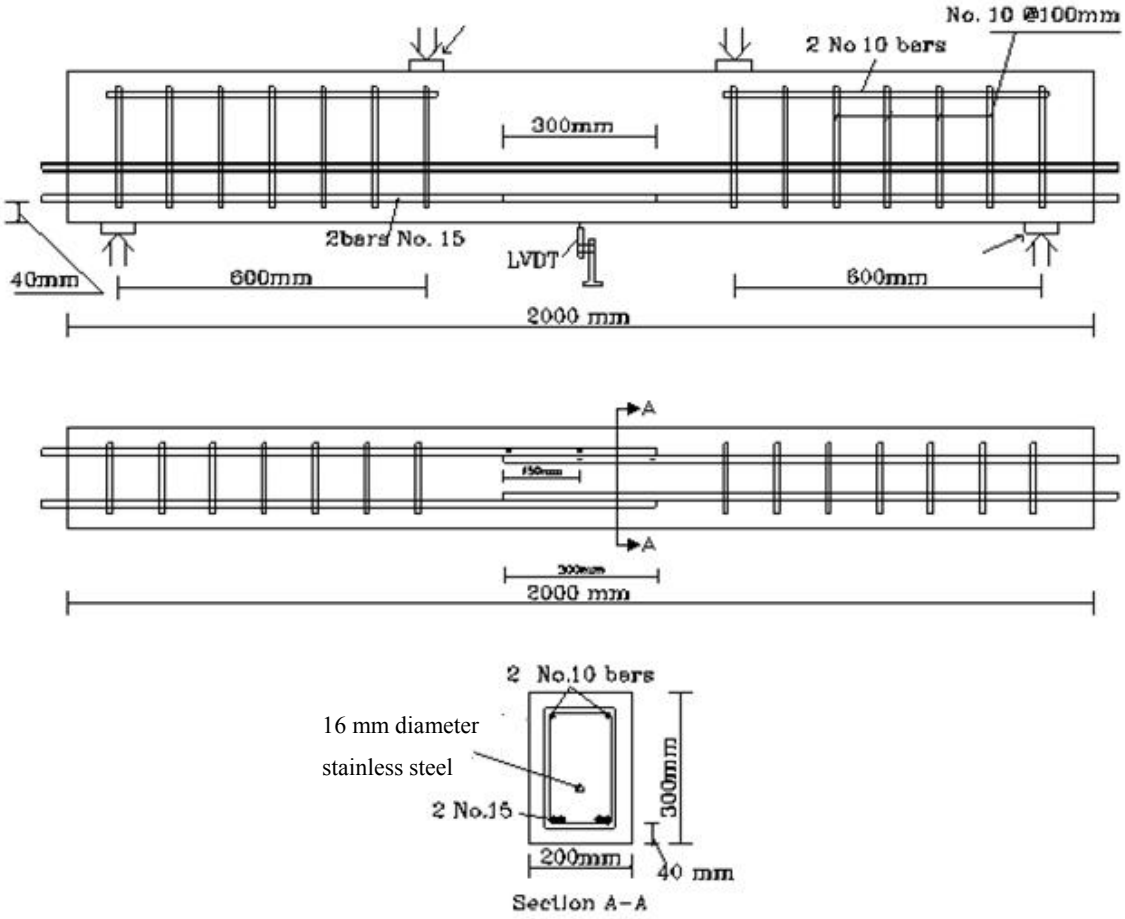

Figure 3-4 Beam configuration and reinforcement details (c/d = 2.67)

A 15 mm diameter hollow stainless steel bar was placed at 120 mm from the soffit of the specimens in all the corroded beams. The hollow stainless steel bar was used as a cathode terminal for the corrosion process. The main tension reinforcements and the stainless steel bar were extended 100 mm from both beam ends. This extension allowed for easy connection to the power supplies used in the accelerated corrosion process. A hole was drilled at the end of each bar to connect them to the power supplies.

The corroded beams were designed in such a way that the main tension reinforcement would corrode only within the lap-splice zone. Salt (NaCl) was added to the concrete mix that was placed in the splice region to induce the localized corrosion. The salted concrete mix was placed over a length of 600 mm within the constant moment region while the rest of the beam was cast with an unsalted concrete mix. The height of the salted concrete was 125 mm from the bottom soffit of the beam so that the stainless steel bar was within the salted concrete. Figure 3.5 shows the location of the salted concrete within the beam.

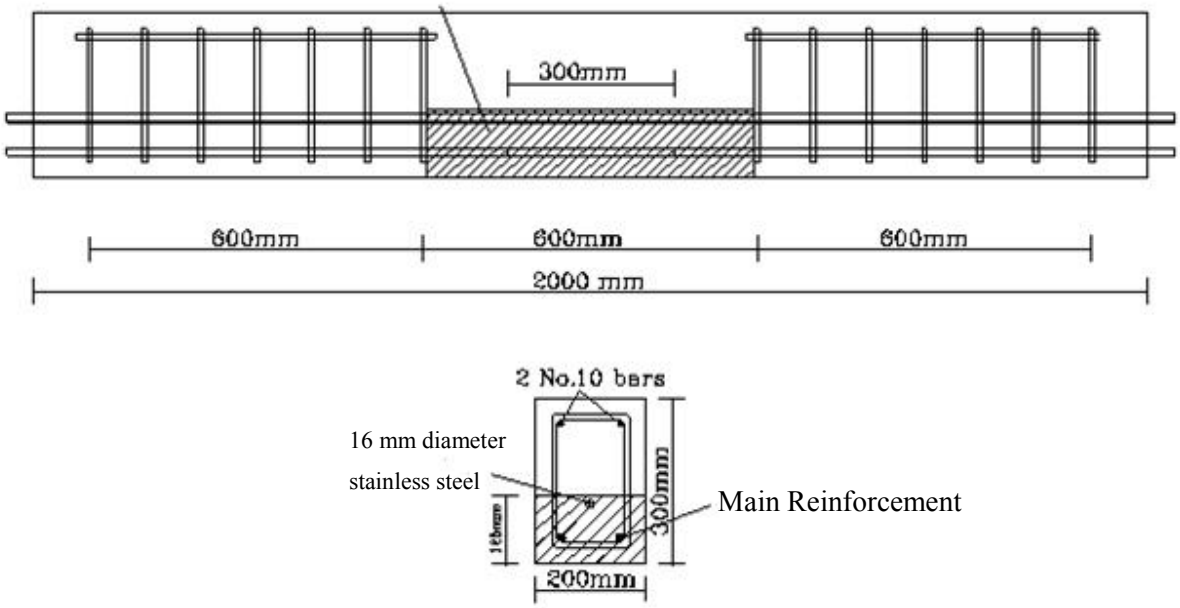

Figure 3-5 Location of the salted concrete within the lap splice region to in the test specimen

Epoxy coated stirrups were used to protect them from corrosion and to prevent the flow of impressed current through the stirrups. The corners of the stirrups were also isolated by the electrical tape to ensure that there was no electrical contact between the main reinforcement

and the stirrups. Figure 3.6 shows the epoxy coated stirrups isolated and coated with electric tape at the corner. The reinforcement steel cages were placed inside the form work as shown in Figure 3.7.

Figure 3-6 Epoxy coated stirrups with electrical tape at the corner

Figure 3-7 Reinforcing steel cages inside the form work

3.4 Formwork

Each beam was cast in a single formwork and the details of the formwork are shown in Figure 3.8. The formwork sides were made from plywood measuring 370 x 20x 2080 mm and the bottom from one steel C- channel measuring 148 x 48 mm. The side faces of the formwork were coated with oil using a brush to allow easy removal of the beams after casting. Plastic plates were used as separators at the transition line between the salted and unsalted concrete zones to ensure that the proper concrete mix was placed while casting. The salted concrete mix was poured first followed by the unsalted concrete mix while the plastic separators were removed. The beams were left to cure for twenty one days to achieve their desired strength and then were stripped from the formwork. The beams were covered by wet burlap during the curing phase.

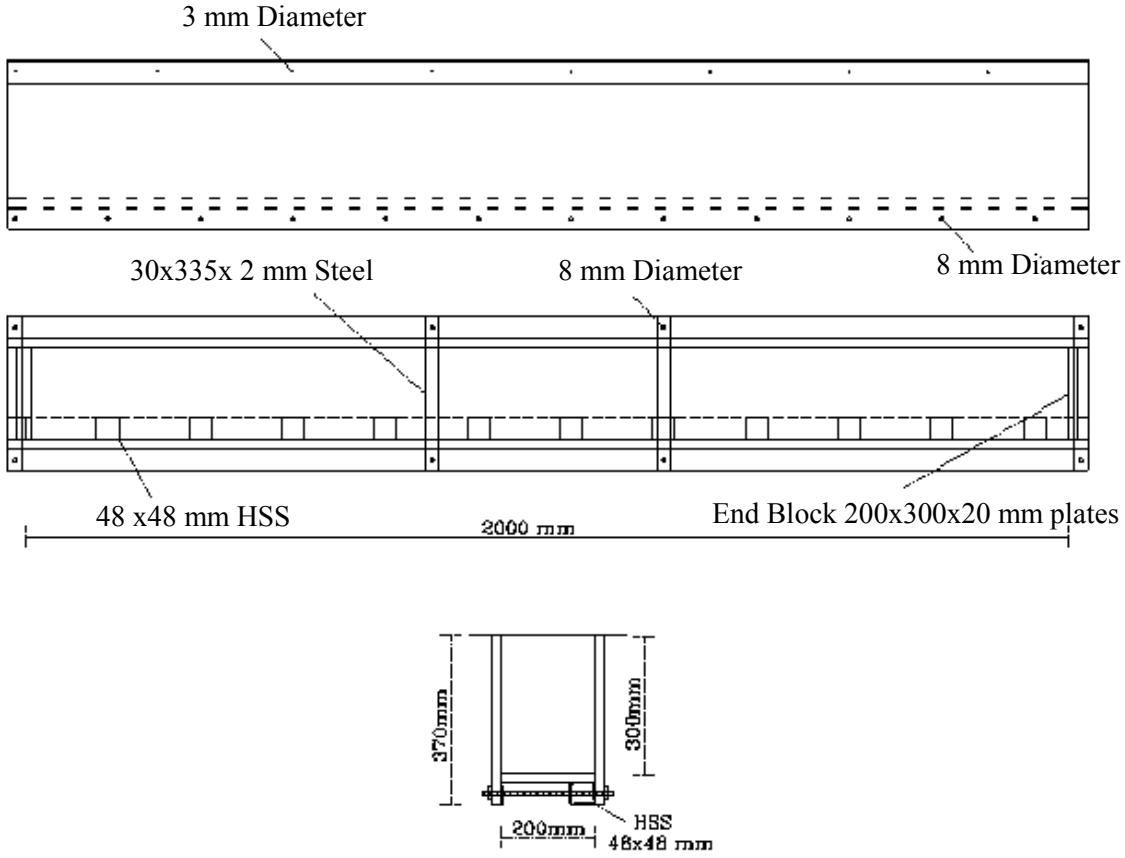

Figure 3-8 Detailing and the dimension of the formwork

3.5 Material properties

The compressive strength of the unsalted and salted concrete was determined by testing 100 x 200 mm cylinders. The average 28-days compressive strength was 41 MPa. The yield strength of the steel reinforcement was 510 MPa according to the manufacturer specifications.

The CFRP laminate was Sika-Wrap-Hex 230C manufactured by Sika Canada Inc. The dry fibre properties are given in Table 3.2. The epoxy resin used was Sika-dur Hex-300 with mechanical properties as given in Table 3.3. The cured CFRP laminate properties for Sika-Wrap-Hex 230C with Sika-dur Hex-300, according to the manufacturer are given in Table 3.4.

Table 3-2 Mechanical properties of Sika-Wrap-Hex 230C

Engineering Property	***Value***
Primary Fibre Direction	0^o
Tensile Strength (GPa)	3.45
Tensile E-modulus (GPa)	230
Tensile Elongation (%)	1.5
Density (g/cm^3)	1.8

Table 3-3 Mechanical Properties of Sikadur-Hex-300

Engineering Property	***Value***
Viscosity(cps)	550
Service Temperature (C)	$40^0$to 60^0
Tensile Strength (MPa)	72.4
Tensile E-modulus (GPa)	3.2
Elongation (%)	4.8

Table 3-4 Cured Sika Wrap Hex 230claminate properties with Sikadur-Hex 30 epoxy

Engineering Property	***Value***
Tensile Strength (MPa)	894
Tensile E-modulus (MPa)	65402
Tensile Elongation (%)	1.33
Ply thickness (mm)	1.8

3.6 Corrosion process

An accelerated corrosion technique was adopted to corrode the reinforcing lap-splice in a reasonable time frame. The corroded beams were placed on steel racks inside the corrosion chamber. A 3 mm of polyvinyl chloride (PVC) plates was placed underneath each beam to isolate the beam from the steel racks and to prevent any current leakage to the ground. A galvanostatic technique was used by impressing an electric current through the main reinforcement. In this system, the current remains constant and the voltage changes depending on the resistance of the beams. The mass loss was predicted based on Faraday's law. Figure 3.9 shows an overview of the corrosion chamber and the power supplies used in the corrosion process

a) Corrosion chamber-racks

b) Corrosion chamber with beams

Figure 3-9 Corrosion chamber

The beams were connected in series with power supplies (Power Rac 1000 with a maximum capacity of 500 μA). The current flows through the circuit with the hollow stainless steel bar acting as a cathode and the main reinforcement as an anode. The main reinforcements in each beam were connected with lead wires to ensure that they will have the same current. Figure 3.10 shows the electrical connections between a group of beams and the power supply.

One of the main requirements for corrosion to occur is the availability of humidity and oxygen. To ensure the availability of moisture and oxygen in the corrosion chamber, plastic sheets were used to enclose the chamber and a water sprinkler was used to provide a mix of water and air. The corrosion chamber consisting of the steel racks, the high pressure water sprinkler and enclosure by plastic sheets to provide a suitable environment for corrosion to occur

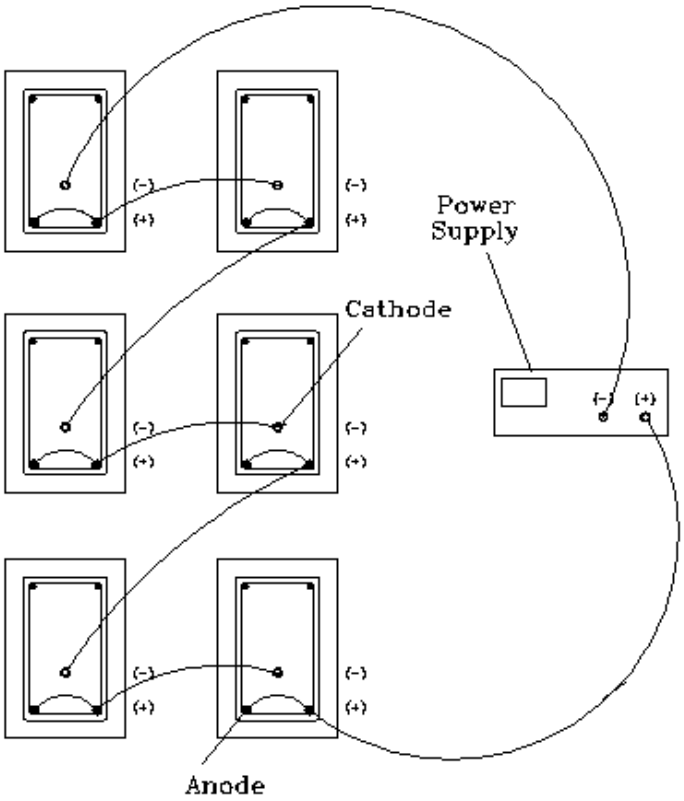

Figure 3-10 Schematic showing the accelerate corrosion Electrical connection details

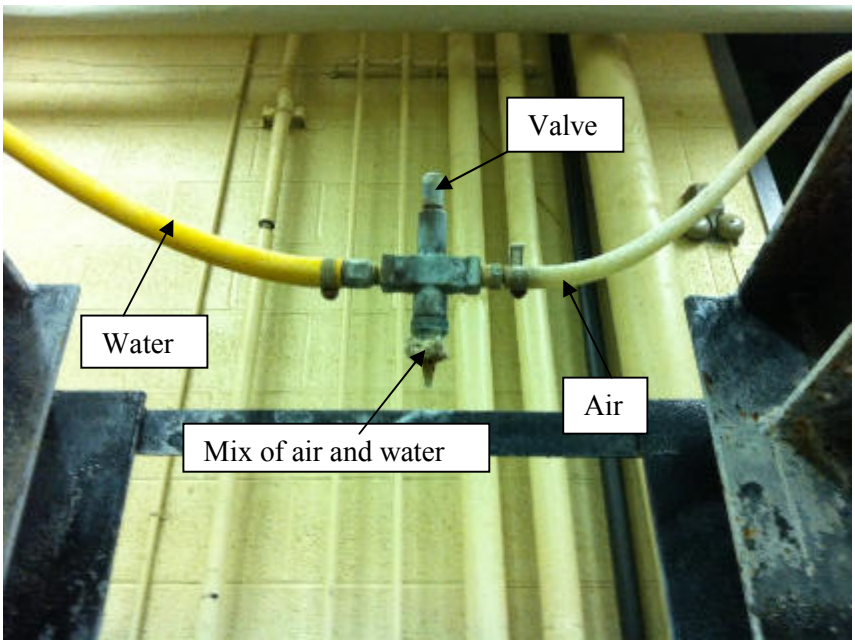

Figure 3-11 High pressure sprinkler used to provide a mix of water and air

3.7 Impressed current

A current density of 150 μA/cm² was used in this study. Each group of beams was connected to a separate power supply with different impressed currents because of the difference in the total surface areas for each group of beams. For beams with 20M reinforcement, the total length of one bar being corroded was 450 mm, and the total surface area for the four bars was 11310 cm². To achieve a current density of 150 μA/cm² in these bars, an impressed current of 160 mA was induced by the power supply. The length of time to induce 2.5% and 5.0% corrosion was 25 days and 50 days, respectively. For beams with 15M reinforcement, the total length of one bar being corroded was 450 mm, and the total surface area for four bars was 8482 cm². The current impressed into the bars was 140 mA to achieve the current density chosen. The length of time to induce 2.5% and 5.0% corrosion was 21 days and 42 days, respectively.

3.8 CFRP repair

The viability of CFRP repair for corroded lap-spliced concrete beams is investigated in this study. The CFRP repair scheme was kept the same for all the repaired beams. It consisted of a 605 mm wide continuous U-wrap placed around the cross section along the constant moment region. Figure 3.12 and 3.13 shows the CFRP repair scheme. This U-wrap will confine the dilation due to bond/splitting stress and increase the bond strength between the reinforcement steel and concrete.

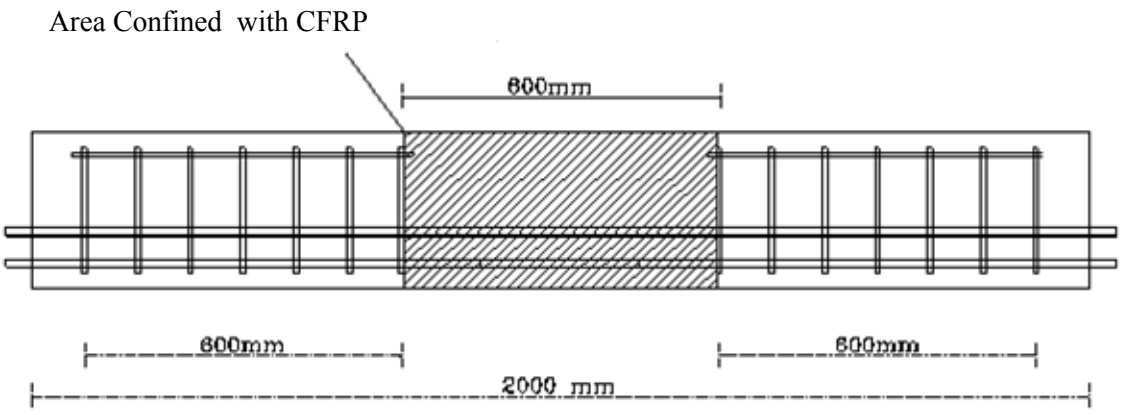

Figure 3-12 Detail of the 605 mm wide continuous u-wrapped along the constant moment region

Figure 3-13 CFRP repair scheme

3.9 Application of the CFRP repair

Concrete surface preparation was done before bonding the CFRP laminates onto the concrete surface of the specimens. The CFRP repair application is describe below.

3.9.1 Surface preparation

Prior to application of the CFRP laminate, a grinder was used to clean the concrete surface from corrosion staining and other foreign particles. The grinder was also used to expose the aggregates to get a sufficiently rough surface to ensure that there will be good bond between the CFRP laminate and the concrete substrate. The corners of the beam's cross section were rounded as per ACI 440.2R-08 to avoid localized stress concentration in the CFRP laminates. Figure 3.14 shows the specimen surface before and after surface preparation.

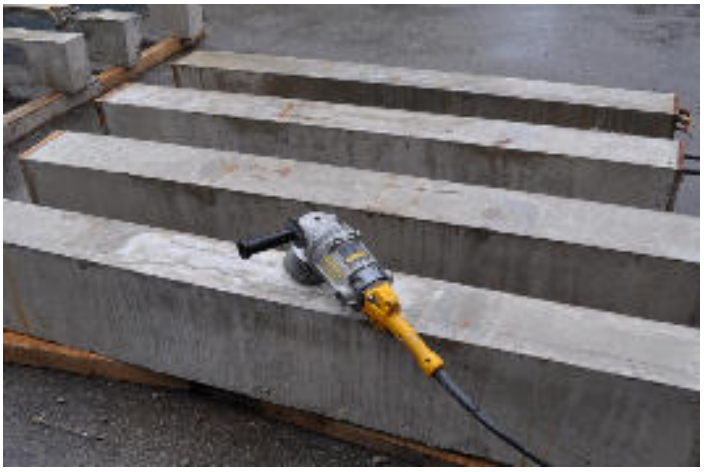

Figure 3-14 The specimen surface before and after cleaning

3.9.2 Installation of the CFRP

After preparing the concrete surface, the CFRP laminates were cut to the required length. The concrete surface was also coated with Sikadur-Hex-300 resin using a brush. The CFRP laminate was impregnated with the same resin and installed onto the concrete surface. Manual pressure was applied on the CFRP laminates by using a steel roller to remove any air voids at the concrete/CFRP interface during the bonding and curing process. The repaired beams were cured for 5 days to allow the CFRP laminates to reach their full strength.

3.10 Instrumentation

Instrumentation used for the test specimens included : i) strain gauges mounted on the steel reinforcing bar, the concrete surface and CFRP laminate to measure the strain, ii) Linear Variable Differential Transformers (LVDT's) to measure mid span deflection of the beam , iii) load cell to measure the applied load.

Strain gauges were mounted on the steel reinforcement and placed inside slots made through the reinforcing bars. Two slots (measuring 2 x 6 mm) were made using milling machine through the reinforcing bars at the middle and the end of the lap-splice length. These strain gauges were used to determine strain distribution along the lap-splice zone. The strain gauges were installed inside the slots using wood sticks to put sufficient pressure to bond the strain gauge onto the bar. Wax was used to cover the slot and to protect the strain gauge from rust during the corrosion process. Figure 3.15 shows the location of the strain gauges on the lap

splice. Figure 3.16 and 3.17 show the slot configurations and the strain gauge installation inside the slot of the reinforcing bars. One strain gauge was mounted on the concrete compression surface at mid span. Two strain gauges were installed on the CFRP laminates. The first strain gauge was placed on the side of the beam at the same level as the main reinforcement in the middle of the constant moment region. The second strain gauge was placed on the bottom side at the end of the lap splice zone. A thin layer of the Sikadur30 was placed to smoothen the location where strain gauge was mounted. After the resin hardened, the surface was polished using sand paper prior to application of the strain gauges. Figure 3.18 shows strain gauge location on the CFRP and on the concrete surface.

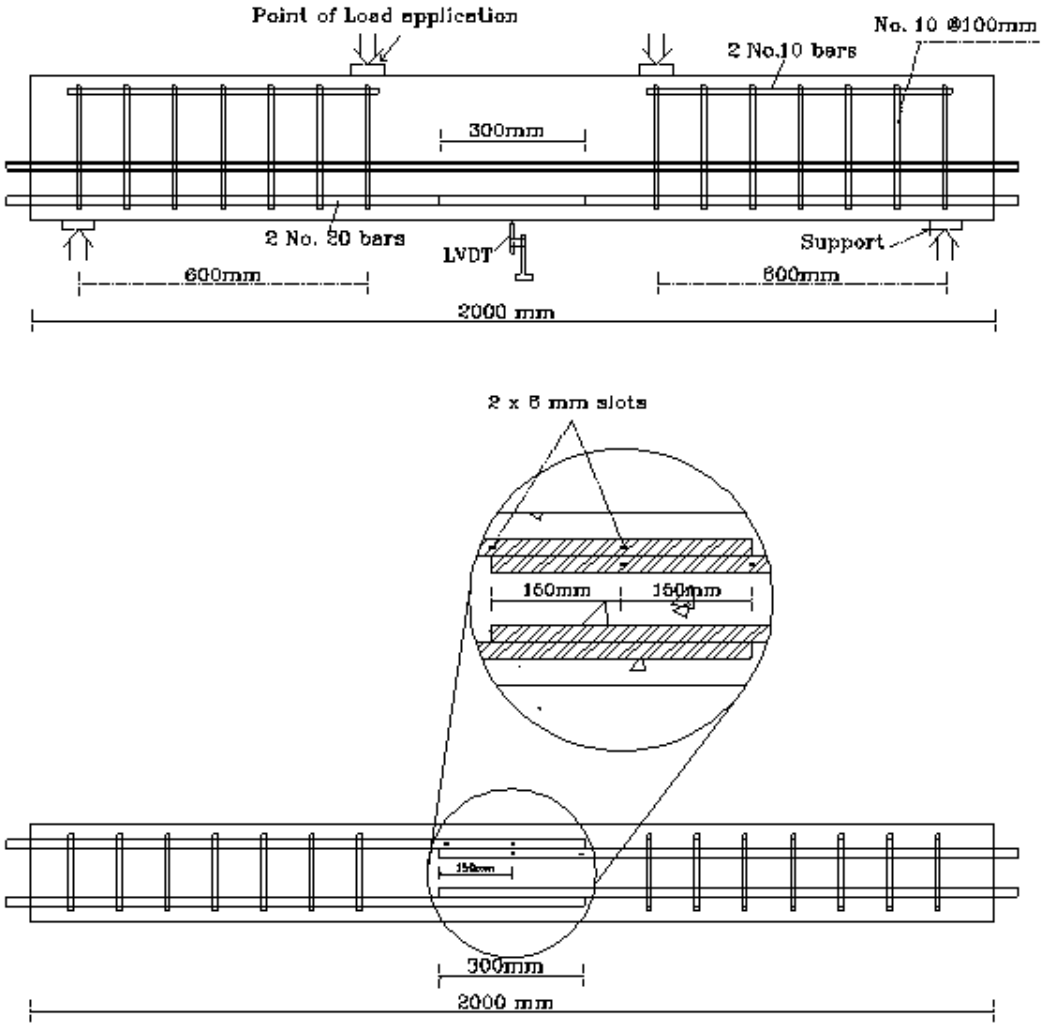

Figure 3-15 Location of the strain gauges on the lap splice

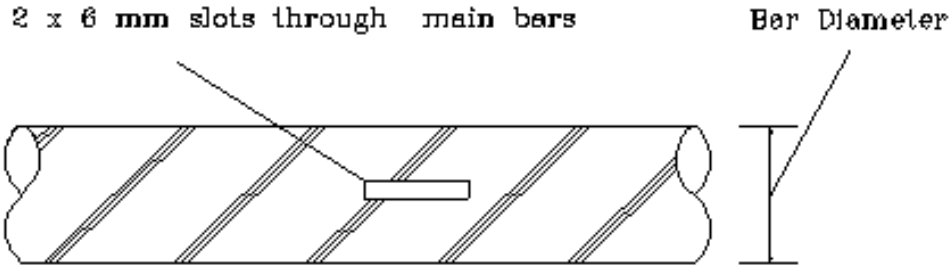

Figure 3-16 2x6 mm slot through the main bars

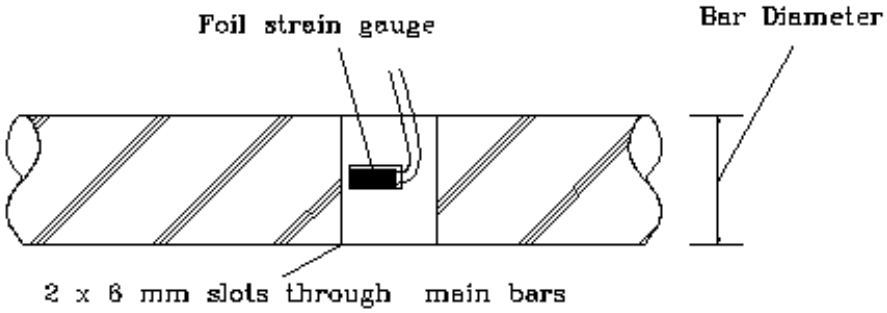

Figure 3-17 Strain gauge installation inside the slot of the reinforcing bar

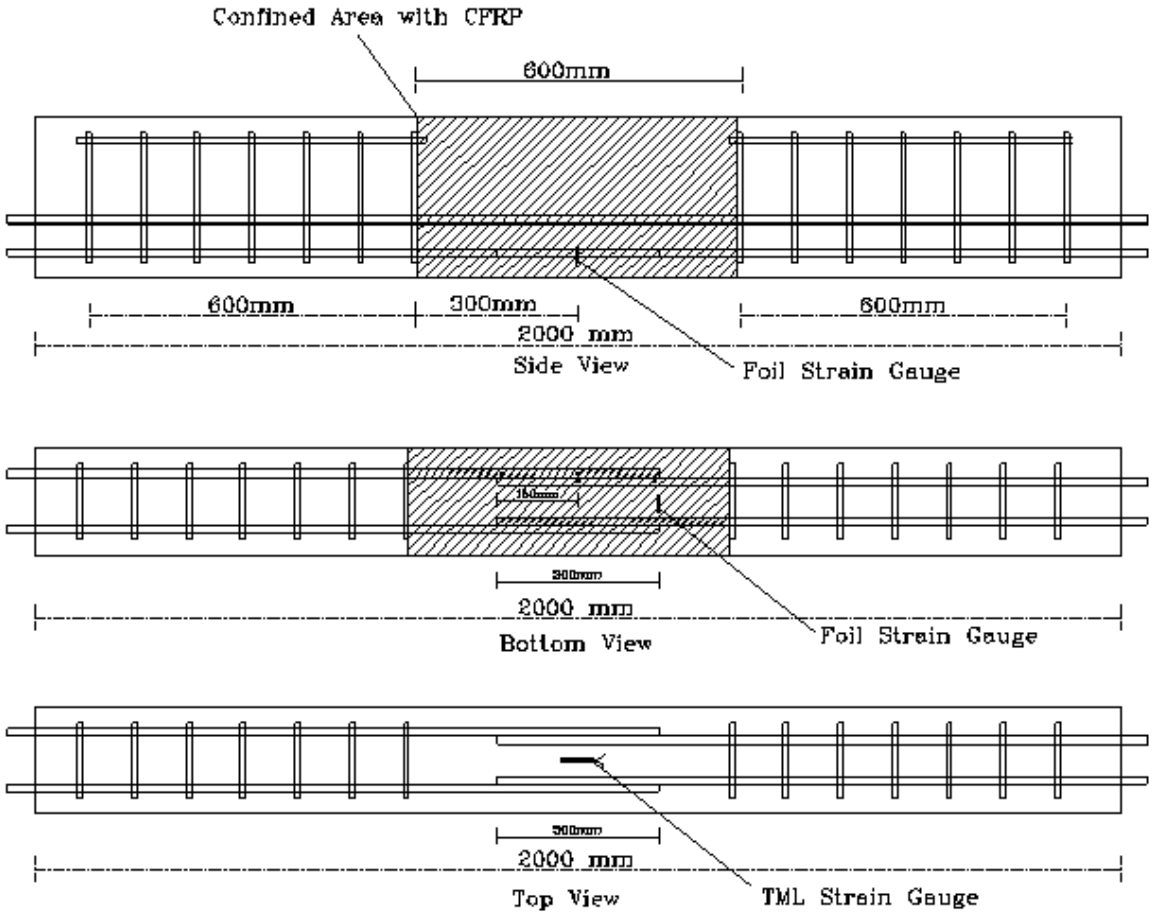

Figure 3-18 Strain gauge locations on the CFRP and the concrete

3.11 Mass loss analysis

ASTM standard G1-90 was followed to determine the mass loss of coupons (150 mm long) extracted from the reinforcing steel bars from the beam following load testing to failure. The reinforcing bars were placed in a bath of diluted hydrochloric acid that was mixed with a buffer solution. Many cleaning cycle were done to get a stable weight measurement of the cleaned corroded bar, then weight and length of the cleaned bars were measured to determine the mass per unit length and compared with the virgin steel rebar. The analysis of the measured mass loss results in comparison to theoretical mass loss was determined based on Faraday's Law and will be presented in Chapter 4.

3.12 Test setup and procedure

All beams were loaded in four-point bending using a servo- hydraulic actuator with a capacity of 332 kN. The loading configuration had a clear span of 1800 mm and a constant moment region 600 mm. The lap-spliced bars placed within constant moment region were subjected only to tension forces using this loading configuration.

The location of the loading points and the supports were marked and grid lines were drawn in the constant moment zone on each beam. Then the beam was placed in the test frame. A linear variable differential transformer (LVDT) with a range of 25 mm was placed at the mid span of the specimen to monitor the mid span deflection. Strain gauges were used to measure the strain on the compression and tension face of the beam. The number and locations of the strain gauges were different for the un- repaired and repaired beams. For the unrepaired beam, one 70 mm strain gauge was placed on the compression face at mid span and no strain gauge was installed on the tension face of the beam. The CFRP repaired beam was instrumented with strain gauges on both the concrete compression face and the CFRP wrap on the tension face. A 70 mm strain gauge was placed at mid span of the specimens on the concrete compression face. Two 30 mm strain gauges aligned with CFRP fibres were bonded onto the CFRP wrap tension face of each beam. One strain gauge was place at the mid of the beam and a second strain gauge was placed at end of the lap splice region. All the instrumentations were zeroed prior to loading. The actuator was controlled by MTS407 controller in stroke control at a displacement rate 0.15 mm/min. All beams were loaded up to failure. Measurements were recorded continuously using SCXI-National instrument data acquisition using LABVIEW software.

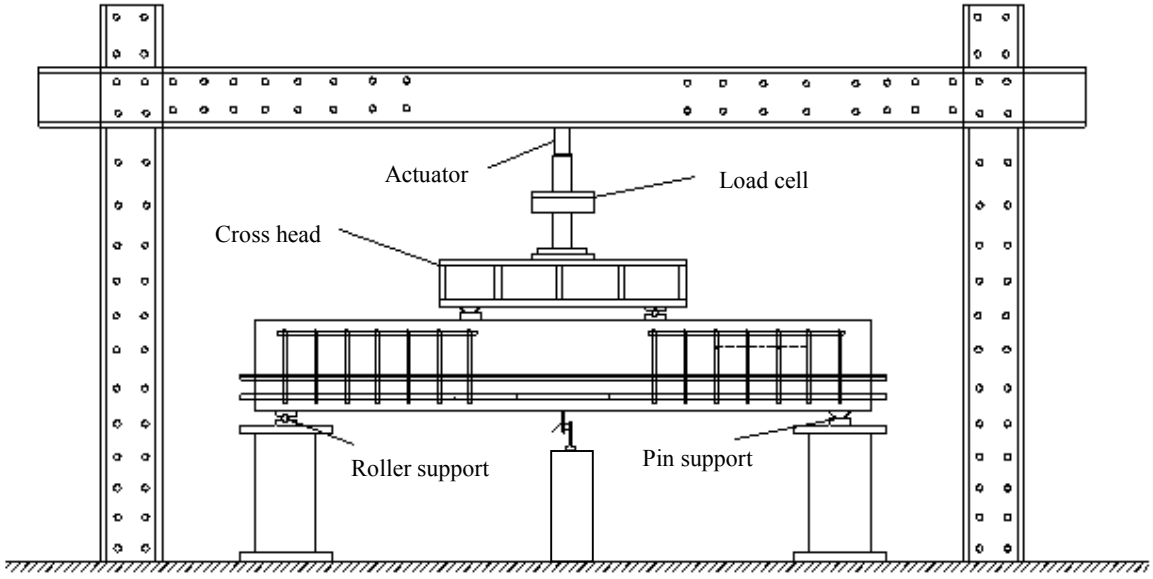

Figure 3-19 Loading test set-up-schematic

Chapter 4

Experimental Results and Discussion

4.1 Introduction

This chapter presents the test results and discussion for the eighteen corroded lap-spliced beams with and without FRP confinement. The test variables were the corrosion level (0%, 2.5%, and 5%), the clear concrete cover to the bar diameter ratio (c/d = 1.5, 2.0, and 2.67), and repair with the fiber reinforced polymer (FRP) sheets. The effect of the variables on the bond strength for lap-spliced beams will be discussed in terms of cracking patterns, mode of failure, load-deflection behavior, beam stiffness, and bond strength. The effect of FRP repair on bond strength the lap-spliced bars in concrete is accounted for by proposing a FRP confinement index ($K_{tr,f}$) in Chapter 5.

4.2 Corrosion cracking

Concrete cracking due to corrosion of the lap splices occurred because the tensile stresses caused by the expansion of the corrosion products exceeded the tensile strength of the concrete. These cracks formed longitudinally along the corroded zone and were parallel to the corroded main reinforcement. Two crack patterns were observed. The first crack pattern consisted of two longitudinal cracks at the soffit of the beam along the corroded region parallel to the main corroded reinforcement. The second pattern consisted of one crack at the bottom of the beam and one crack on the side of the beam. The possible reason for the different cracking pattern is that the corrosion products are not uniformly distributed around the cross section of the bar.

The crack length and width depends on many factors including the concrete strength, the concrete permeability, the concrete cover, and the corrosion level. The maximum crack width differed among the beam series because of the differences in the concrete cover to the bar diameter (c/d) ratio and the level of corrosion. The crack patterns for beams with (c/d) ratios of 1.5, 2.0 and 2.67 are shown in Figures 4.1, 4.2, and 4.3, respectively. Each figure is divided into two parts: (a) shows the crack pattern for 2.5% theoretical corrosion level and the second part (b) shows the crack patterns for 5% theoretical corrosion level. It is evident

from these figures that the corrosion level had a significant effect on the crack width. Beams with (c/d) =1.5 had maximum crack widths of 0.5 mm and 0.8 mm for the 2.5% and 5.0% corrosion level (Figure 4.1). Beams with c/d = 2.0 had a maximum crack widths of 0.4 mm and 0.6 mm for the 2.5% and 5.0% corrosion level (Figure 4.2). Beams with c/d = 2.67, also had maximum crack widths of 0.4 mm and 0.6 mm for the 2.5% and 5.0% corrosion levels (Figure 4.3).

The second parameter affecting the crack width is the concrete cover to the bar diameter (c/d) ratio. Figures 4.1, 4.2, and 4.3 show the differences in crack widths for (c/d) ratios of 1.5, 2.0, and 2.67, respectively. From the figures, it is clear that increasing the bar diameter for a given concrete cover results in higher crack width. For beams with c/d =1.5, the maximum crack width was 0.8 mm and for beams with c/d =2.0, it was 0.6 mm. For a given concrete cover (c = 30 mm), the maximum crack width for beams reinforced with 20M steel bar was greater than that for beams reinforced with 15M bar. Increasing the concrete cover for the same bar diameter decreased the crack width as shown in Figures 4.2a and 4.3a. The maximum crack width for the 30 mm concrete cover was 0.6 mm and for the 40 mm concrete cover was 0.5 mm for bar diameter of 15 mm.

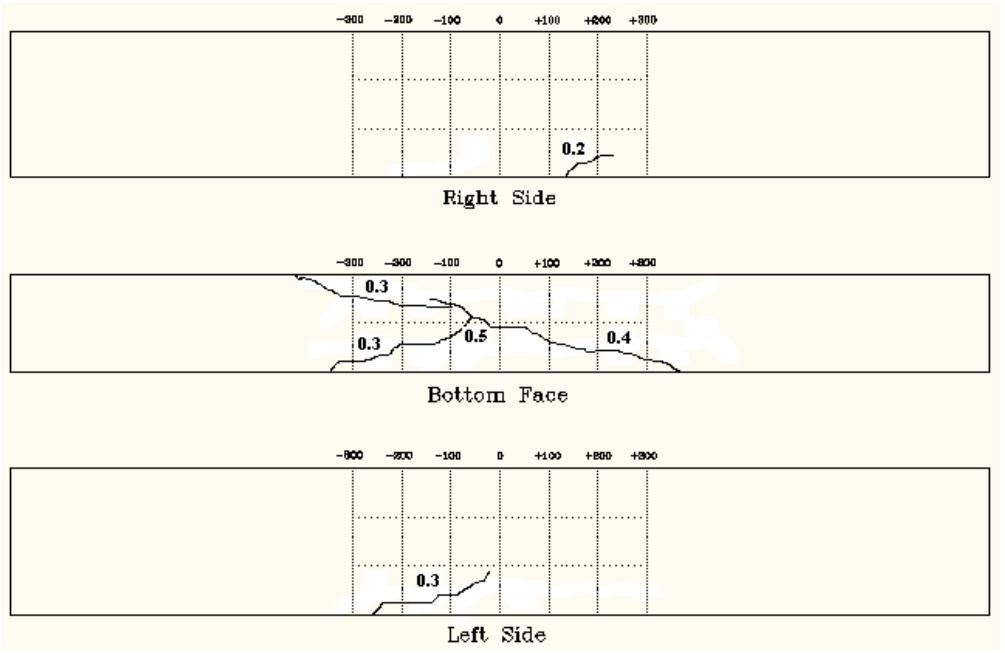

(L-1.5)

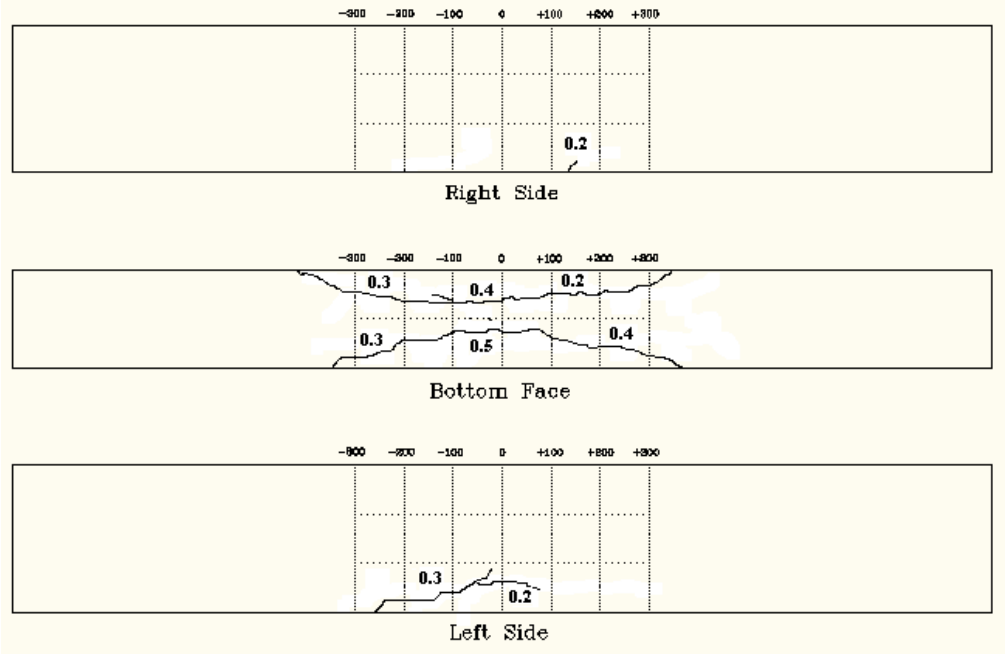

(WL-1.5)

(a) Corrosion level = 2.5%

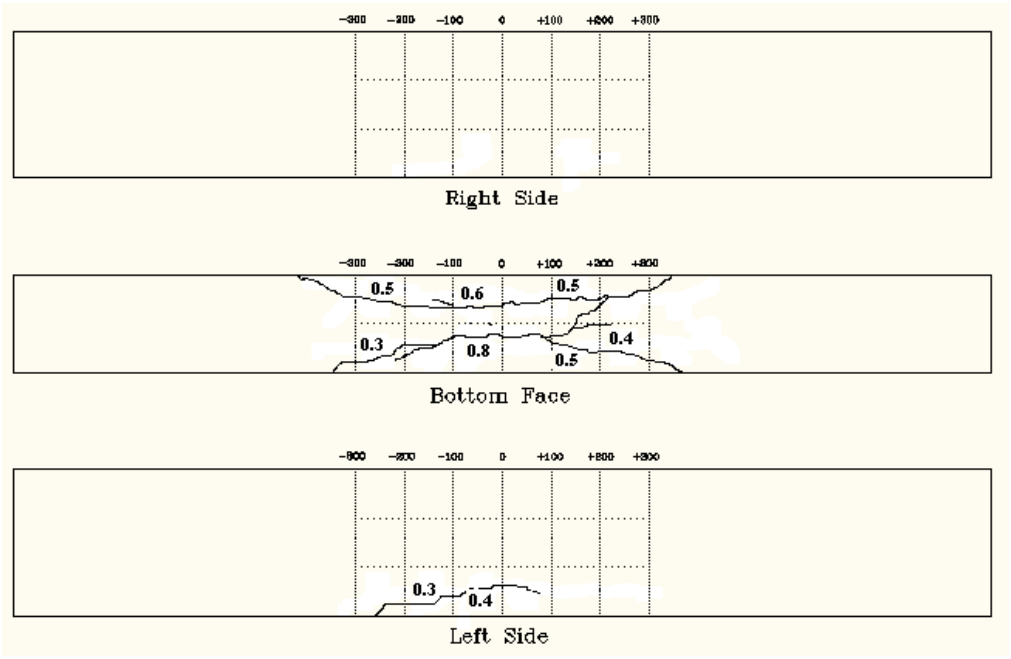

(M-1.5)

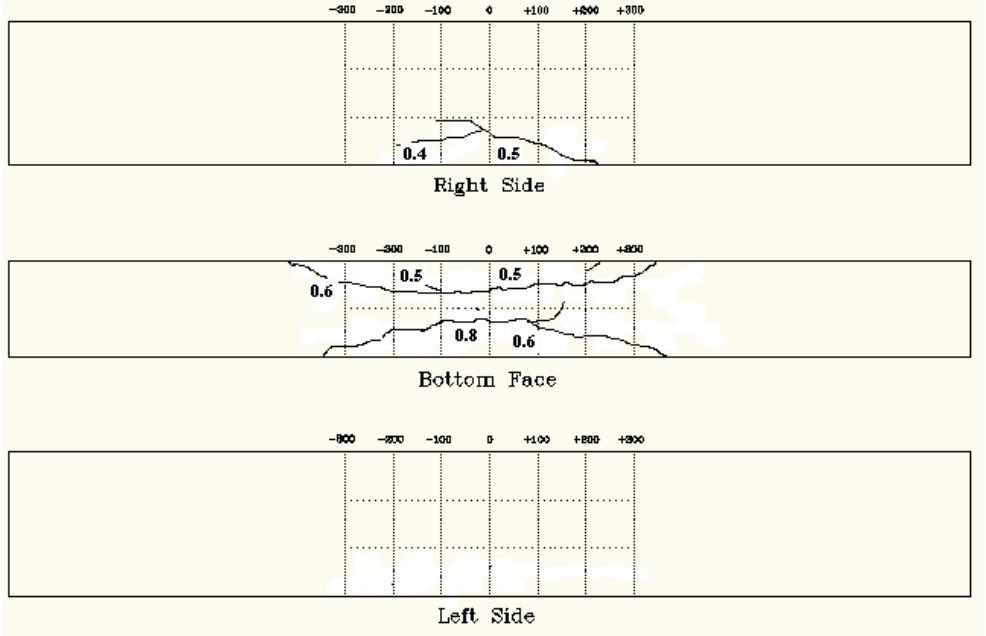

(MW-1.5)

(b) corrosion level =5.0%

Figure 4-1 Crack patterns for beams with (c/d) = 1.5 and

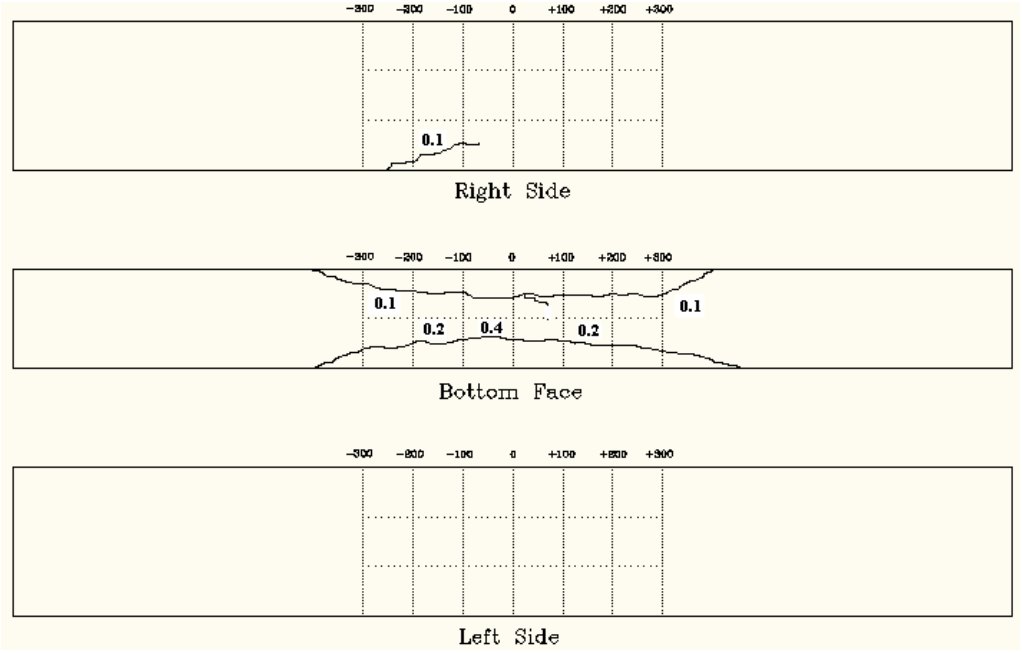

(L-2.0)

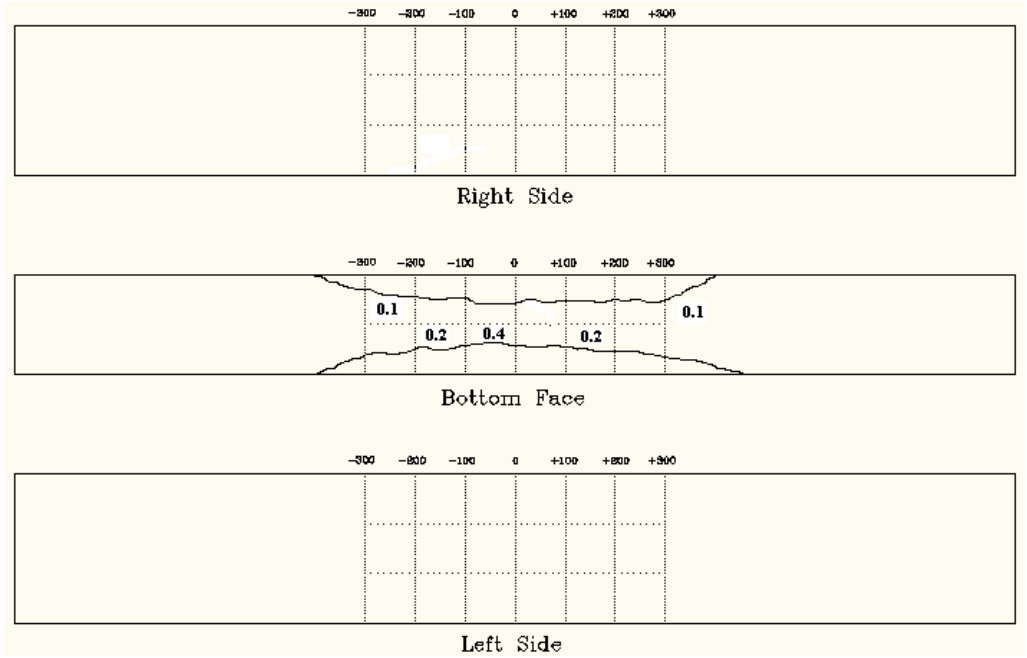

(LW-2.0)

(a) corrosion level = 2.5%

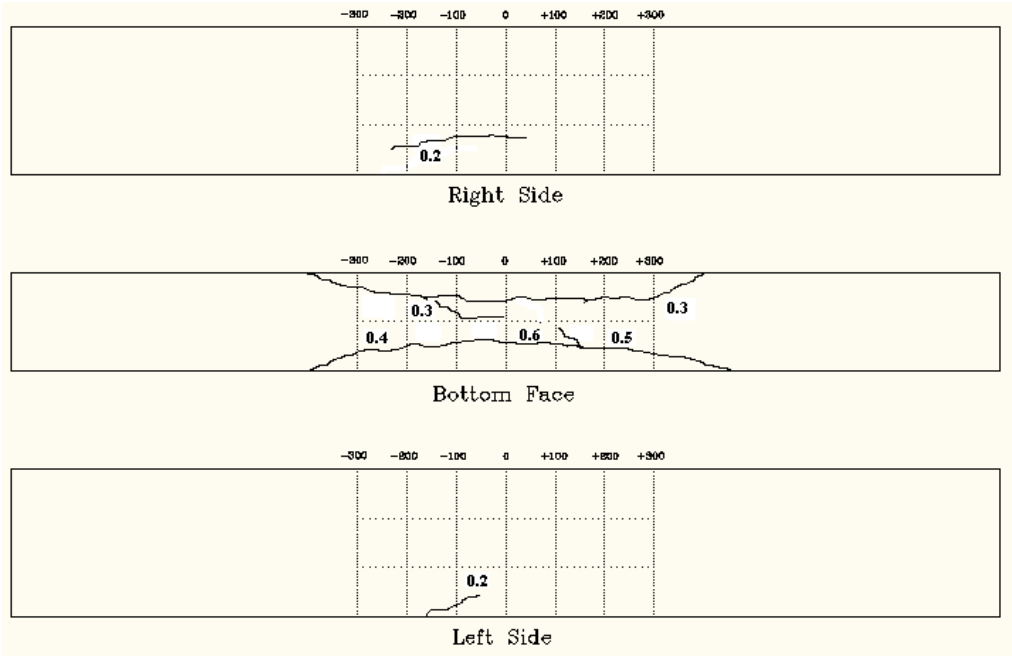

(M-2.0)

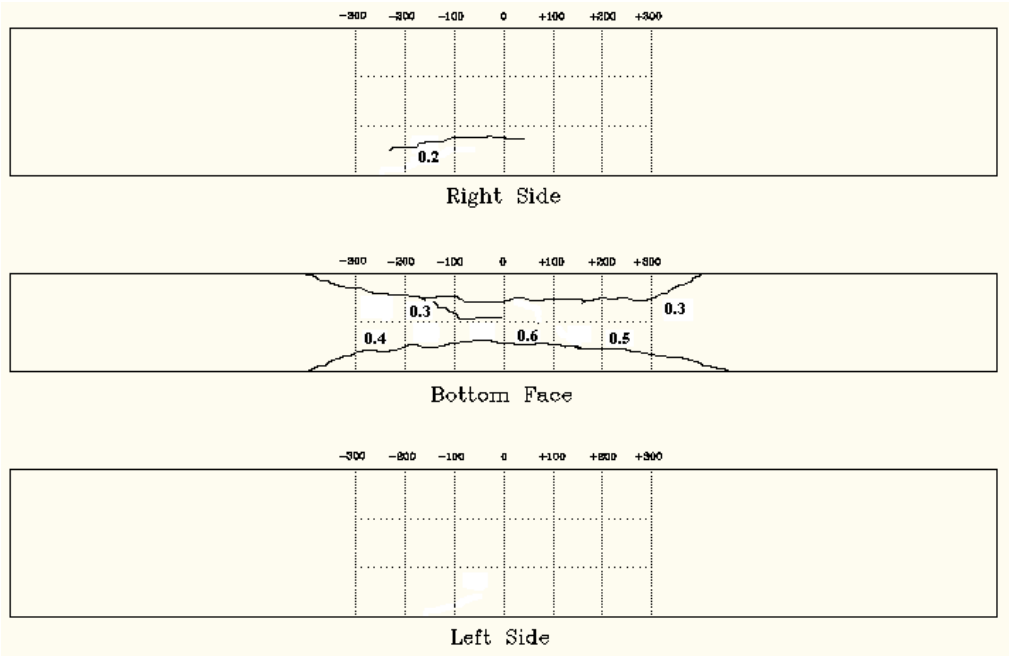

(MW-2.0)

(a) corrosion level =5.0%

Figure 4-2 Crack patterns for beams with (c/d) = 2.0

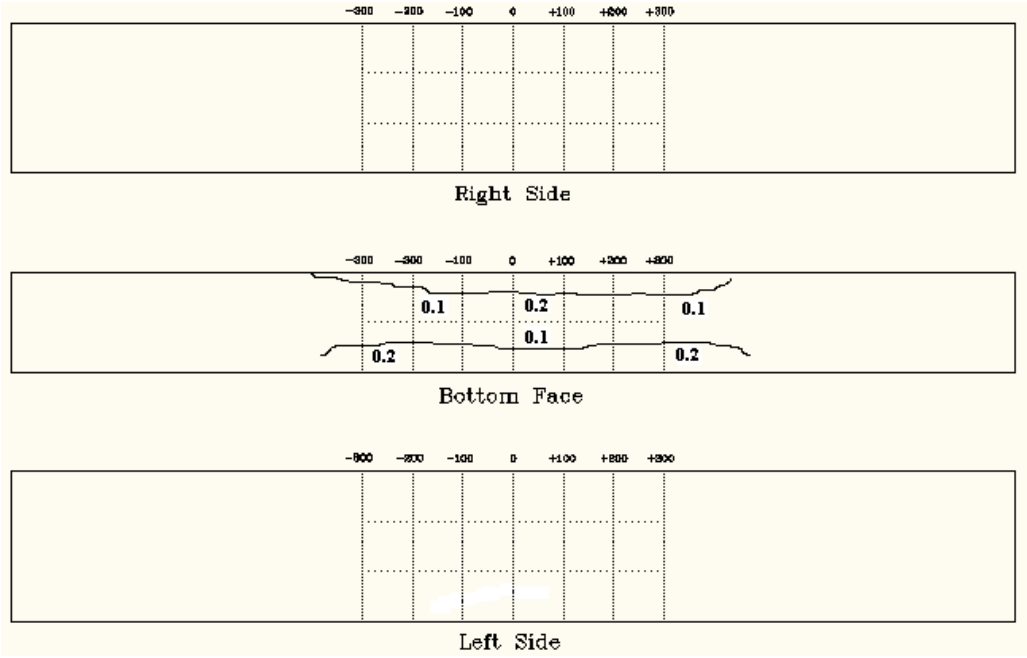

(L-2.67)

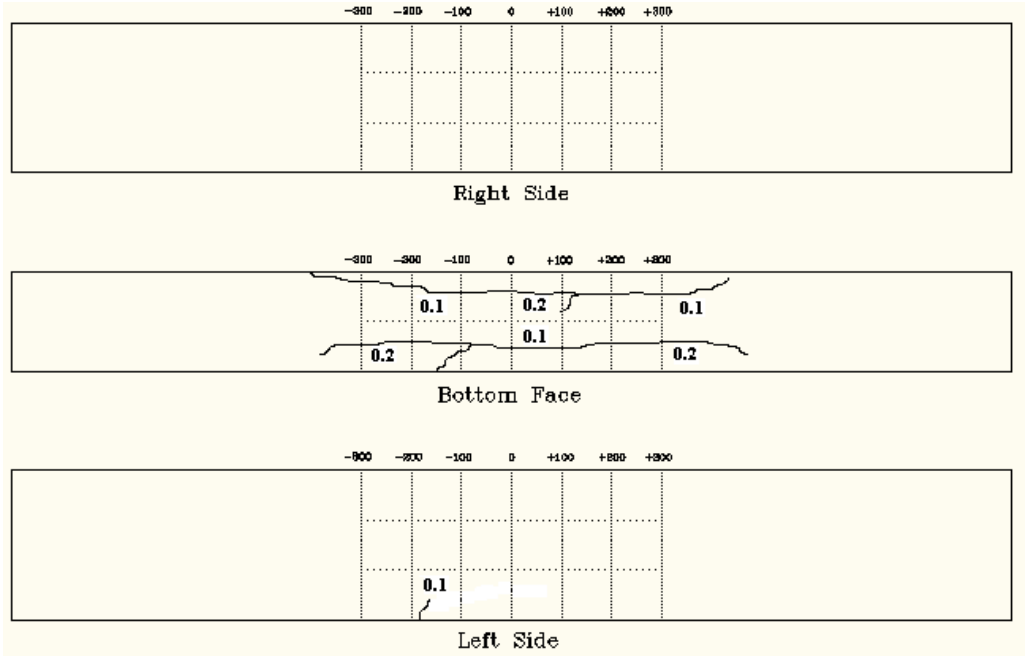

(LW-2.67)

a) corrosion level = 2.5%

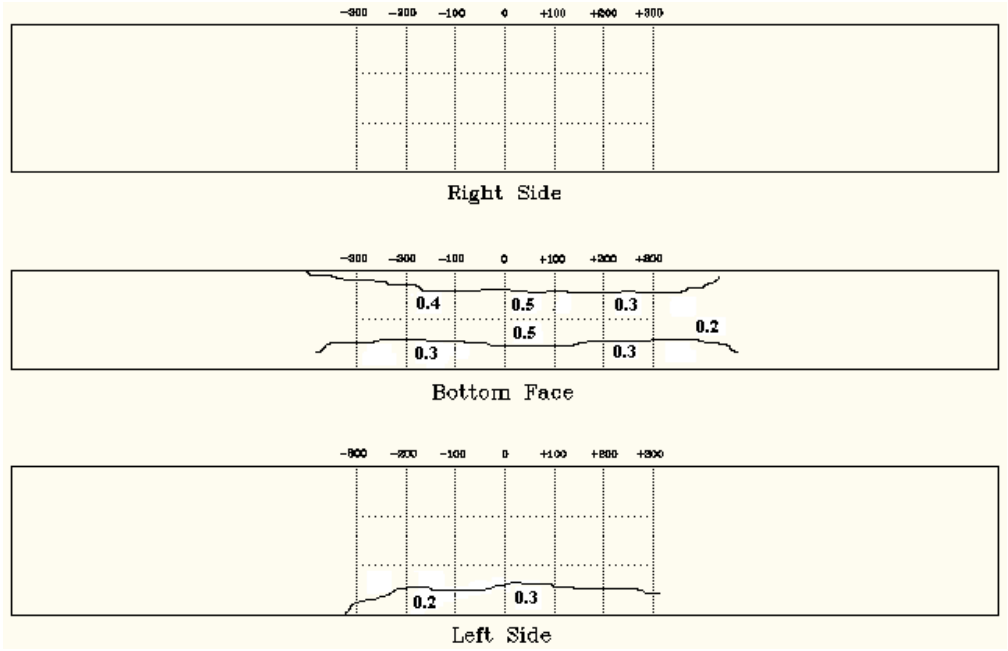

(M-2.67)

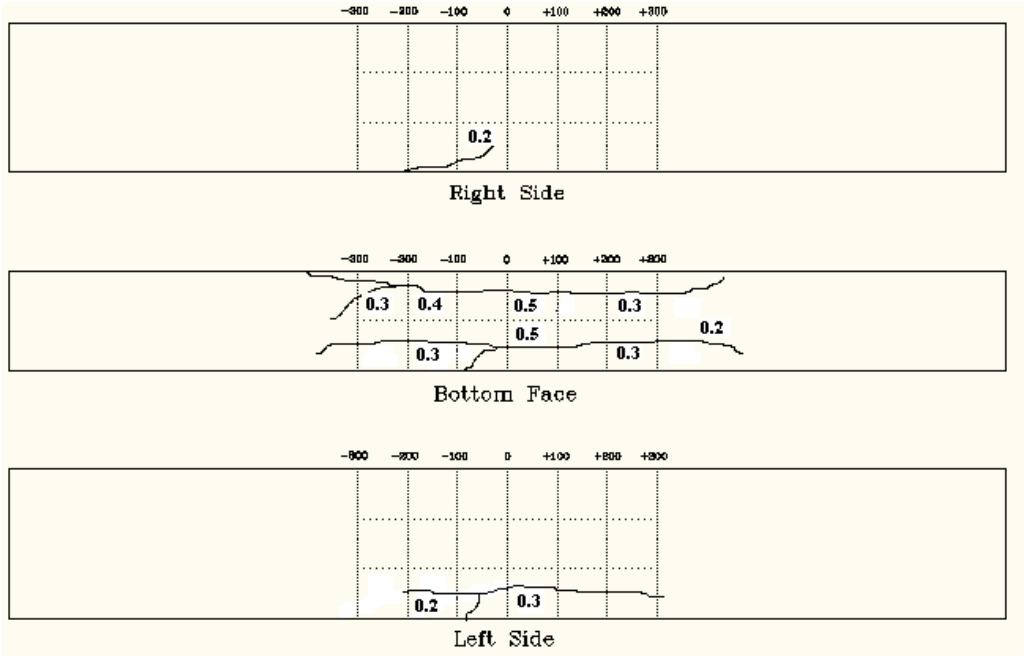

(MW-2.67)

Corrosion level = 5.0%

Figure 4-3 Crack patterns for beams with (c/d) = 2.67

4.3 Mass loss analysis

After load testing the beams to failure, the corroded tension steel bars in the lap-splice were extracted as explained in Chapter 3 to determine the actual mass loss due to corrosion. The mass loss analysis was carried out according to the procedure given in ASTM standard G1-90, designation C.3.5. The average measured mass losses for all the beams were 2.01% and 3.33% for 2.5% and 5% theoretical mass loss, respectively. The difference between the actual and the theoretical mass loss is due to the way the current induced was in the lap-spliced bars. The electrical current was connected to a steel bar at one end of the beam and the current travelled to the second bar through the lap splice. It seems that the electrical connectivity in the lap-splice decreased with higher corrosion level because of the formation of corrosion products on the spliced bars. The theoretical and experimental mass losses along with the attack penetration depth are shown in Table 4.1. Figure 4.4 shows the average mass loss results for beams with different c/d ratios (1.5, 2.0, and 2.67) at all three corrosion levels (2.5%, 5.0% and 7.5%).

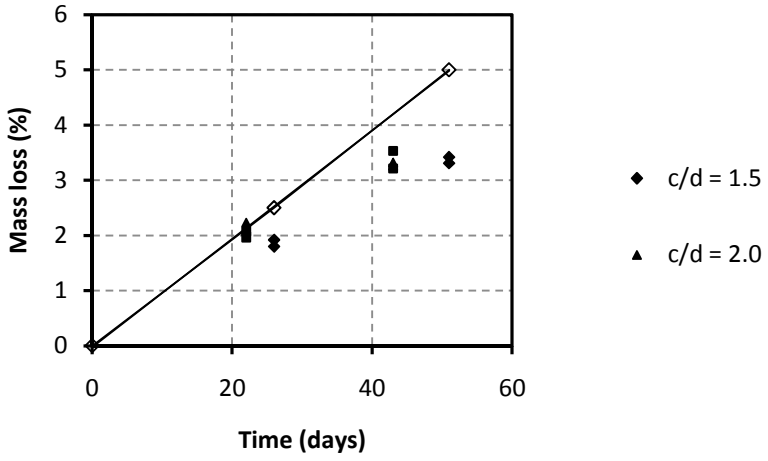

Figures 4-4 Average mass losses vs. time relationship

Table 4-1 Measured corrosion mass loss

Beam designation	Theoretical mass loss (%)	Experimental mass loss (%)	Corrosion attack Penetration depth (mm)
L-1.5	2.5	1.92 ± 0.27	0.39
WL-1.5	2.5	1.80 ± 0.48	0.28
M-1.5	5.0	3.31 ± 0.51	0.38
WM-1.5	5.0	3.42 ± 0.49	0.55
L-2.0	2.5	2.12 ± 0.49	0.62
WL-2.0	2.5	2.23 ± 0.30	0.42
M-2.0	5.0	3.21 ± 0.50	0.76
WM-2.0	5.0	3.53 ± 0.51	0.77
L-2.67	2.5	2.07 ± 0.35	0.59
WL-2.67	2.5	1.96 ± 0.27	0.62
M-2.67	5.0	3.26 ± 0.49	0.72
WM-2.67	5.0	3.32 ± 0.29	0.74

4.4 General behavior of un-wrapped lap-spliced beams

A total of nine lap-spliced beams were tested monotonically in four point bending to failure. The beams were divided into three series based on the concrete cover to bar diameter ratio (c/d). The three series were as follows:(c / d) ratio equal to 1.5 (the clear concrete cover was 30 mm and the bar diameter was 20 mm), (c / d) ratio equal to 2.0 (the clear concrete cover was 30 mm and the bar diameter was 15 mm), and (c / d) ratio equal to 2.67 (the clear concrete cover was 40 mm and the bar diameter was 15 mm). Each series consisted of three beams: one control (0% corrosion level), one corroded to 2.5% (low corrosion level), and one corroded to 5% (medium corrosion level). The longitudinal reinforcement was lap spliced within the constant moment region for a length of 300 mm. The main reinforcement was only corroded within the constant moment region with no corrosion induced in the shear zones. The shear reinforcements (stirrups) were epoxy coated to prevent their corrosion. The strain gauges were installed on the steel bar within the spliced region for beams with c/d =1.5 and c/d = 2.67 while there were not any strain gauges installed on the steel bar for beams with c/d

= 2.0. All un-wrapped beams failed in bond by splitting of the concrete cover surrounding the tension lap-splices. Upon failure by bond splitting, an abrupt loss of the load-carrying capacity accompanied with spalling of the concrete cover occurred.

4.4.1 Lap-spliced beams with (c/d) ratio equal to 1.5

4.4.1.1 Cracking behavior

The first cracks that appeared during load testing were flexural cracks and were located randomly within the constant moment region. As the loading continued, shear, flexural, and splitting cracks developed. Shear cracks were observed only in the shear spans between the loading point and the support. At higher load levels, the crack pattern became complicated around internal discontinuities. Flexural cracks were observed at mid span and at one or both ends of the lap-splice region. Additional flexural and shear cracks formed and the initial cracks at the end of the splice region extended to the compression zone. Splitting cracks were initially observed at the end of splice region on the tension face of the specimen. These splitting cracks originated from flexural cracks and propagated along the spliced bars as loading continued. As the load increased, the crack at the end of the lap-splice propagated to the compression zone and the width of the splitting crack increased until failure. The failure mode of the beams was by splitting of the concrete cover from the side and soffit of the beam in the tension zone. Figures 4.5a and 4.5b show an elevation and bottom view of the control beam (0% corrosion level) at failure. Figures 4.6a and 4.6b show an elevation and bottom view of the corroded beam (2.5% corrosion level) at failure. Figures 4.7a and 4.7b show an elevation and bottom view of the corroded beam (5.0% corrosion level) at failure.

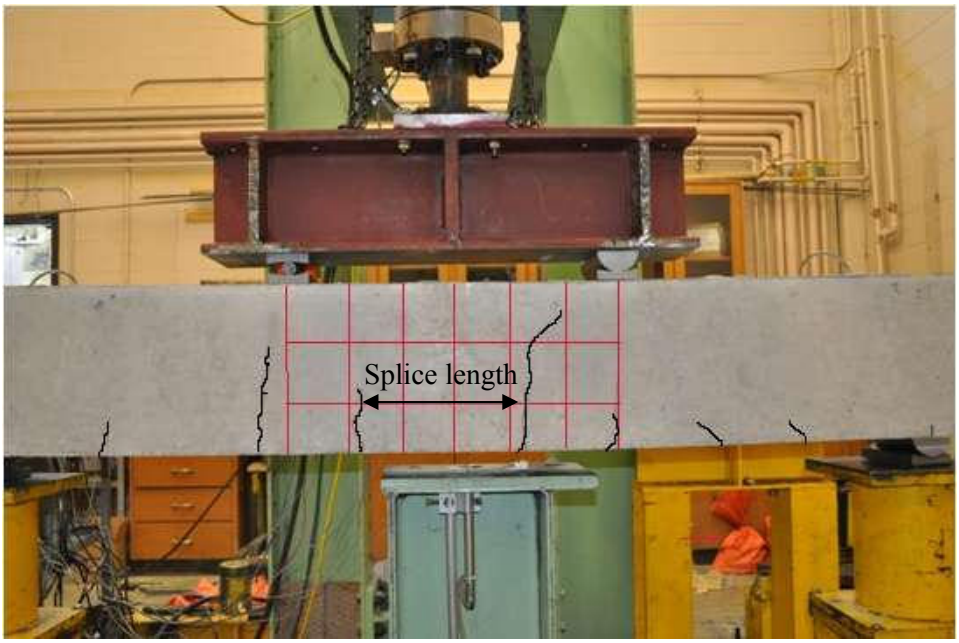

(a) Elevation view

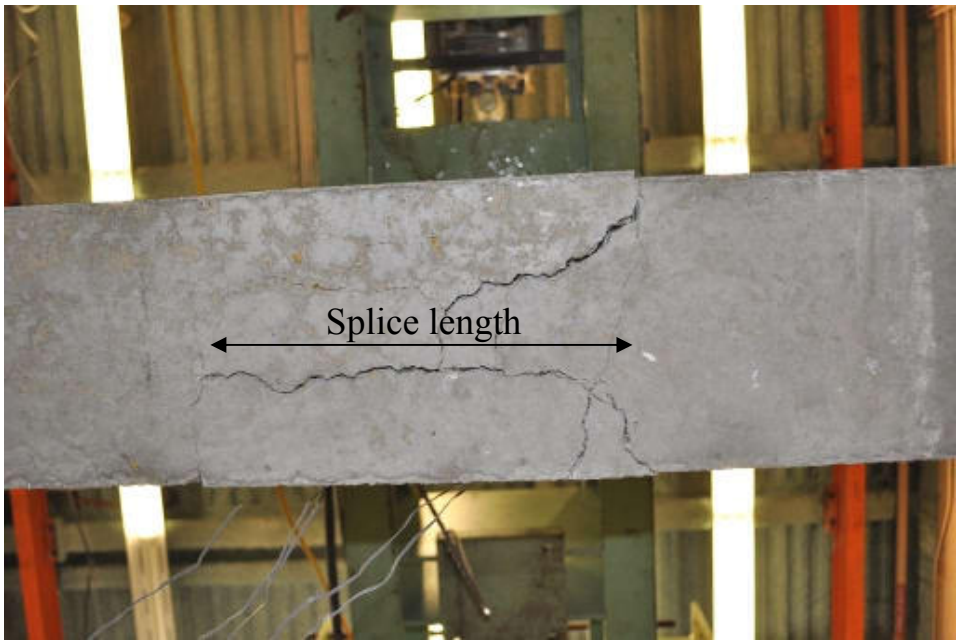

b) Bottom view

Figure 4-5 The failure mode for the control beam (0% corrosion)

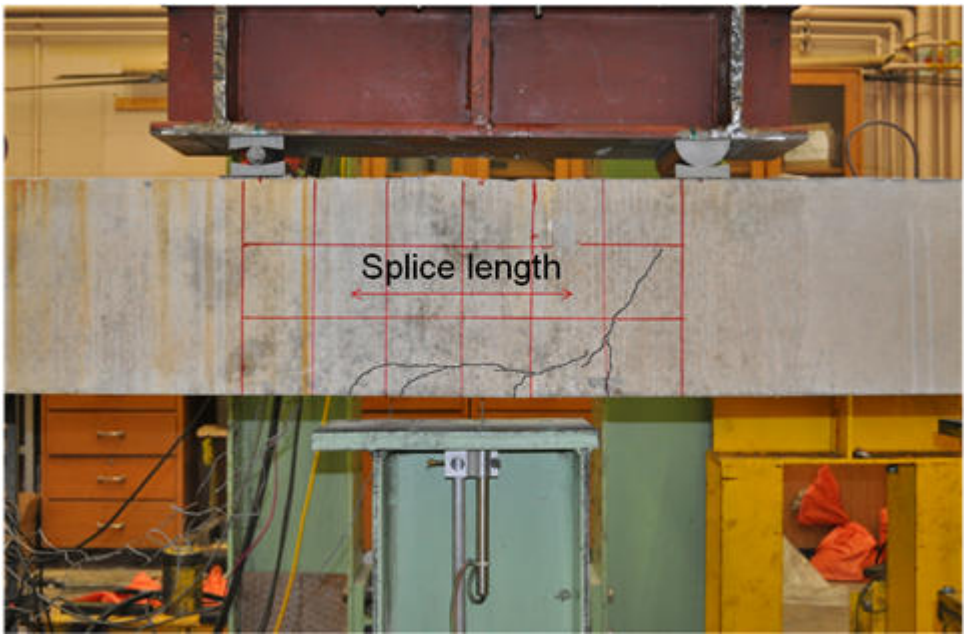

(a) Elevation view

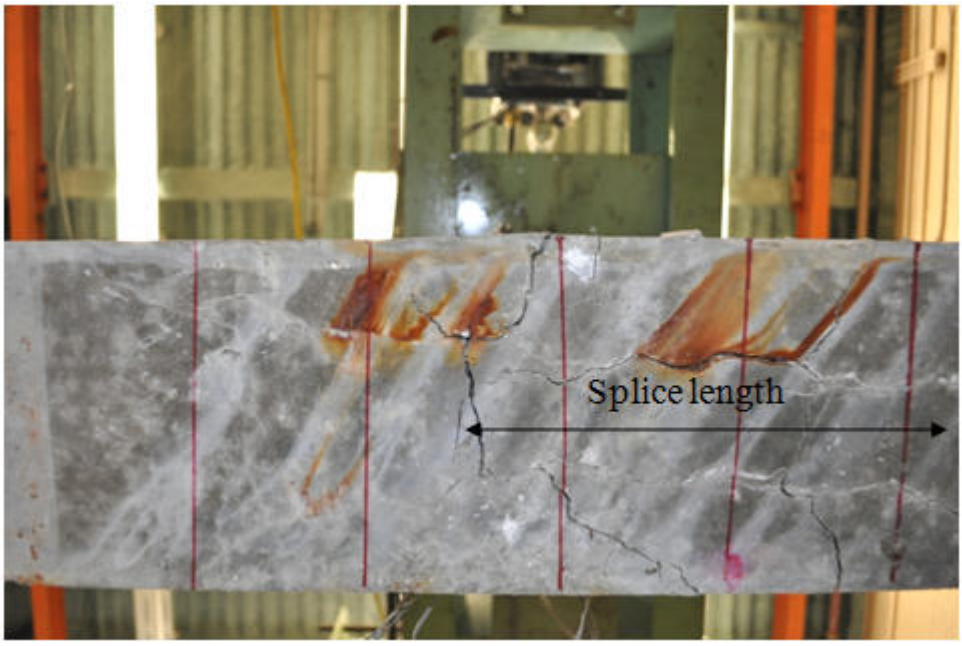

b)Bottom view

Figure 4-6 The failure mode for the corroded beam (2.5% corrosion)

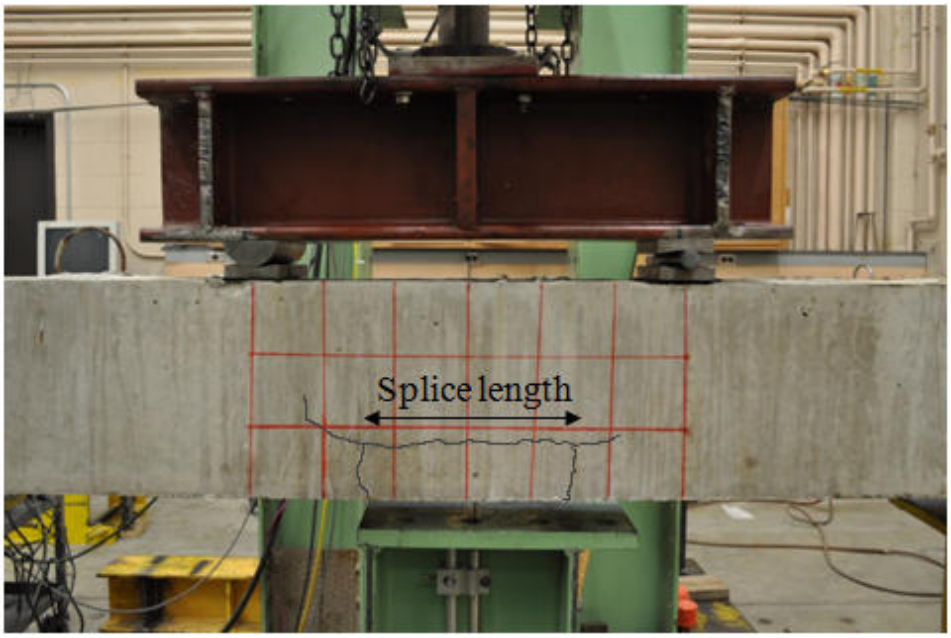

(a) Elevation view

b)Bottom view

Figure 4-7 The failure mode for the corroded beam (5.0% corrosion)

4.4.1.2 Load deflection behavior

The load-deflection curves for beams with (c/d) ratio = 1.5 at different corrosion levels (0%, 2.5%, and 5.0%) are compared as shown in Figure 4.8. The flexural stiffness for the three beams was almost identical regardless of the corrosion level. The cracking load for beams with 0%, 2.5%, and 5.0% corrosion level was 42 kN, 38 kN, and 37 kN, respectively.

Figure 4.8 shows a consistent decrease in the maximum load as the corrosion level increased. The maximum loads for beams with different corrosion levels (0%, 2.5%, and 5%) were 120 kN, 89 kN, and 74 kN, respectively. The maximum predicted flexure failure load was 243 kN. The maximum loads for the beam with low and medium corrosion level (2.5%, and 5.0%) were 26% and 38% lower than that of the control (un-corroded) specimen, respectively. Beyond the maximum load, the load dropped rapidly and the deflection slightly increased as shown in Figure 4.8.

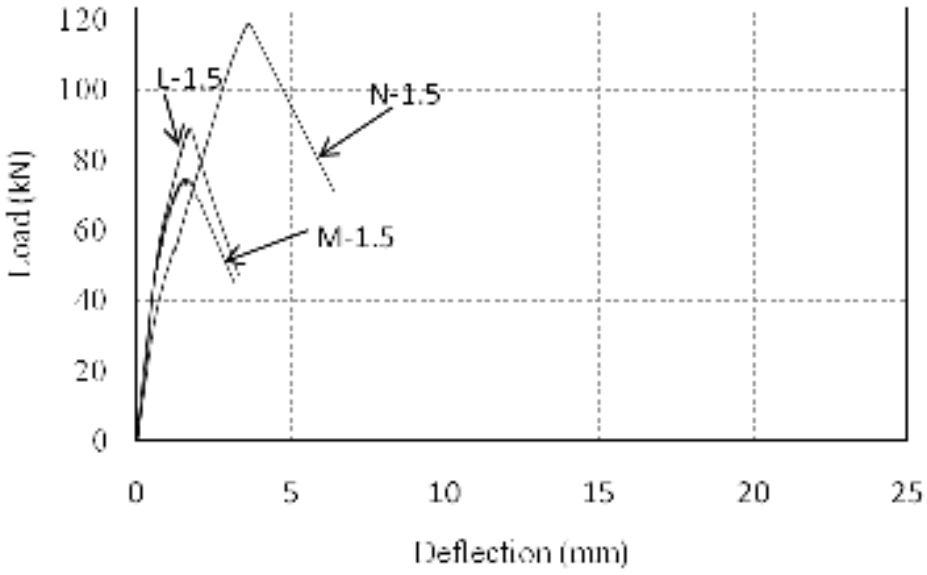

Figure 4-8 Load-deflection curves of beam specimens with (c/d) ratio equal to 1.5

4.4.1.3 Measured strain

Figure 4.9 shows the load- strain response for one bar in Beam N-1.5. As the load increases from zero to 42kN, the concrete is un-cracked and resists all the tensile forces. At 42 kN, the concrete cracks at a steel strain of 267με. Once the crack occurs, all of the tensile forces carried by the concrete at the crack are transmitted to the steel reinforcement. As the load increases from 42 kN to 58 kN, the steel strain increases from 267 με at 42 kN to 985 με at 58 kN. The slip of the main reinforcement due to the splitting cracks occurred at the end of the spliced bars at load levels between 42 kN and 58 kN. As loading continues further, the steel strain increases almost linearly until reaching a peak load of 120 kN with a corresponding steel strain of 2400 με.

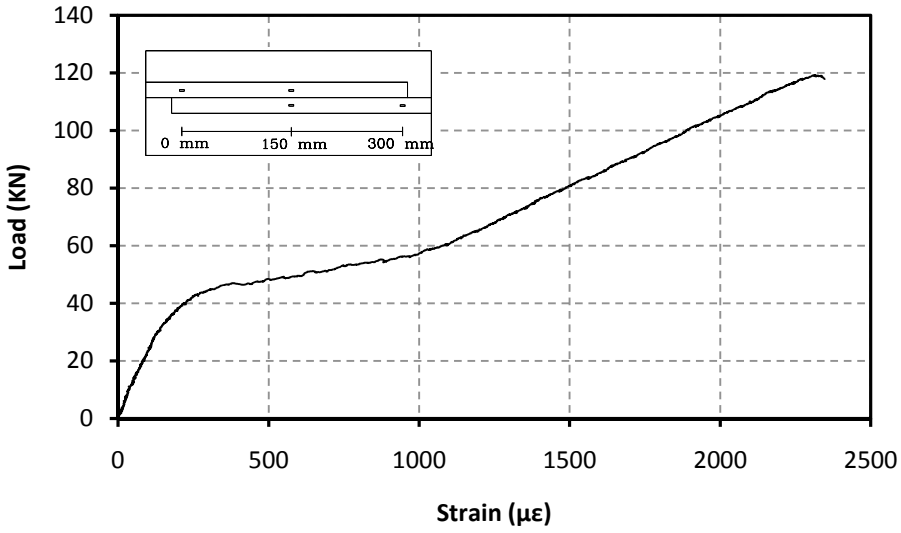

Figure 4-9 Strain response in bar (1) of gauge at (0 mm) distance along the lap splice

The measured strain profile along the lap splice was almost identical for all the beams in this series. Figure 4.10a and 4.10b show typical strain distribution with distance along the lap splice for the two bars in beam N-1.5. The strain gauges on a steel bar were located at the middle and the end of the lap splice. The strain reading increase gradual until the middle of the lap splice and more rapidly between the middle and the loaded end of the lap splice. These results indicate that the maximum strain is concentrated at the loaded end of the spliced steel bars. Beyond a load

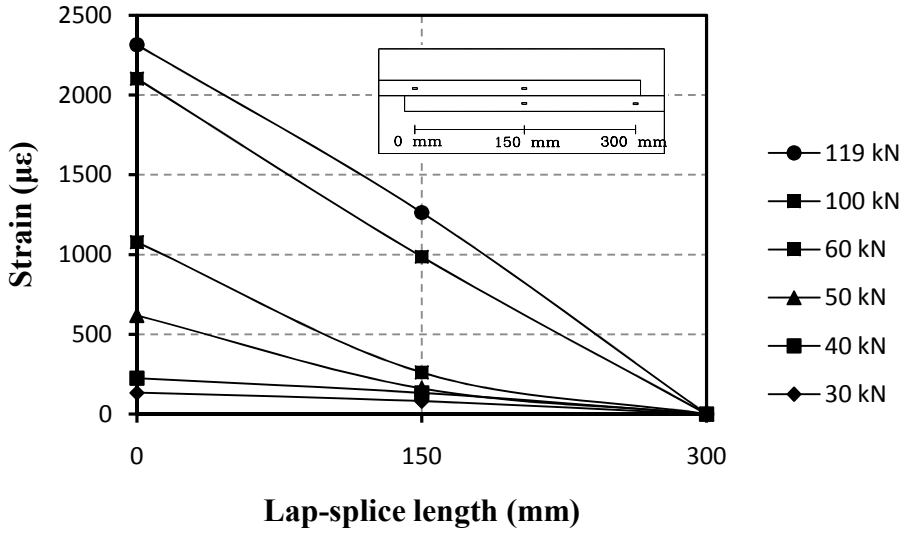

(a) Strain distribution along the first bar of the lap splice

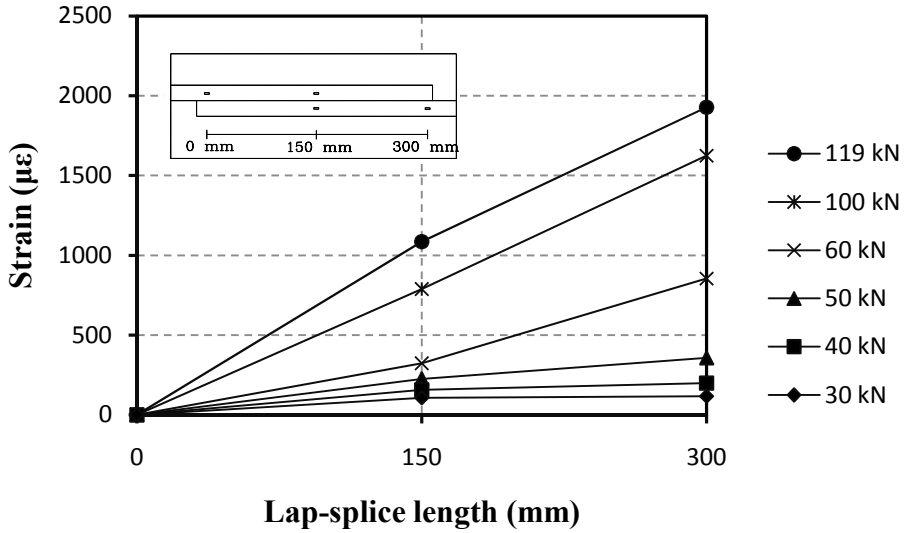

b)Strain distribution along the second bar of the lap splice

Figure 4-10 Strain distribution along the lap splice in beam N-1.5

4.4.2 Lap-spliced beam with (c/d) ratio equal 2.0

4.4.2.1 Cracking behavior

The cracking behavior of the beams with c/d = 2.0 was similar to that of beams with c/d = 1.5. The first cracks that appeared during load testing were flexural cracks within the constant moment region. Shear, flexural, and splitting cracks developed as the loading was increased, Shear cracks were observed in the shear spans between the loading point and the supports. The crack pattern became complicated around internal discontinuities. Flexural cracks were observed at mid span and at one or both ends of the lap-splice region. Additional flexural and shear cracks formed and the initial cracks at the end of the splice region extended to the compression zone as loading continued. Splitting cracks were initially observed at the end of splice region on the tension face of the specimen. These splitting cracks originated from flexural cracks and propagated along the spliced bars. As the load increased, the crack at the end of the lap-splice propagated to the compression zone and the width of the splitting crack increased until failure. The failure mode of beams was by was splitting of the concrete cover from the side and soffit of the beam in the tension zone. Figures 4.11a and 4.11b show an elevation and bottom view of the control beam (0% corrosion level) at failure. Figures 4.12a and 4.12b show an elevation and bottom view of the corroded beam (2.5% corrosion level) at failure. Figures 4.13a and 4.13b show an elevation and bottom view of the corroded beam (5.0% corrosion level) at failure.

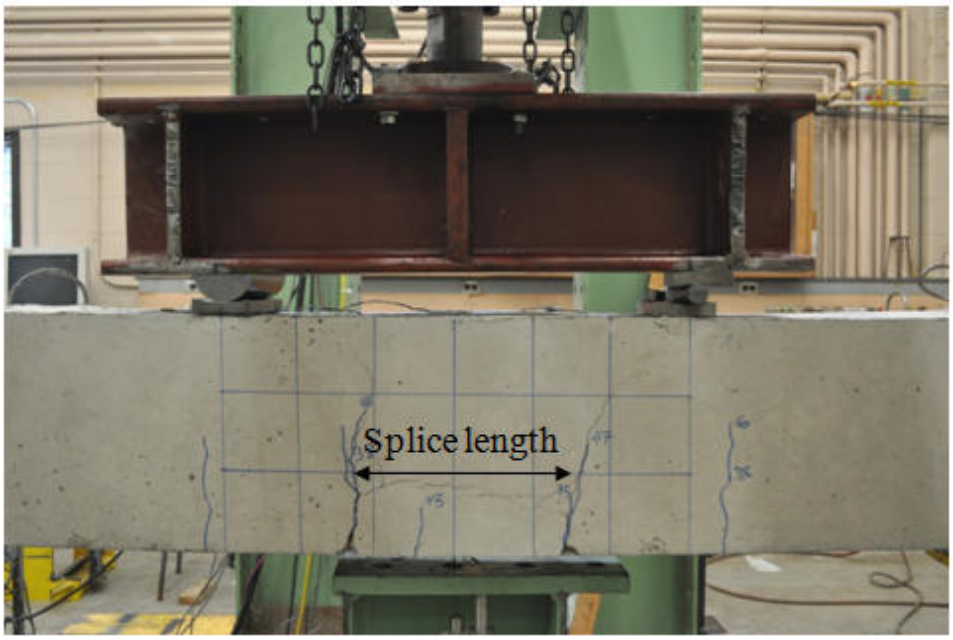

a) Elevation view

b) Bottom view

Figure 4-11 The splitting crack of the control beam (0%) at failure

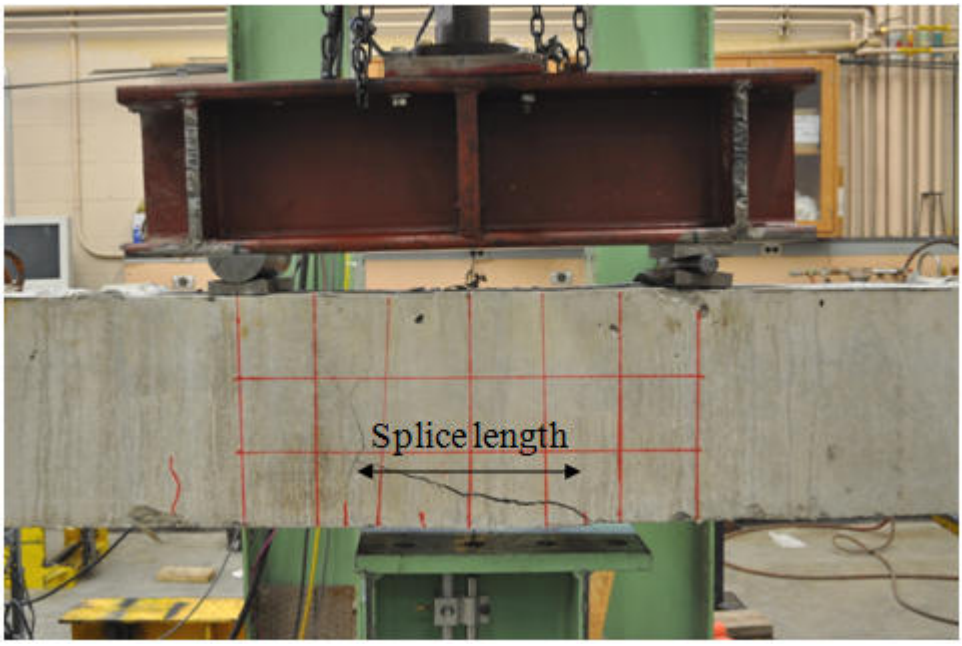

a) Elevation view

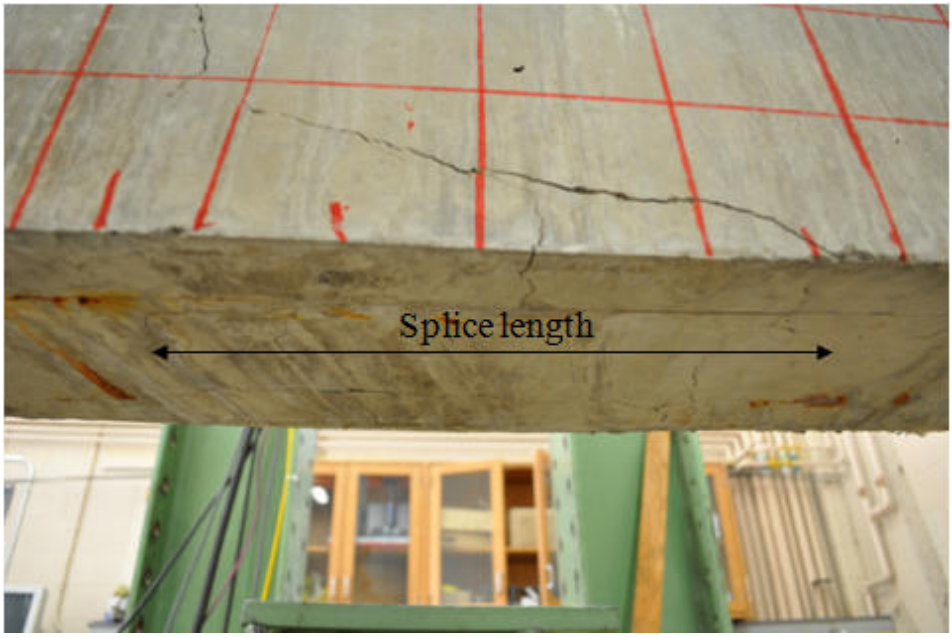

b) Bottom view

Figure 4-12 The splitting crack of the corroded beam (2.5%) at failure

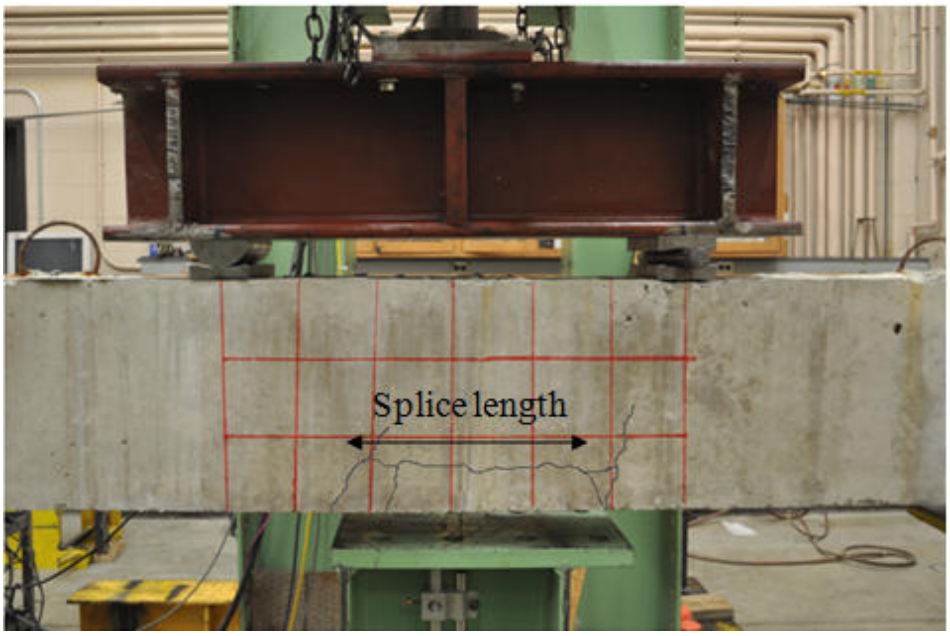

a) Elevation view

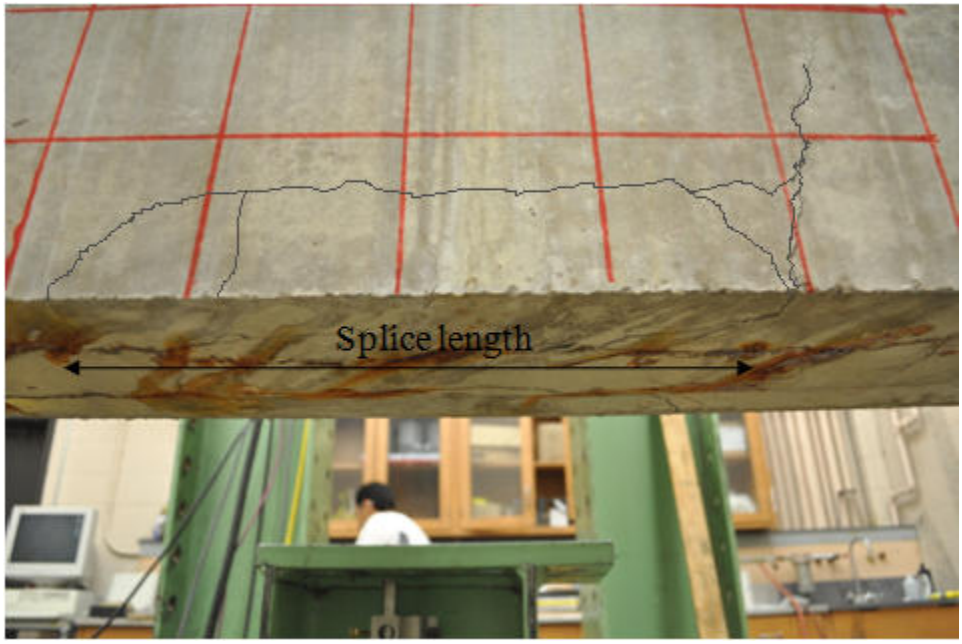

b) Bottom view

Figure 4-13 The splitting crack of the corroded beam (5.0%) at failure

4.4.2.2 Load deflection behavior

The load-deflection curves for beams with (c/d) ratio = 2.0 at different corrosion levels (0%, 2.5%, and 5.0%) are compared as shown in Figure 4.14. The flexural stiffness for the three beams was almost identical regardless of the corrosion level (0%, 2.5%, and 5.0%). The cracking load for beam with 0%, 2.5%, and 5.0% corrosion level was 56 kN, 50 kN, and 45 kN, respectively.

Figure 4.14 shows a consistent decrease in the maximum load as the corrosion level increased. The maximum loads for beams with different corrosion levels (0%, 2.5%, and 5%) were 103 kN, 82 kN, and 63 kN, respectively. The maximum predicted flexure failure load was 167 kN. The maximum loads for the beam with low and medium corrosion level (2.5%, and 5.0%) were 21% and 39% than that of the control (un-corroded) specimen, respectively. Beyond the maximum load, the load dropped rapidly and the deflection slightly increased as shown in Figure 4.14.

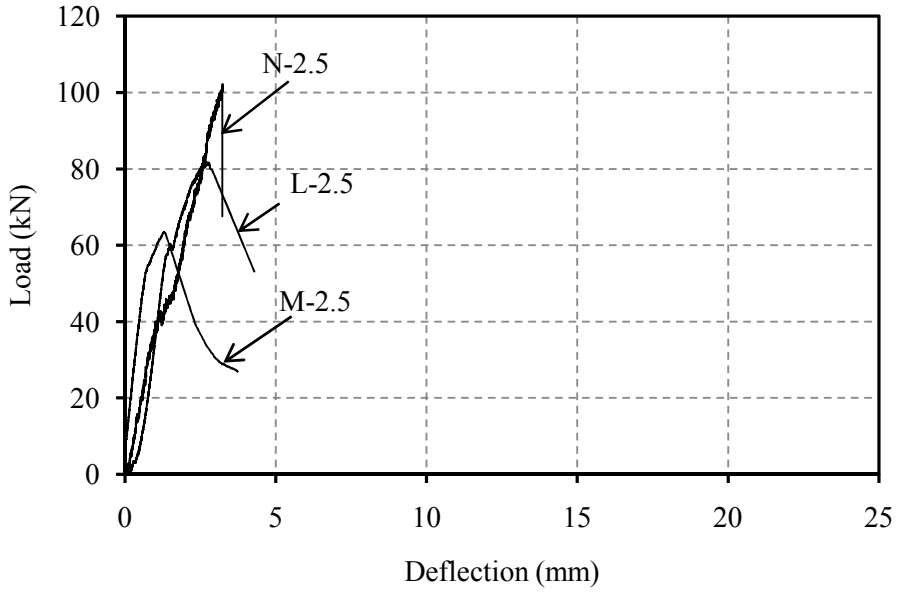

Figure 4-14 Load-deflection curves of beam specimens with (c/d) ratio equal to 1.5

4.4.3 Lap spliced beams with (c/d) ratio equal 2.67

4.4.3.1 Cracking behavior

The cracking behavior of the beams with c/d = 2.67 was similar to that of beams with c/d = 1.5 and 2.0. The first cracks that appeared during load testing were flexural cracks within the constant moment region. As the loading continued, shear, flexural, and splitting cracks developed. Shear cracks were observed only in the shear spans between the loading point and the support. The crack pattern became complicated around internal discontinuities. Flexural cracks were observed at mid span and at one or both ends of the lap-splice region. Additional flexural and shear cracks formed and the initial cracks at the end of the splice region extended to the compression zone as loading continued. Splitting cracks were initially observed at the end of splice region on the tension face of the specimen. These splitting cracks originated from flexural cracks and propagated along the spliced bar. As the load increased, the crack at the end of the lap-splice propagated to the compression zone and the width of the splitting crack increased until failure. The failure mode of beams was by was splitting of the concrete cover from the side and soffit of the beam in the tension zone. Figures 4.15a and 4.15b show an elevation and bottom view of the control beam (0% corrosion level) at failure. Figures 4.16a and 4.16b show an elevation and bottom view of the corroded beam (2.5% corrosion level) at failure. Figures 4.17a and 4.17b show an elevation and bottom view of the corroded beam (5.0% corrosion level) at failure.

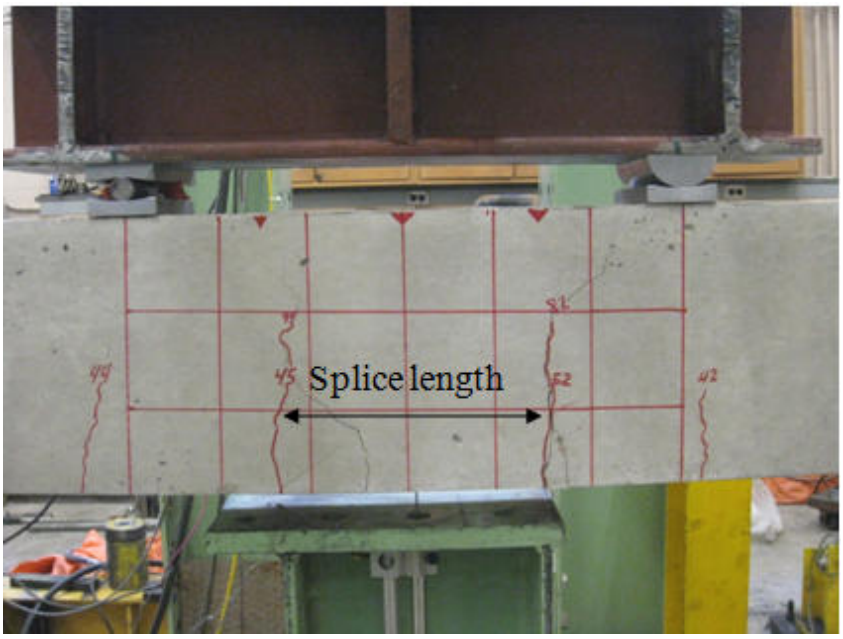

a) Elevation view

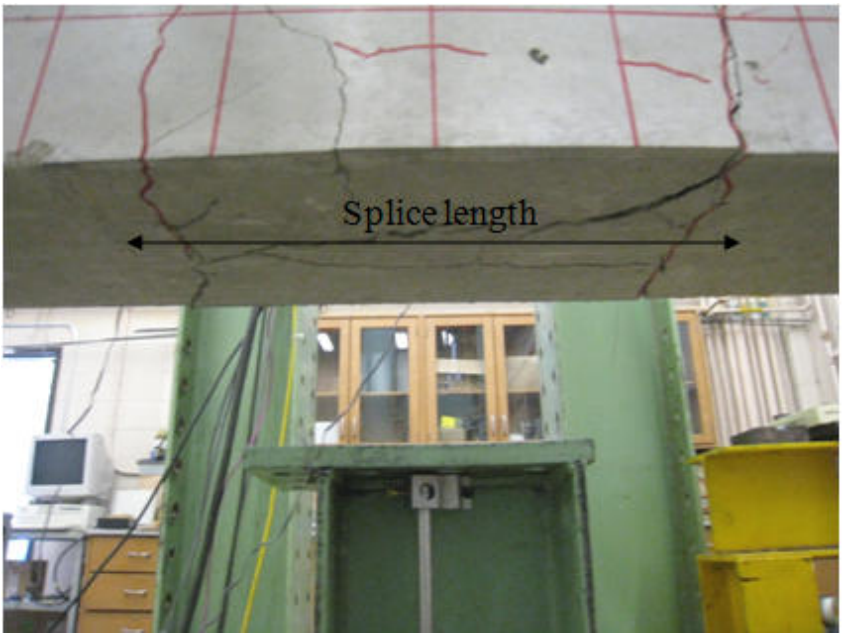

b) Bottom view

Figure 4-15 The splitting crack of the control beam (0%) at failure

a) Elevation view

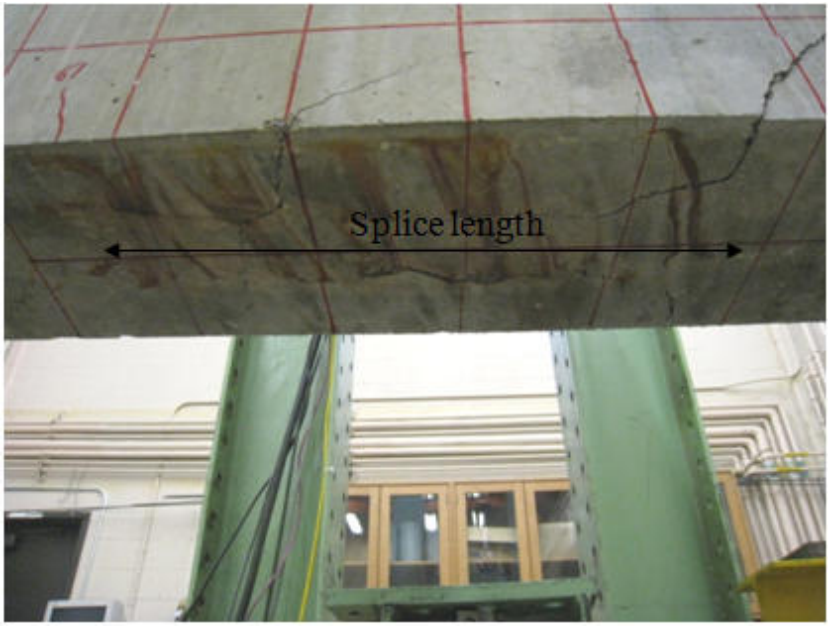

b) Bottom view

Figure 4-16 The splitting crack of the corroded beam (2.5%) at failure

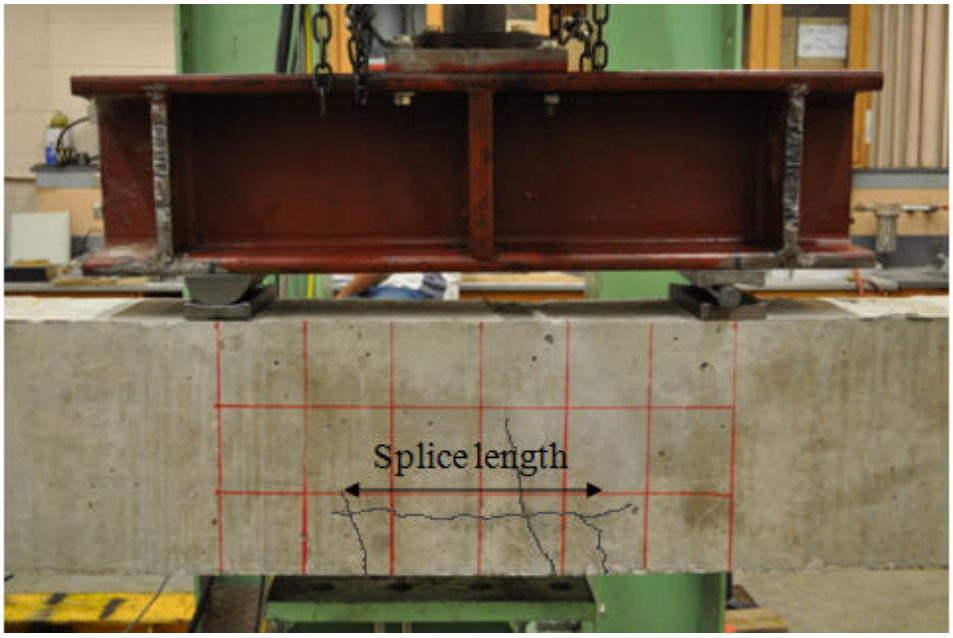

a) Elevation view

b) Bottom view

Figure 4-17 The splitting crack of the corroded beam (5.0%) at failure

4.4.3.2 Load deflection behavior

The load-deflection curves for beams with (c/d) ratio = 2.67 at different corrosion levels (0%, 2.5%, 5.0%) are compared as shown in Figure 4.18. The flexural stiffness for the three beams was almost identical regardless of the corrosion level. The cracking load for beam with 0%, 2.5%, and 5.0% corrosion level was 42 kN, 41 kN, and 38 kN, respectively.

Figure 4.18 shows a consistent decrease in the maximum load as the corrosion level increased. The maximum loads for beams with different corrosion levels (0%, 2.5%, and 5%) were 104 kN, 92 kN, and 81 kN, respectively. The maximum predicted flexure failure was 161 kN. The maximum loads for the beam with low and medium corrosion level (2.5%, and 5.0%) were 12% and 22% lower than that of the control (un-corroded) specimen, respectively. Beyond the maximum load, the load dropped rapidly and the deflection slightly increased as shown in Figure 4.18.

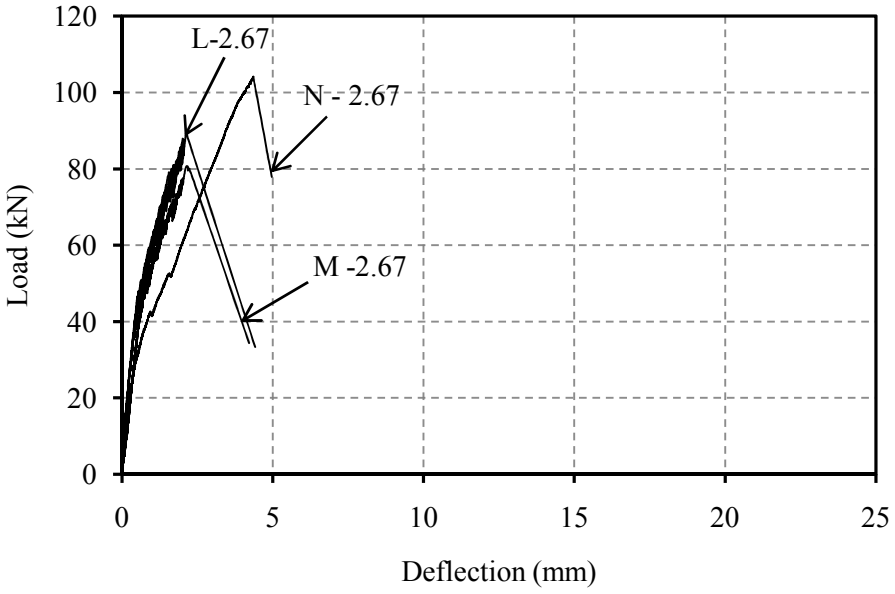

Figure 4-18 Load-deflection curves of beam specimens with (c/d) equal 2.67

4.4.3.3 Measured strain

Figure 4.19 shows the load- strain response for one bar in beam N-2.67. As the load increases from zero to 43kN, the concrete is un cracked and resists tensile forces. The concrete cracks at a load of 43 kN and steel strain of 277με. Once the crack occurs, all the tensile forces carried by the concrete at the crack are transferred to the steel bar. As the load increase from 43 kN to 56 kN, the steel strain increases from 277 με to 974 με. The slip of the main reinforcement due to the splitting cracks occurred at the end of the spliced bars at load levels between 43 kN and 56 kN. As loading continues further, the steel strain increases almost linearly until reaching a peak load of 104 kN with a corresponding steel strain of 2556 με.

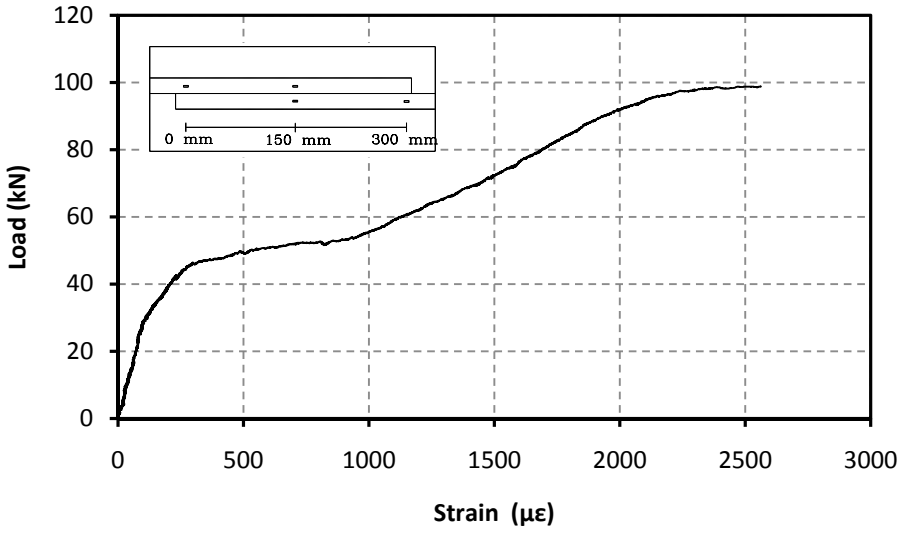

Figure 4-19 Strain response in bar (1) at 0 mm distance along the lap splice

The measured strain profile along the lap splice was almost identical for all the beams in this series. Figure 4.20a and 4.20b show typical strain distribution with distance along the lap splice for the two bars in beam N-2.67. The strain gauges on a steel bar were located at the middle and the end of the lap splice and more rapidly between the middle and the loaded end of the lap splice. These results indicate that the maximum strain is concentrated at the loaded end of the spliced steel bars. Beyond a load level of 60 kN, the strain distribution was linear between the free end and loaded end of the lap splice. In all cases, the strain in the splice was lower than the yield strain of the steel bars.

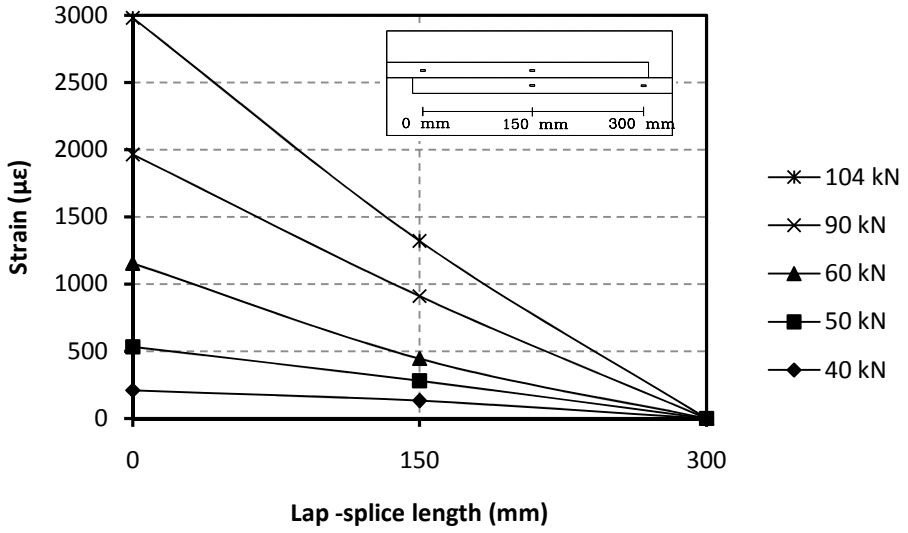

a) Strain distribution along the first bar of the lap splice

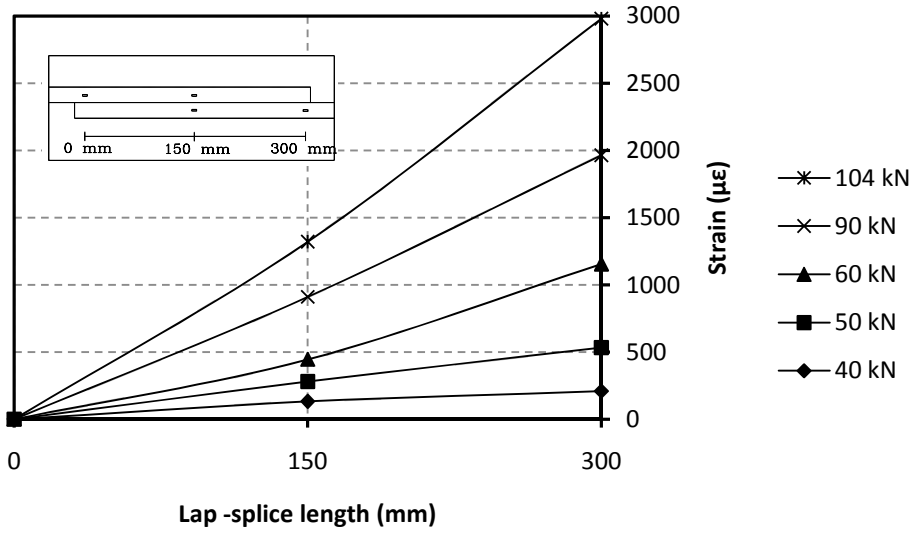

b) Strain distribution along the first bar of the lap splice

Figure 4-20 Strain distribution along the lap splice in beam N-2.67

4.5 General behavior of wrapped lap-spliced beams

A total of nine lap-spliced beams wrapped with CFRP sheets were tested monotonically in four point bending to failure. Similar to the un-wrapped beams, the wrapped beams were divided into three series based on their concrete cover to the diameter (c/d) ratio as follow: (c/d) ratio equal to 1.5 (the clear concrete cover was 30 mm and the bar diameter was 20 mm), (c / d) ratio equal to 2.0 (the clear concrete cover was 30 mm and the bar diameter was 15 mm), and (c / d) ratio equal to 2.67 (the clear concrete cover was 40 mm and the bar diameter was 15 mm). Each series consisted of three beams; one control (0% corrosion level), one corroded to 2.5% (low corrosion level), and one corroded to 5% (medium corrosion level). The longitudinal reinforcement was lap spliced within the constant moment region within a length of 300 mm. The reinforcement was corroded only within the constant moment region with no corrosion induced in the shear spans. The shear reinforcements were epoxy coated to prevent their corrosion.

The CFRP repair scheme was identical for all the repaired beams. It consisted of a 600 mm wide continuous CFRP U-wrap sheet placed, around the cross section, in the constant moment region. All the wrapped beams failed in bond by splitting of the concrete cover at the end of the lap-splice region. The crack width at the end of the lap-splice increased and propagated toward the compression zone as the loading increased until failure.

Strain gauge measurements were taken only on the lap spliced bars for specimen with c/d = 1.5 and 2.67.

4.5.1 Lap spliced beams with (c/d) equal to 1.5

4.5.1.1 Cracking

The first cracks that appeared during testing were the flexural cracks located within the constant moment region. With further loading, shear, flexural, and splitting crack developed. Shear cracks were observed only in the shear spans between the loading point and the support. Flexural cracks were observed in the mid span and at one or both ends of the lap-splice region. As loading continued, some additional flexural and shear cracks formed and the initial cracks at the end of the splice region extended to the compression zone. The crack width at the end of the lap splice increased and propagated towards the compression zone until failure occurred. There were no horizontal cracks along the lap spliced region. Figures 4.21a and 4.21b show an elevation view of the control beam (0% corrosion level) at failure. Figures 4.22a and 4.22b show an elevation view of the corroded beam (2.5% corrosion level) at failure. Figures 4.23a and 4.23b show an elevation view of the corroded beam (5.0% corrosion level) at failure.

a) Elevation view

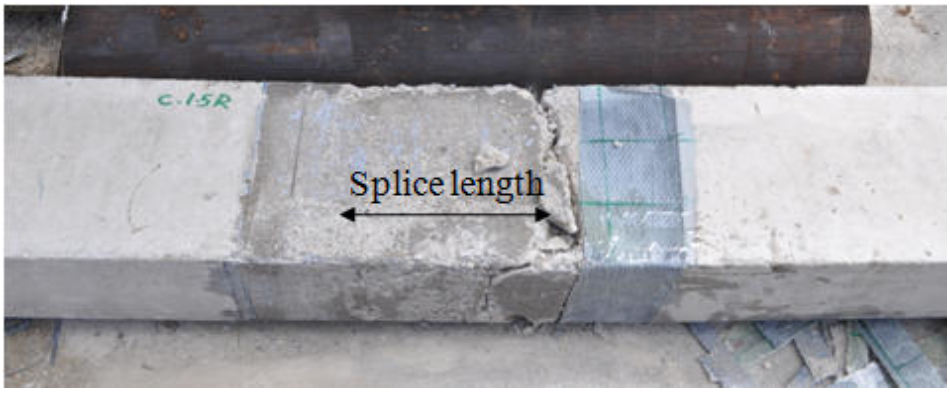

b) Elevation view after removing the CFRP

Figure 4-21 The failure mode for the control strengthened beam (0% corrosion)

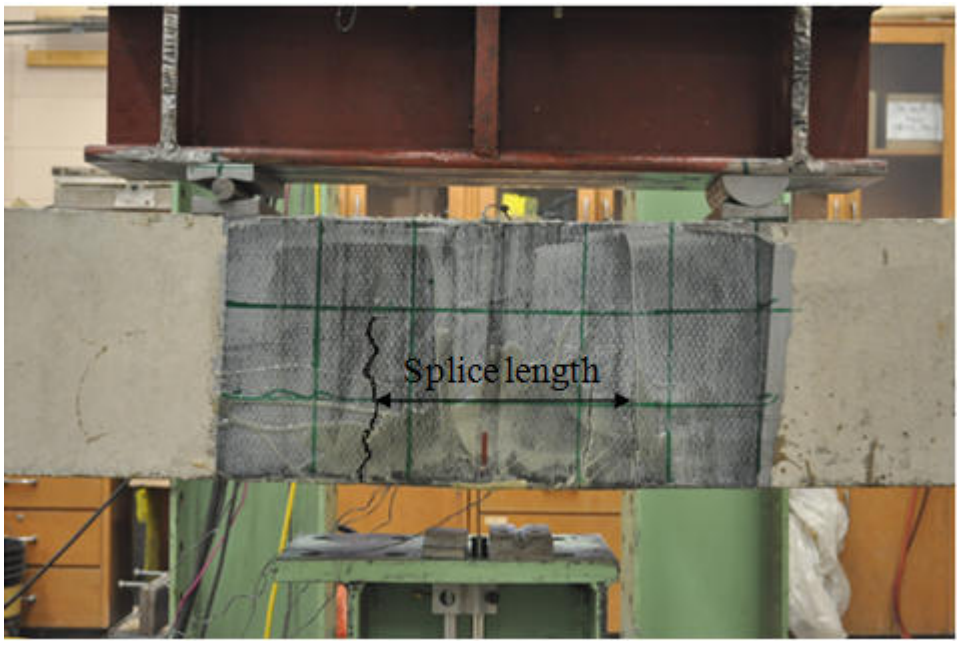

a) Elevation view

b) Elevation view after removing the CFRP wrap.

Figure 4-22 The failure mode for the repaired corroded beam (5.0 % corrosion)

4.5.1.2 Load deflection behavior

The load-deflection curves of the CFRP wrapped beams with (c/d) ratio = 1.5 at different corrosion levels (0%, 2.5%, and 5.0%) are compared as shown in Figure 4.24. The flexural stiffness for the three beams was almost identical regardless of the corrosion level. The cracking load for beam with 0%, 2.5%, and 5.0% corrosion level was 62 kN, 60 kN, and 59 kN, respectively.

Figure 4.24 shows a consistent decrease in the maximum load as the corrosion level increased. The maximum loads for the CFRP wrapped beams with different corrosion levels (0%, 2.5%, and 5%) were 154 kN, 117 kN, and 82 kN, respectively. The maximum loads for the beam with low and medium corrosion level (2.5%, and 5.0%) were decreased by 12% and 22% in comparison to than that of the CFRP wrapped control (un-corroded) specimen, respectively.

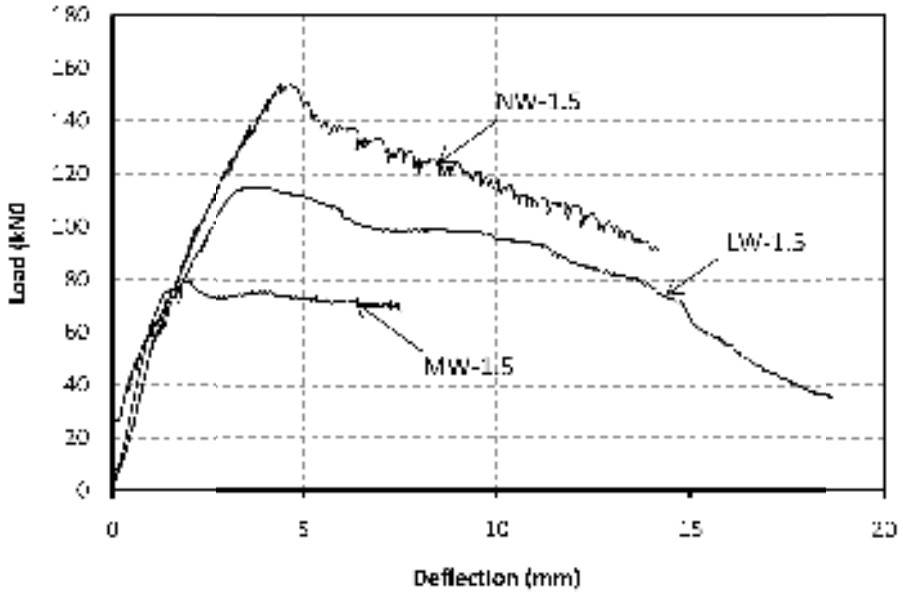

Figure 4-23 Load-deflection curves of CFRP wrapped beams of (c/d) ratio =1.5

4.5.1.3 Measured strain

Figure 4.25 shows the load- strain response for one bar in beam NW-1.5. As the load increases from zero to 62kN, the concrete is un-cracked and resists tensile forces. At a load of 62 kN, the concrete cracks and the strain in the tensile steel is 325με. Once the crack occurs, all the tensile forces carried by the concrete at the crack are being transmitted to the steel reinforcement. As the load increase from 62 kN to 68 kN, the steel strain increases from 325 με at 62 kN to 689 με at 68 kN. The slip of the main reinforcement due to the splitting cracks occurred at the end of the spliced bars at load levels between 62 kN and 68 kN. As loading continues further, the steel strain increases almost linearly until reaching a peak load of 154 kN with a corresponding steel strain of 1834 με.

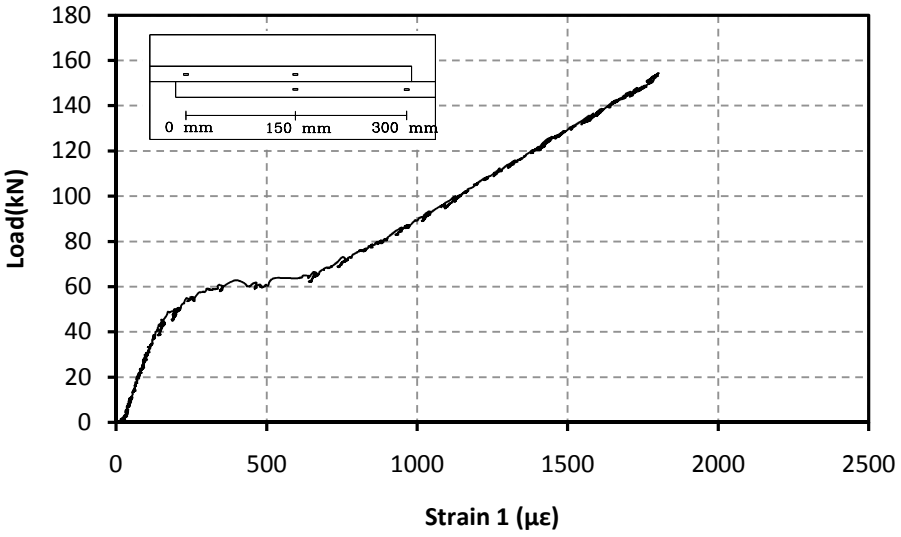

Figure 4-24 Strain response in bar (1) at (0 mm) distance along the lap splice

The measured strain profile along the lap splice was almost identical for all the beams in this series. Figure 4.26a and 4.26b show typical strain distribution with distance along the lap splice for the two bars in beam NW-1.5. The strain gauges on a steel bar were located at the middle and the end of the lap splice and more rapidly between the middle and the loaded end of the lap splice. These results indicate that the maximum strain is concentrated at the loaded end of the spliced steel bars. Beyond a load level of 90 kN, the strain distribution was linear between the free end and loaded end of the lap splice. In all cases, the strain in the splice was lower than the yield strain of the steel bars.

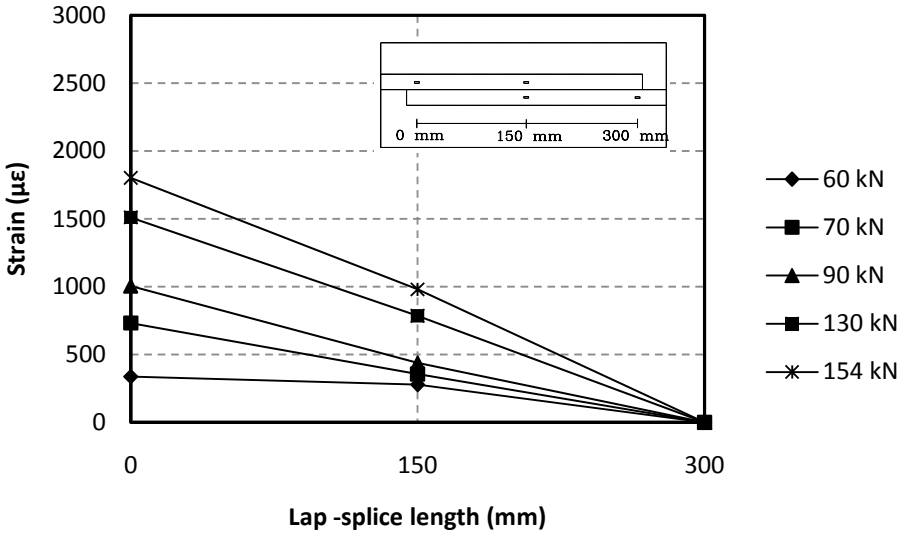

a) Strain distribution along the first bar of the lap splice

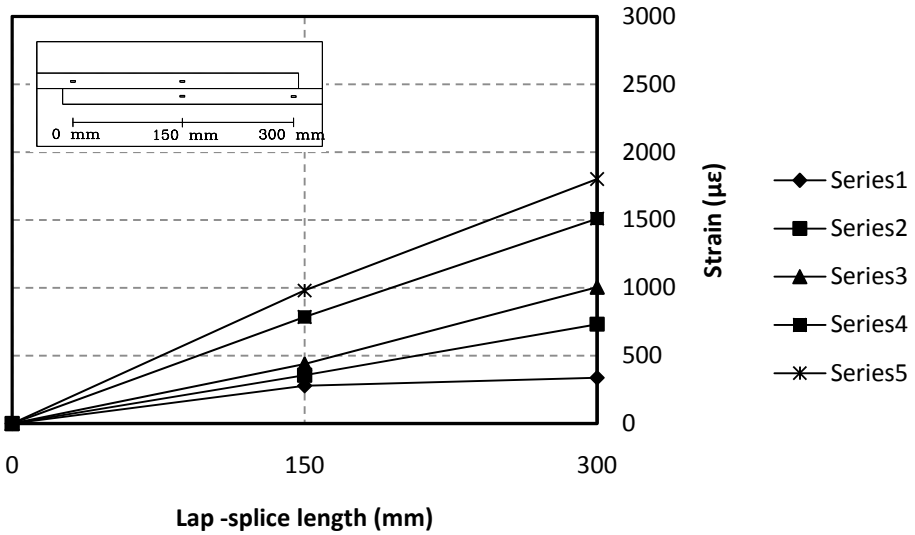

b) Strain distribution along the second bar of the lap splice

Figure 4-25 Strain distribution along the lap splice in beam NW-1.5

Figure 4.27 shows the strain in the FRP versus the deflection at mid span. The curve can be divided into three main regions as shown in Figure 4.27. In region 1, the beam is un cracked and as the load increases the deflection increases but the strain in the FRP remains almost zero until reaching 4.35 mm deflection. At this deflection, the bond/splitting cracks occurred. In region 2, as the deflection increases from 4.3 to 13.6 mm, the strain in the FRP increases from 90 με to a peak strain of 4400 με. Past the peak strain, the FRP strain decreases and the deflection increases due to gradual rupture of FRP fibers.

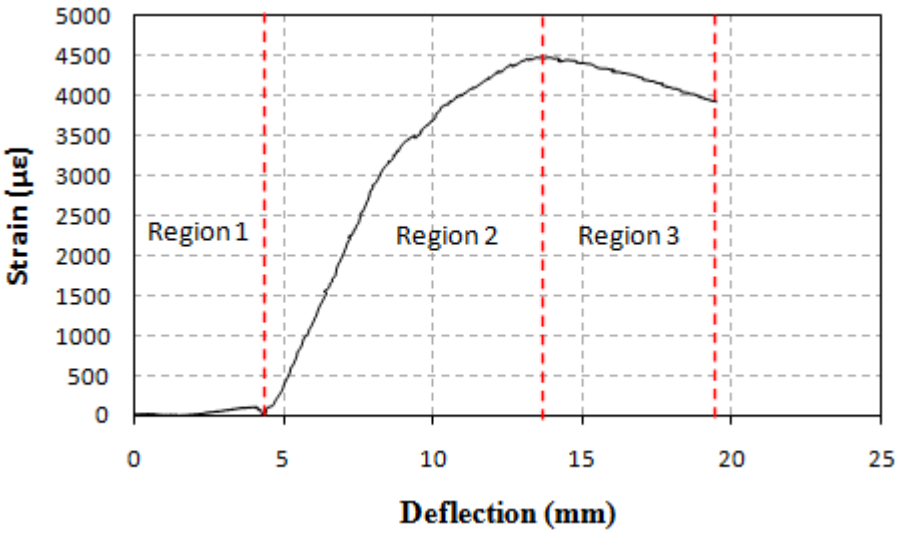

Figure 4-26 Strain vs. Deflection curve for the beam with (c/d) ratio =1.5

4.5.2 Lap-spliced beams with (c/d) ratio equal to 2.0

4.5.2.1 Cracking

The cracking behavior of the CFRP wrapped beams with c/d = 2.0 was similar to that of CFRP wrapped beams with c/d = 1.5. The first cracks that appeared during testing were the flexural cracks that were located within the constant moment region. As loading continued, shear, flexural, and splitting cracks developed. Shear cracks were observed only in the shear spans between the loading point and the supports. Flexural cracks were observed in the mid span and at one or both ends of the lap-splice region. As loading continued, additional flexural and shear cracks formed. The crack width at the end of the lap splice increased and propagated towards the compression zone until failure occurred. There were no horizontal cracks along the lap spliced region. Figures 4.28a and 4.28b show an elevation view of the control beam (0% corrosion level) at failure with and without CFRP wrap. Figures 4.29a and 4.29b show an elevation view of the corroded beam (2.5% corrosion level) at failure with and without CFRP wrap. Figures 4.30a and 4.30b show an elevation view of the corroded beam (5.0% corrosion level) at failure with and without CFRP wrap. The vertical crack is evident in all these Figures.

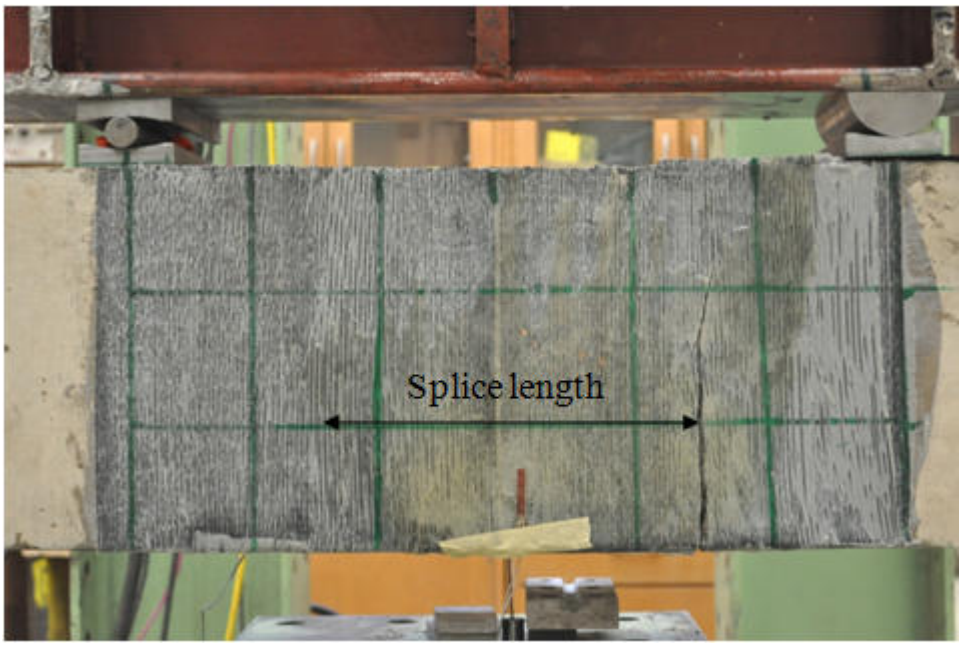

a) Elevation view

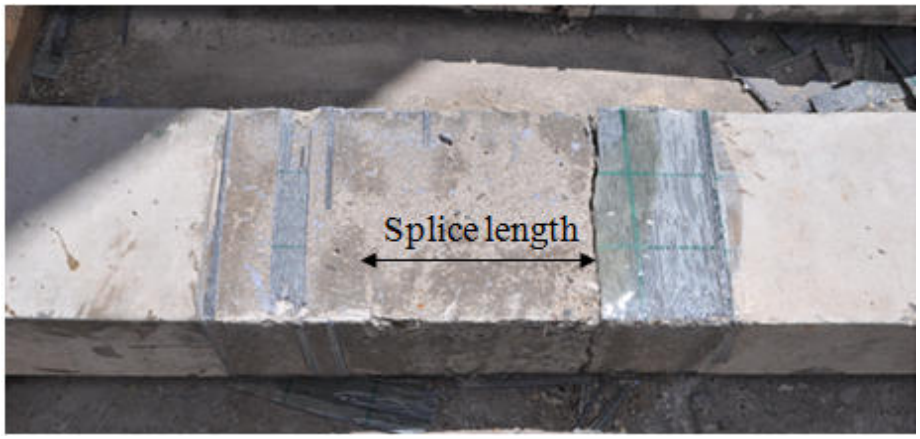

b) Elevation view after removing the CFRP wrap

Figure 4-27 The failure mode for the control beam (0%)

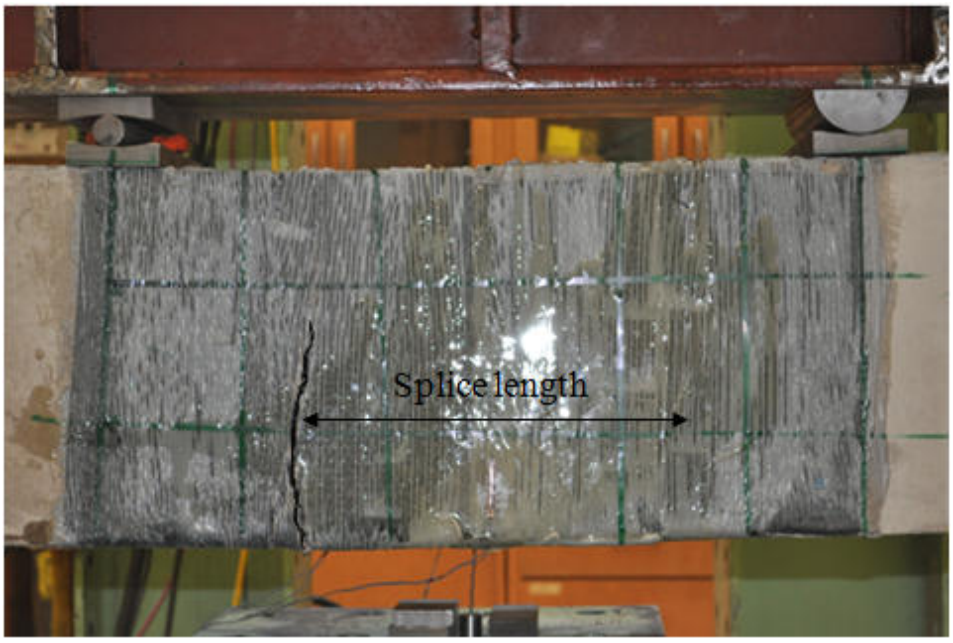

a) Elevation view

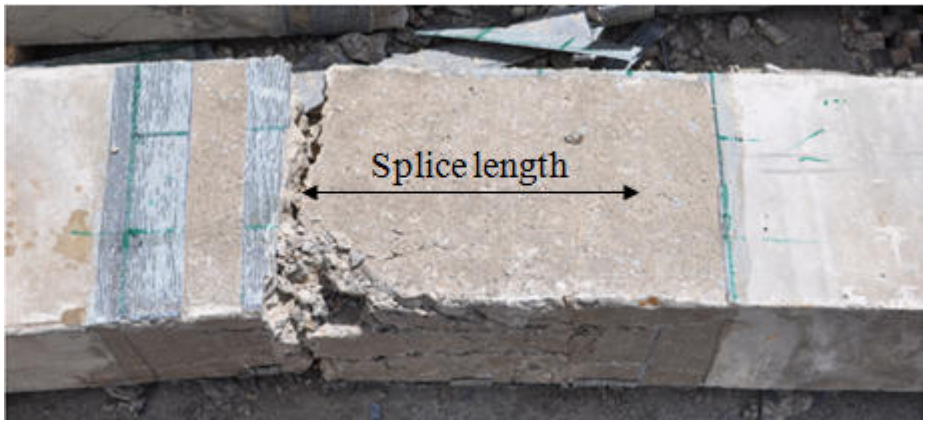

b) Elevation view after removing the CFRP wrap

Figure 4-28 The failure mode for the repaired corroded beam (2.5%)

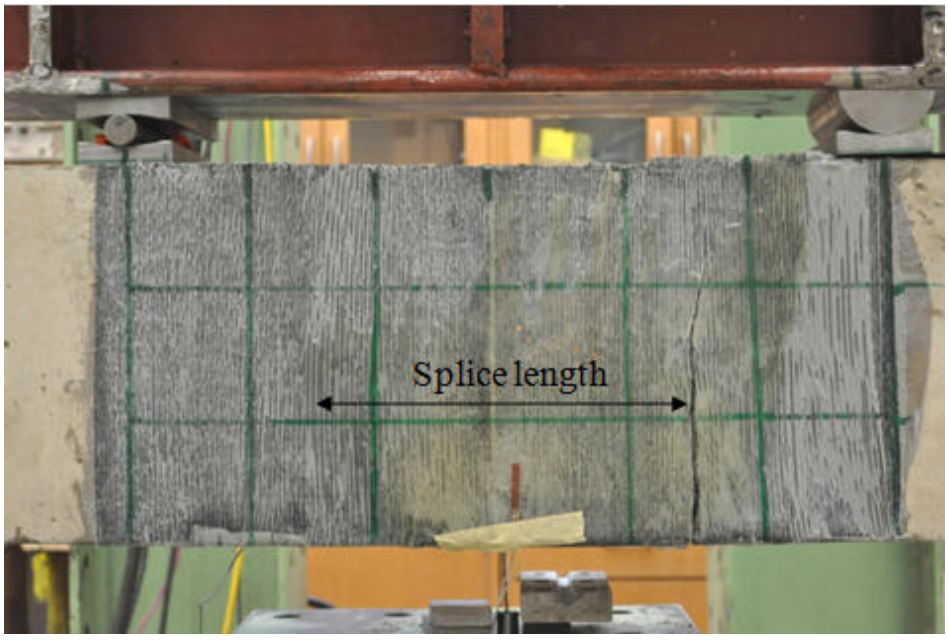

a) Elevation view

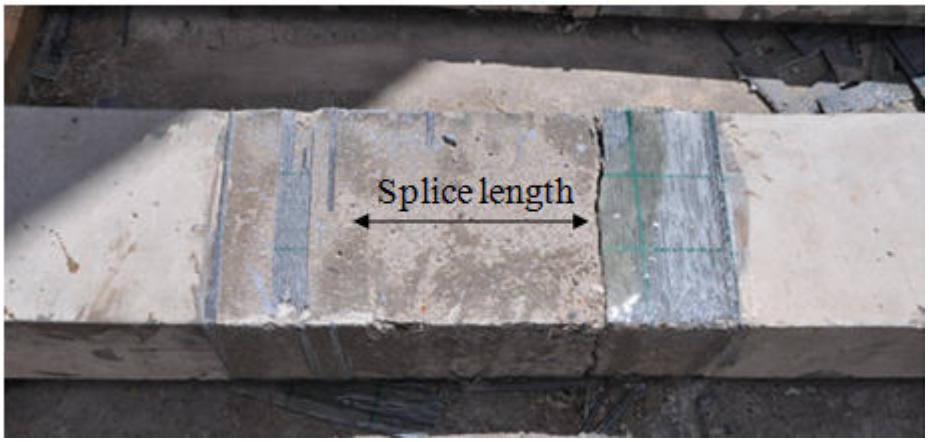

b) Elevation view after removing the CFRP wrap

Figure 4-29 The failure mode for the corroded repaired beam (5.0%)

4.5.2.2 Load deflection behavior

The load-deflection curves of the CFRP wrapped beams with (c/d) ratio = 2.0 a different corrosion levels (0%, 2.5%, and 5.0%) are compared as shown in Figure 4.31. The flexural stiffness for the three beams was almost identical regardless of the corrosion level (0%, 2.5%, and 5.0%). The cracking load for beam with 0%, 2.5%, and 5.0% corrosion level was 55 kN, 51 kN, and 53 kN, respectively.

Figure 4.31 shows a consistent decrease in the maximum load as the corrosion level increased. The maximum loads for the CFRP wrapped beams with different corrosion levels (0%, 2.5%, and 5%) were 153 kN, 117 kN, and 115 kN, respectively. The maximum loads for the beam with low and medium corrosion level (2.5%, and 5.0%) were decreased by 23% and 25% in comparison to that of the CFRP wrapped control (un-corroded) specimen, respectively.

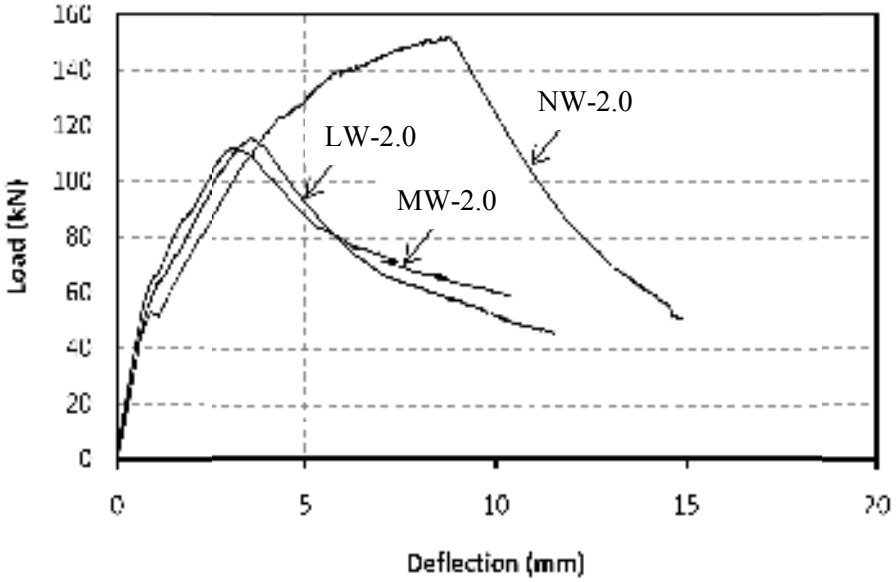

Figure 4-30 Load-deflection curves of CFRP wrapped beams of (c/d) ratio = 2.0

4.5.3 Lap-spliced beams with (c/d) ratio equal to 2.67

4.5.3.1 Cracking

The cracking behavior of the CFRP wrapped beams with c/d = 2.67 was similar to that of CFRP wrapped beams with c/d ratio = 1.5 and 2.0. The first cracks that appeared during testing were the flexural cracks that were located within the constant moment region. As loading continued, shear, flexural, and splitting cracks developed. Shear cracks were observed only in the shear spans between the loading point and the supports. Flexural cracks were observed in the mid span and at one or both ends of the lap-splice region. As loading continued, additional flexural and shear cracks formed. The crack width at the end of the lap splice increased and propagated towards the compression zone until failure occurred. There were no horizontal cracks along the lap spliced region. Figures 4.32a and 4.32b show an elevation view of the control beam (0% corrosion level) at failure with and without CFRP wrap. Figures 4.33a and 4.33b show an elevation view of the corroded beam (2.5% corrosion level) at failure with and without CFRP wrap. Figures 4.34a and 4.34b show an elevation view of the corroded beam (5.0% corrosion level) at failure with and without CFRP wrap. The vertical crack is evident in all these Figures.

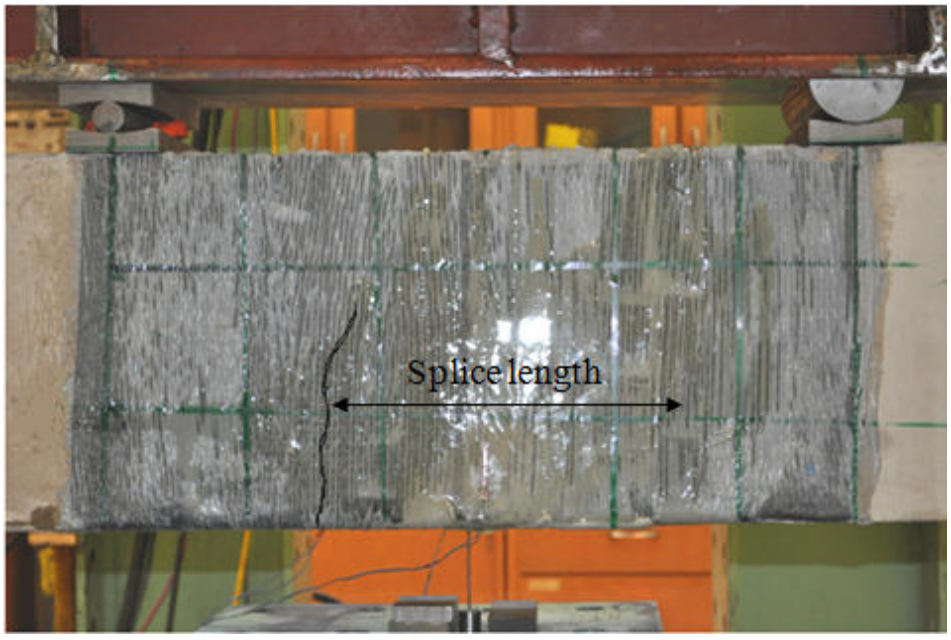

a) Elevation view

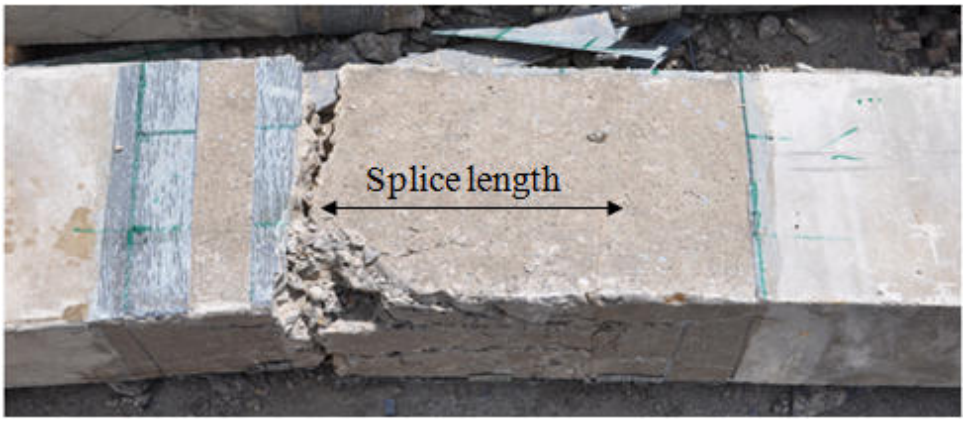

b) Elevation view after removing the CFRP wrap

Figure 4-31 The failure mode for of the control strengthen beam (0%)

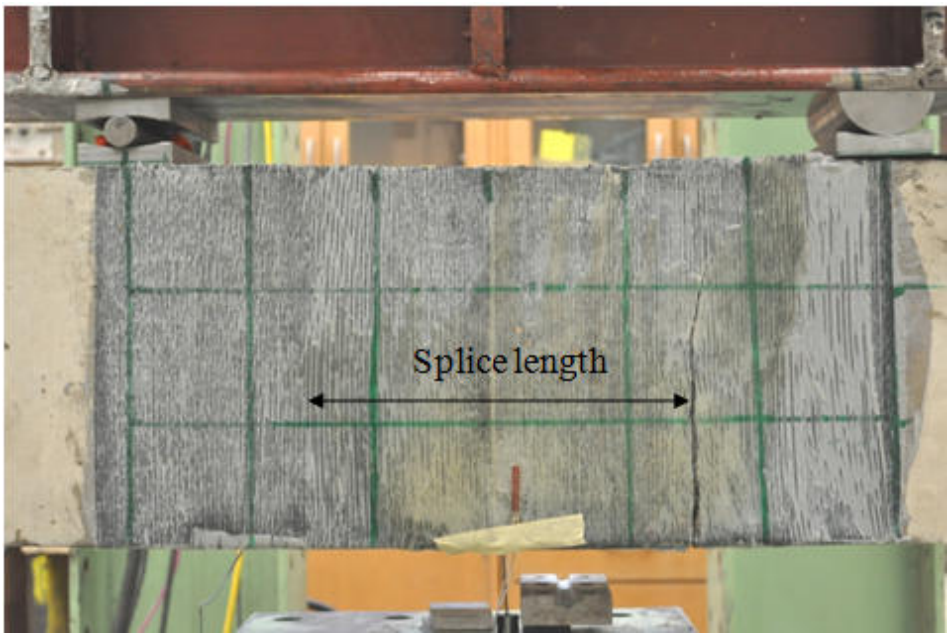

a) Elevation view

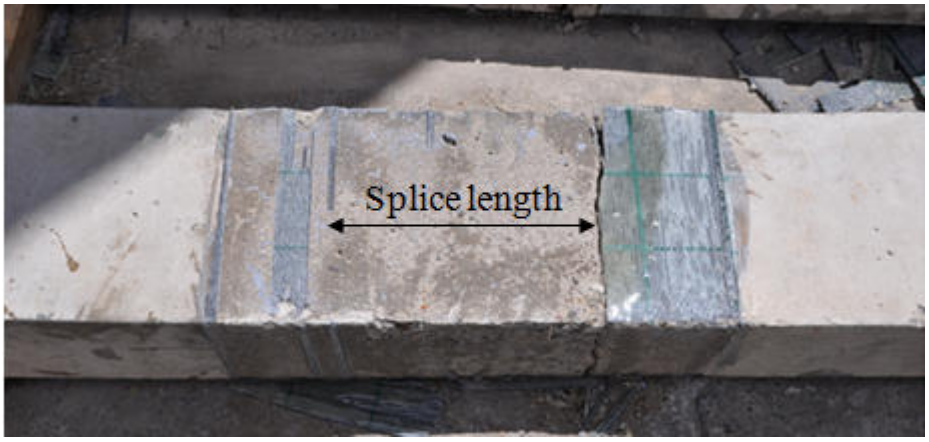

b) Elevation view after removing the CFRP wrap

Figure 4-32 The failure mode for the corroded repaired beam (2.5%)

a) Elevation view

b) Elevation view after removing the CFRP wrap

Figure 4-33 The failure mode for the corroded repaired beam (5.0%)

4.5.3.2 Load deflection behavior

The load-deflection curves of the CFRP wrapped beams with (c/d) ratio = 2.0 at different corrosion levels (0%, 2.5%, and 5.0%) are compared as shown in Figure 4.35. The flexural stiffness for the three beams was almost identical regardless of the corrosion level (0%, 2.5%, and 5.0%). The cracking load for beam with 0%, 2.5%, and 5.0% corrosion level was 44 kN, 45 kN, and 43 kN, respectively.

Figure 4.35 shows a consistent decrease in the maximum load as the corrosion level increased. The maximum loads for the CFRP wrapped beams with different corrosion levels (0%, 2.5%, and 5%) were 142 kN, 117 kN, and 92 kN, respectively. The maximum loads for the beam with low and medium corrosion level (2.5%, and 5.0%) were decreased by 17% and 35% in comparison to than that of the CFRP wrapped control (un-corroded) specimen, respectively.

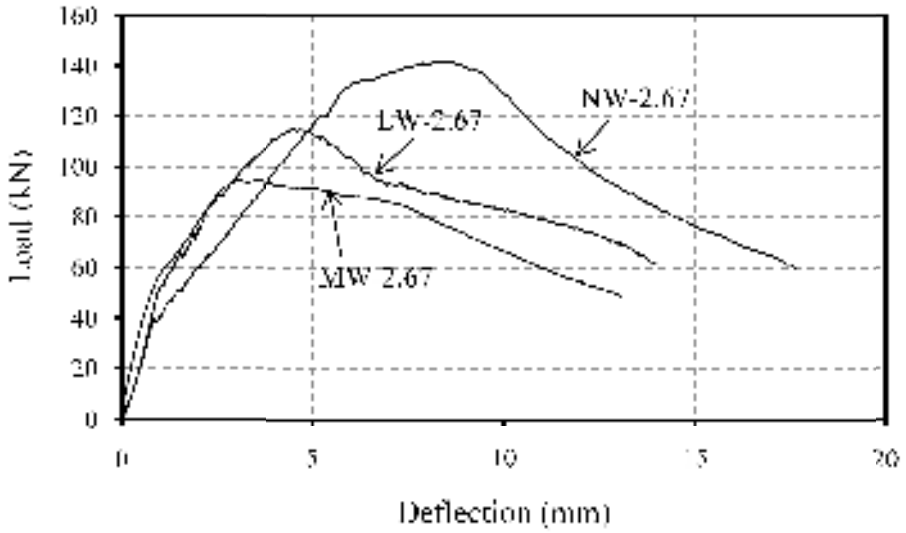

Figure 4-34 Load-deflection curves of CFRP wrapped beams of (c/d) ratio = 2.67

Figure 4.36 shows the strain in the FRP versus the deflection at mid span. The curve can be divided into three main regions as shown in Figure 4.36. In region 1, the beam is un-cracked and as the load increases the deflection increases but the strain in the FRP remains almost zero until reaching 2.14 mm deflection. At this deflection, the bond/splitting cracks occurred. In region 2, as the deflection increases from 2.14 to 13.6 mm, the strain in the FRP increases from 90 με to a peak strain of 4100 με. Past the peak strain, the FRP strain decreases and the deflection increases due to gradual rupture of FRP fibers.

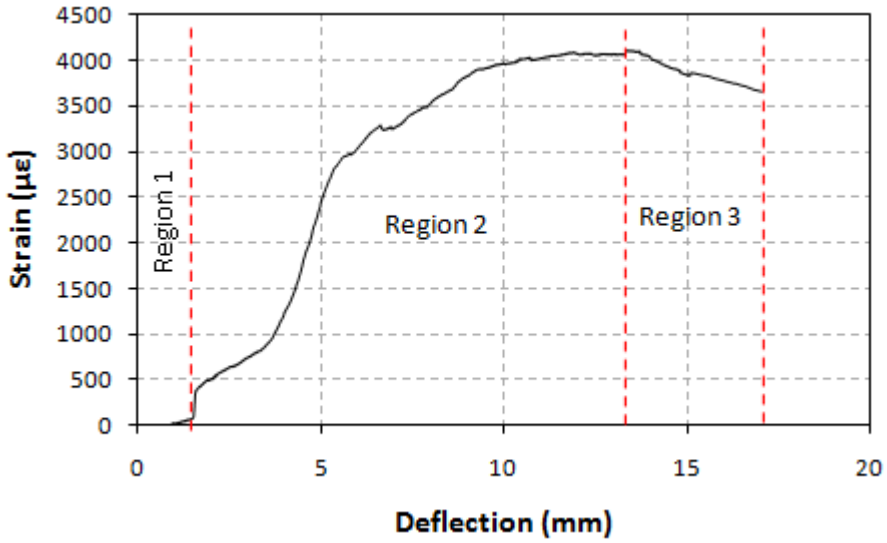

Figure 4-35 Strain vs. Deflection curve for the beam with (c/d) ratio =2.67

4.6 Effect of the (c/d) ratios on the maximum load of beams

4.6.1 Un-wrapped beams

The load-deflection curves for beams with different (c/d) ratios (1.5, 2.0, and 2.67) at different corrosion levels 0%, 2.5%, and 5.0% are shown in Figures 4.37, 4.38, and 4.39, respectively. Figure 4.37 shows the load deflection curves for beams with different (c/d) ratios (1.5, 2.0, and 2.67) at 0% corrosion level. The cracking load for non-corroded (0%) beams with (c/d) ratios 1.5, 2.0, and 2.67 was 42 kN, 49 kN, and 56 kN, respectively. For beams with (c/d) ratios 1.5 and 2.0 (constant concrete cover and different bar diameter), the maximum load for the beam with (c/d) ratio of 1.5 was greater than the beam with (c/d) ratio of 2.0 due to the larger bar diameter. For beams with (c/d) ratios of 2.0 and 2.67 (constant bar diameter and different concrete cover), the maximum load for both beams was almost identical. the difference in the effective depth between the two beams is only 10 mm, and this has no effect on the peak load

Figure 4.38 and Figure 4.39 show the load deflection curves for beams with (c/d) ratios 1.5, 2.0, and 2.67 at 2.5% and 5.0% corrosion level. The cracking load for beams with (c/d) ratio of 1.5, 2.0, and 2.67 was 37 kN, 42 kN, and 48 kN. For beams with (c/d) ratios equal 1.5 and 2.0 (constant concrete cover and different in bar diameter), the maximum load for the beam with (c/d) ratio of 1.5 was greater than the beam with (c/d) ratio of 2.0 due to larger bar diameter. For beams with (c/d) ratios of 2.0 and 2.67 (constant bar diameter and different concrete cover) the maximum load for the beam with (c/d) ratio = 2.67 was greater than the beam with (c/d) of 2.0. The difference in the maximum measured load is due to the differences of the corrosion crack. The corrosion cracks for the beam with (c/d) ratio of 2.0 were wider than those in the beam with (c/d) ratio = 2.67 as mentioned in Section 4.1.

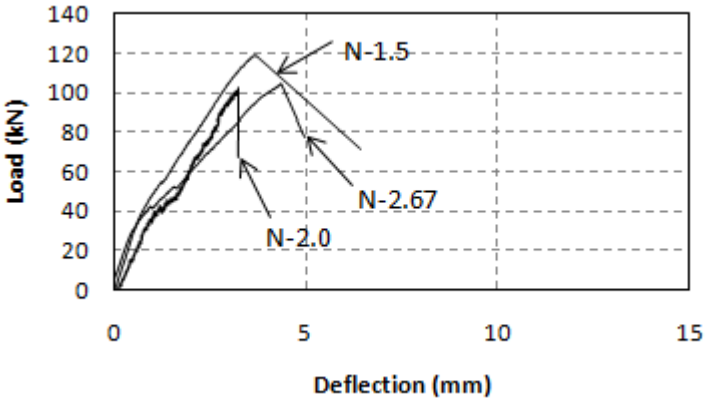

Figure 4-36 Load vs. deflection for beams with no corrosion

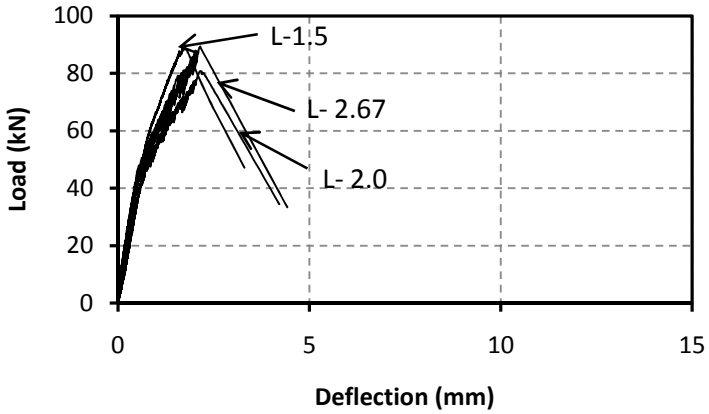

Figure 4-37 Load vs. deflection for beams with 2.5% corrosion

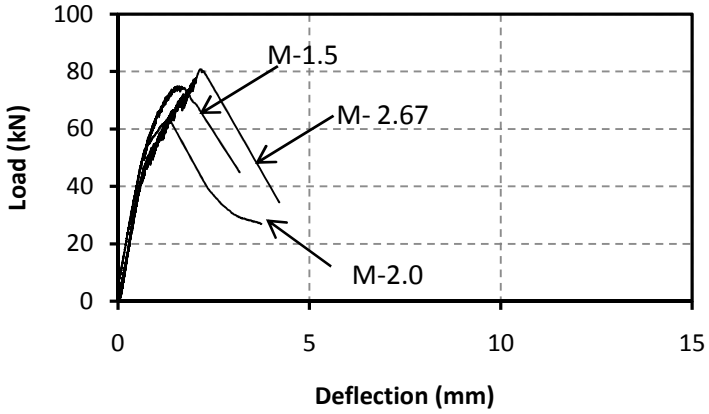

Figure 4-38 Load vs. deflection for beams with 5.0% corrosion

4.6.2 Wrapped beams

The load-deflection curves for wrapped beams with different (c/d) ratios (1.5, 2.0, and 2.67) at different corrosion levels 0%, 2.5%, and 5.0% are shown in Figures 4.40, 4.41, and 4.42, respectively. From Figure 4.40, the cracking load for beams with (c/d) ratios 1.5, 2.0, and 2.67 was 48 kN, 55 kN, and 62 kN, respectively. For the two beams with (c/d) ratios of 1.5 and 2.0 (constant concrete cover and different in bar diameter), the maximum loads were almost identical. For beams with (c/d) ratios of 2.0 and 2.67 (constant bar diameter and different concrete cover), the maximum load for the beam with (c/d) ratio equal to 2.0 was greater than the beam with (c/d) equal to 2.67. The difference in the maximum load between the two series is due to the effect of the (c/d) ratio. For beams with constant bar diameter and different concrete cover, the effect of the FRP depends on the dilation of the confined concrete resulting from bond/splitting stresses; greater dilation means greater confinement.

Figure 4.41 shows the load deflection curves for beams with different (c/d) ratios 1.5, 2.0, and 2.67 at 2.5% corrosion level. The cracking load for beams with c/d ratios 1.5, 2.0, and 2.67 was 44 kN, 52 kN, and 56 kN, respectively. The maximum load for all beams was almost identical.

Figure 4.42 shows that the load deflection curves for beams with different (c/d) ratios (1.5, 2.0, and 2.67) at 5.0% corrosion level. The cracking load for beams with (c/d) ratios 1.5, 2.0, and 2.67 was 43 kN, 48 kN, and 52 kN. For beams with (c/d) ratios equal 1.5 and 2.0 (constant concrete cover and different in bar diameter), the maximum load for the beam with (c/d) ratio of 2.0 (bar diameter = 15 mm) was greater than the beam with (c/d) ratio of 1.5 (bar diameter =20 mm) because of the effect of the (c/d) ratio. As the bar diameter increase, the dilation area due bond/splitting increases and the effective stress due to the FRP decreases. For the beams with (c/d) ratios 2.0 and 2.67 (constant bar diameter and different concrete cover), the maximum load for the beam with (c/d) ratio equal to 2.0 was greater than the beam with (c/d) equal 2.67. The difference in the maximum load between the two series was because of the effect of the (c/d) ratio. For beams with constant bar diameter and different concrete cover, the effect of the FRP depends on the dilation of the confined concrete resulting from bond/splitting stresses; greater dilation means greater confinement.

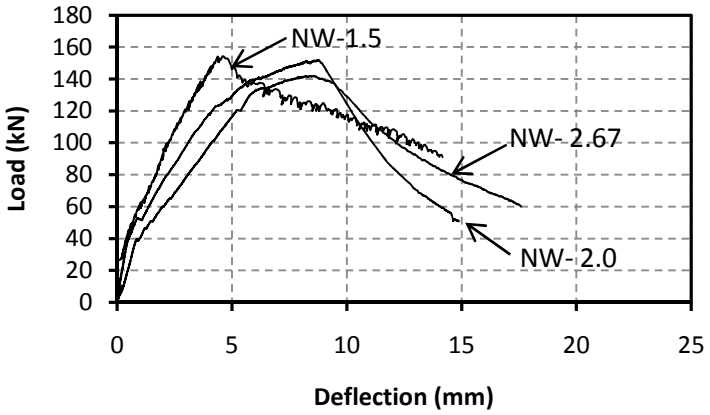

Figure 4-39 Load vs. deflection response of wrapped beams with no-corrosion

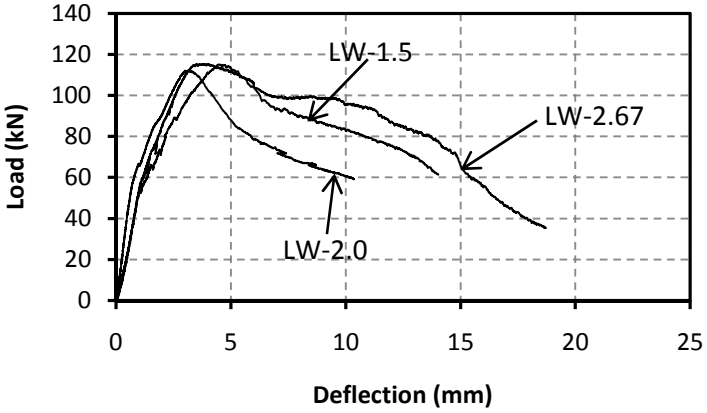

Figure 4-40 Load vs. deflection response of wrapped beams with 2.5% corrosion

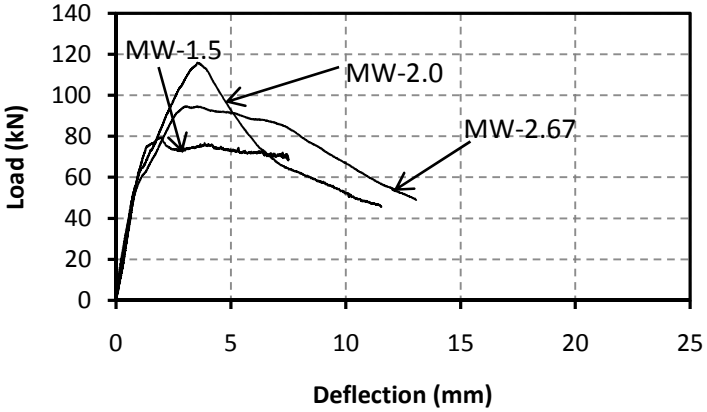

Figure 4-41 Load vs. deflection response of wrapped beams with 5.0% corrosion

4.7 Effect of CFRP repair

4.7.1 Beams with (c/d) ratio = 1.5

For the repaired specimens, the maximum load and the ductility increased compared to the beams without CFRP sheets. The maximum load for the CFRP wrapped beams at 0% , 2.5% , and 5.0% corrosion level increased by 22% , 24%, and 10% , respectively in comparison with the corresponding un-wrapped specimens as seen in Figures 4.43 a, b, and c. The load deflection behavior beyond the maximum load was ductile for the CFRP wrapped beams as seen in figure 4.43 a, b, and c .The load dropped slightly and continued to decrease gradually with increasing deflection

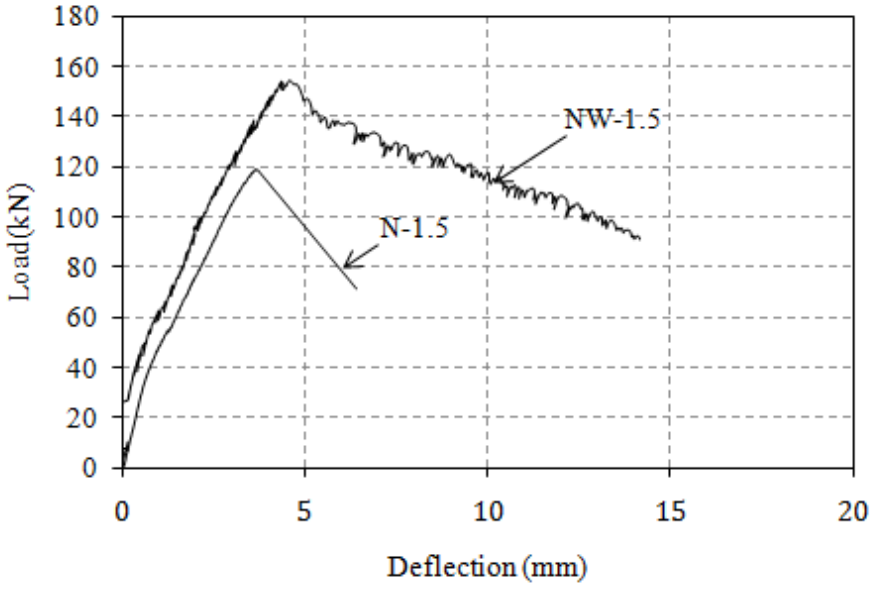

a) 0% corrosion

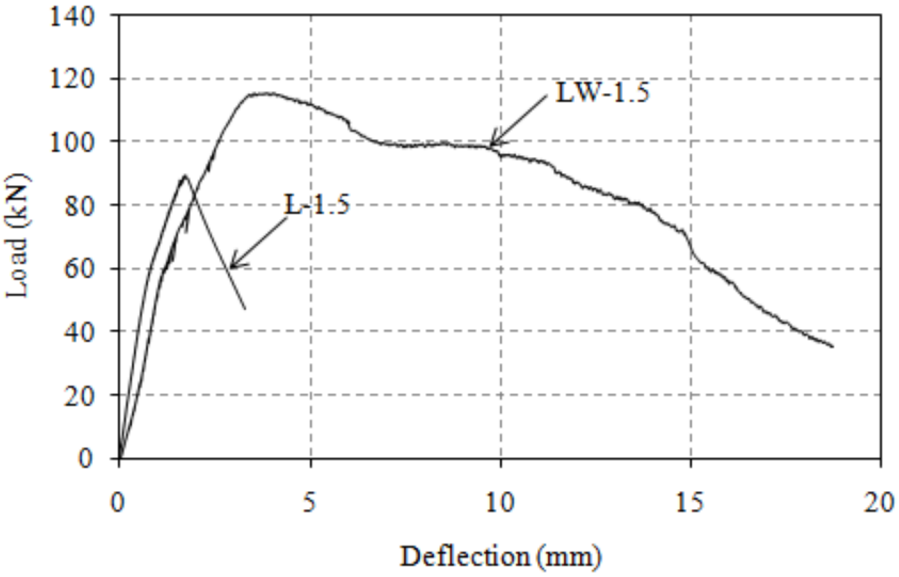

b) 2.5% corrosion level

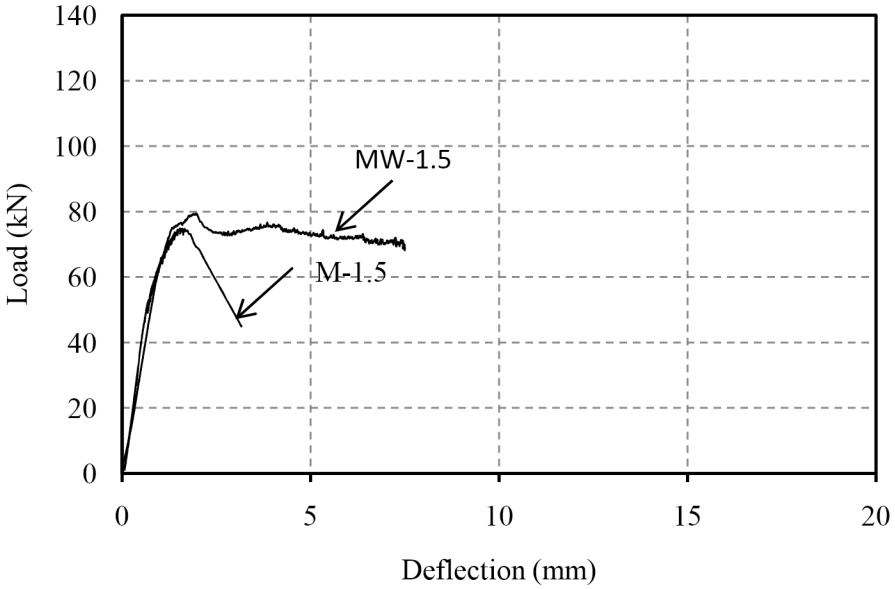

c) 5.0% corrosion level

Figure 4-42 Comparison of load-deflection curves of CFRP wrapped vs. unwrapped beams: a) 0% corrosion, b) 2.5% corrosion, and c) 5.0% corrosion

4.7.2 Beams with (c/d) ratio = 2.0

For the repaired specimens, the maximum load and the ductility increased compared to the beams without CFRP sheets. The maximum load for the CFRP wrapped beams at 0% , 2.5% , and 5.0% corrosion level increased by 33% , 30%, and 46% , respectively in comparison with the corresponding un-wrapped specimens as seen in Figures 4.44a, b, and c. The load deflection behavior beyond the maximum load was ductile as seen in Figure 4.44a, b, and c. The load dropped slightly and continued to decrease gradually with increasing deflection.

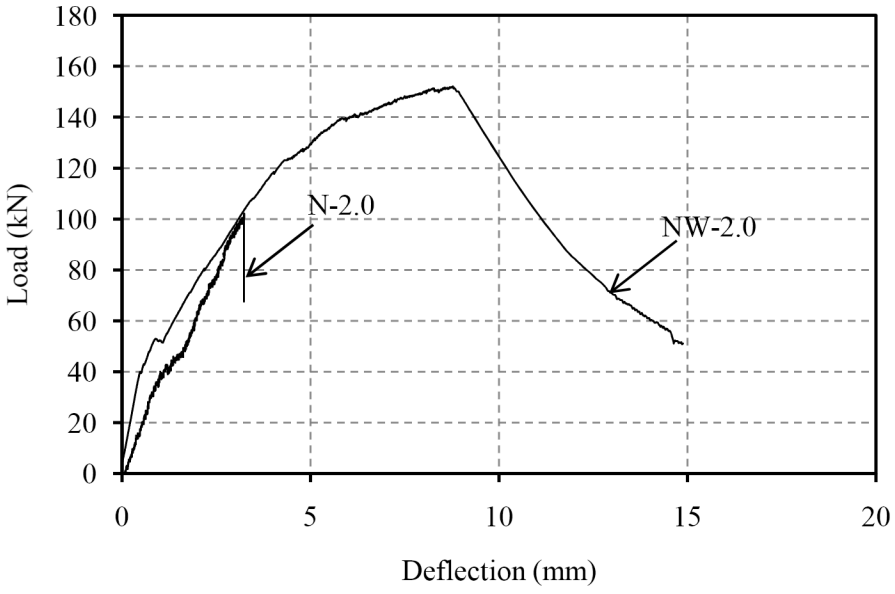

a) 0% corrosion level

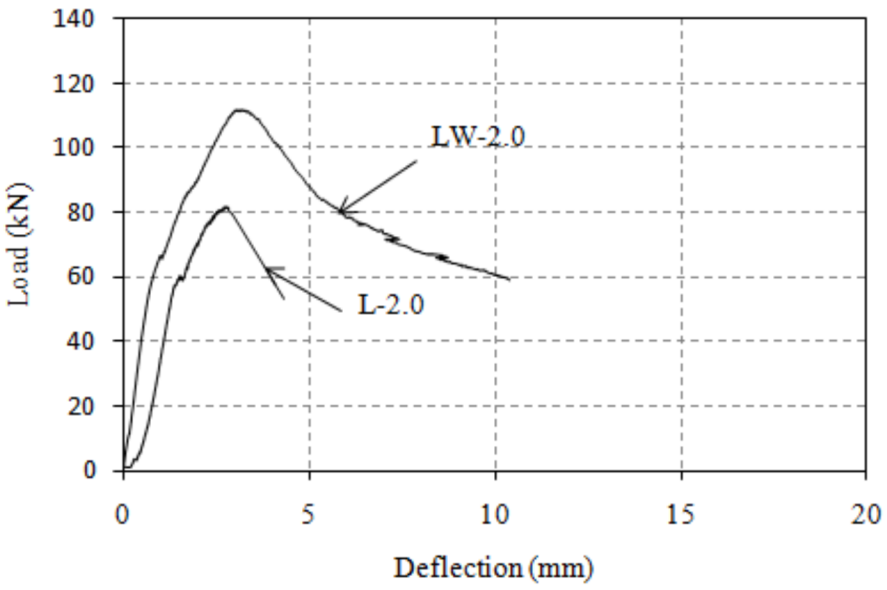

b) 2.5% corrosion level

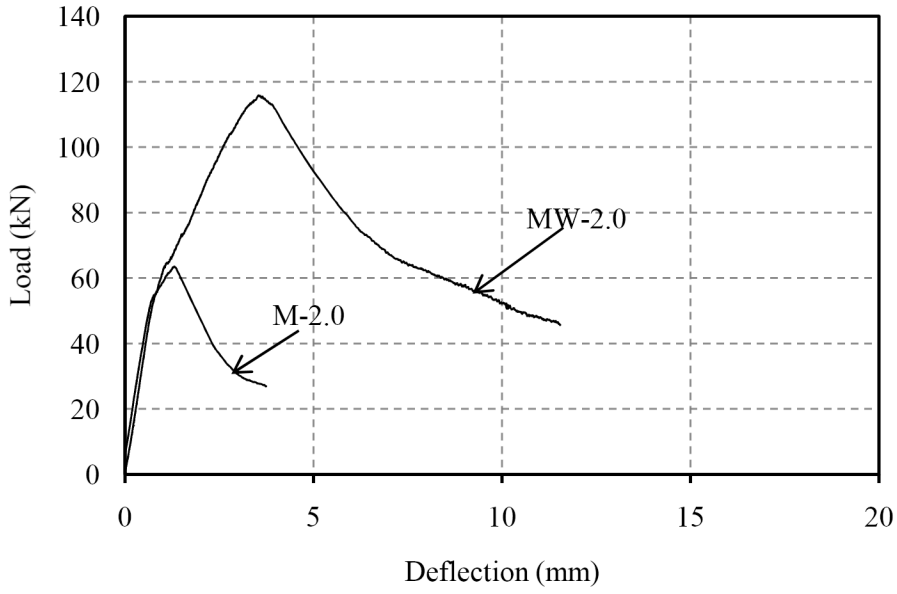

c) 5.0% corrosion level

Figure 4-43 Comparison of load-deflection curves of CFRP wrapped vs. unwrapped beams: a) 0% corrosion, b) 2.5% corrosion, and c) 5.0% corrosion

4.7.3 Beams with (c/d) ratio = 2.67

For the repaired specimens, the maximum load and the ductility increased compared to the beams without CFRP sheets. The maximum load for CFRP wrapped beams at 0% , 2.5% , and 5.0% corrosion level increased by 27% , 21%, and 12% , respectively in comparison with the un-wrapped specimens as seen in Figures 4.45a, b, and c. The load deflection behavior beyond the maximum load was ductile as seen in figure 4.45a, b, and c. The load dropped slightly and continued to decrease gradually with increasing deflection.

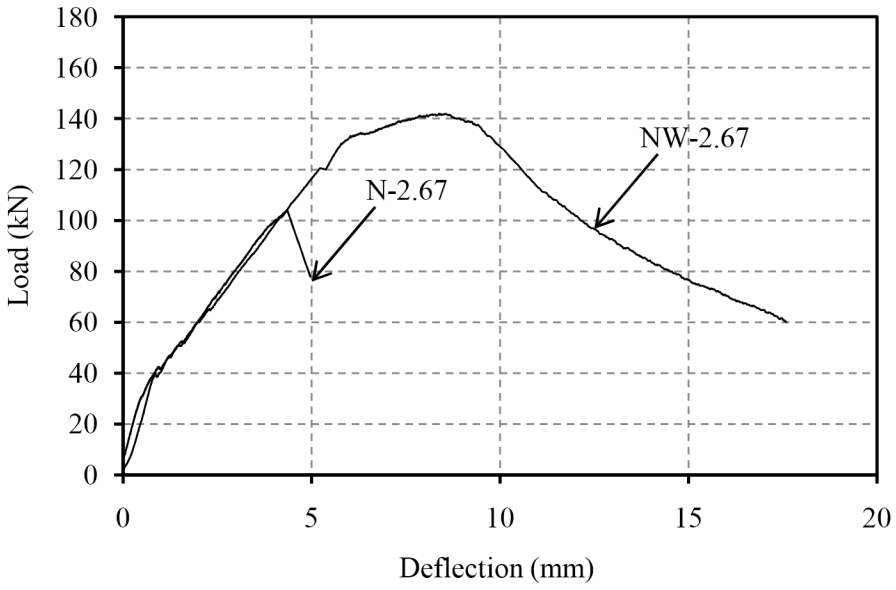

a) 0% corrosion level

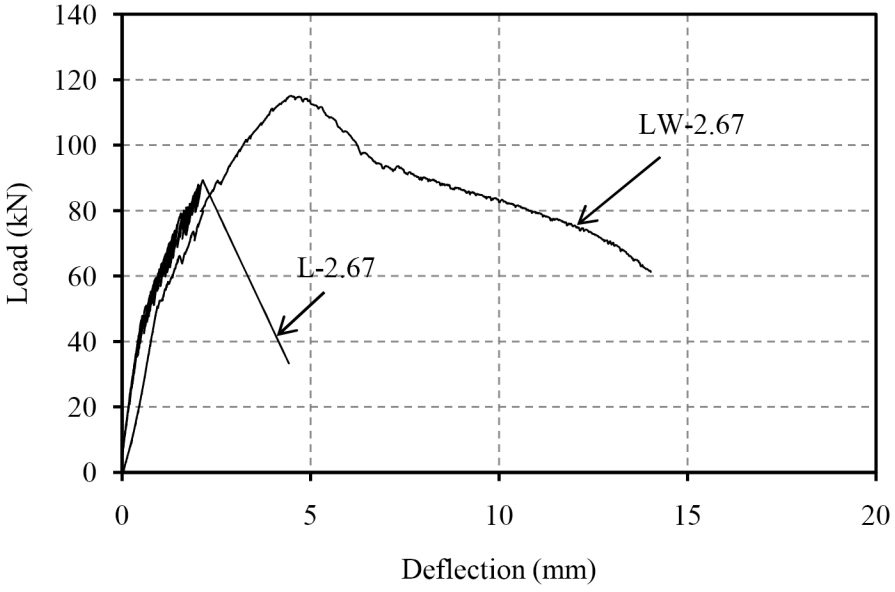

b) 2.5% corrosion level

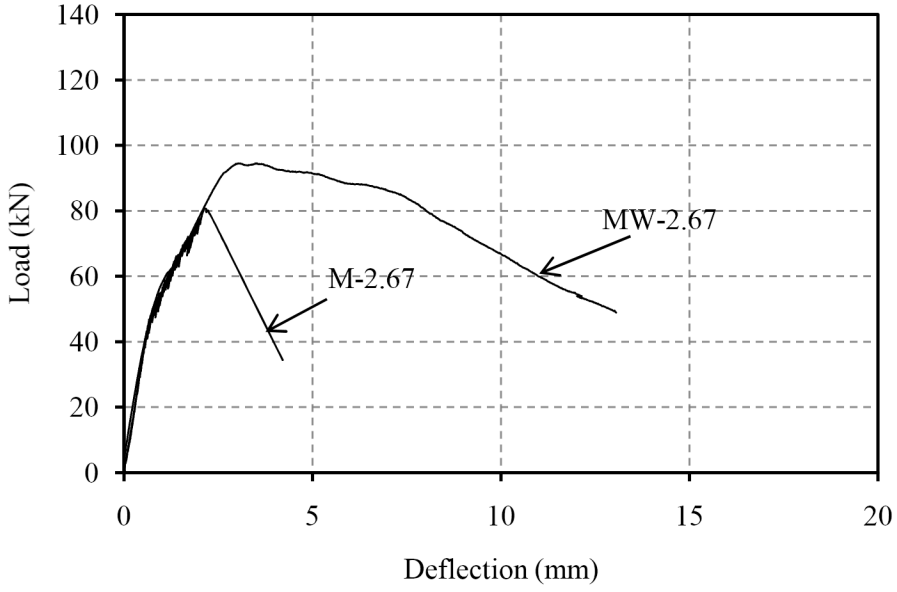

c) 5.0% corrosion level

Figure 4-44 Comparison of load-deflection curves of CFRP wrapped vs. unwrapped beams: a) 0% corrosion, b) 2.5% corrosion, and c) 5.0% corrosion

4.8 Bond strength

The maximum tensile stress developed in the longitudinal steel reinforcing bars in a beam specimen was calculated according to elastic cracked section analysis. The analysis assumes linear concrete stress-strain behavior and ignores the tensile strength of the concrete below the neutral axis. The average bond stress between the bar and concrete was calculated based on the assumption that the tensile force in the bar is resisted by a uniform bond stress along the full length of the splice.

$$U_t = \frac{A_b f_s}{\pi d_b l_s} \tag{4.1}$$

Where:

U_t : Average bond stress (MPa)

A_b: Cross sectional area of the rebar (mm^2)

f_s: stress in the steel rebar (MPa)

d_b: Rebar diameter of steel rebar (mm)

l_s: splice length (mm)

The bond strength can be determined directly from the tensile stress developed in the steel rebar. The stress in the steel rebar, (fs), is calculated based on the elastic cracked section analysis. The stress was determined at the maximum measured load. The steel stress and bond stress for all un-repaired and repaired beams are presented in Table 4.2. Table 4.2 also gives the concrete strength at 28-days, and the ultimate load. It is clear that there is a consistent decrease in the maximum bond stress as the corrosion level increases see Figures 4.46, 4.47, and 4.48. For beams with (c/d) ratio equal to 1.5, the maximum bond stress in

specimens with low and medium corrosion decreased by 25% and 41% respectively when compared to the control ones. For beams with (c/d) ratio equal to 2.0, the maximum bond stress in specimens with low and medium corrosion level decreased by 20% and 33% respectively when compared to the control ones. For beams with (c/d) ratio equal to 2.67, the maximum bond stress in specimens with low and medium corrosion level decreased by 14% and 22% respectively when compared to the control ones. After wrapping the beams with CFRP sheets, the maximum bond stress increased. For beams with (c/d) ratio equal to 1.5, the maximum load of the repaired beams at 0%, 2.5%, and 5.0% corrosion increased by 23%, 22%, and 13%, respectively. For beams with (c/d) ratio equal to 2.0, the maximum load of the repaired beam for (0%, 2.5%, and 5.0%) increased by 33%, 30%, and 34%, respectively. For beams with (c/d) ratio equal to 2.67, the maximum load of the repaired beam for (0%, 2.5%, and 5.0%) increased by 27%, 22%, and 15%, respectively.load of the repaired beam for (0%, 2.5%, and 5.0%) increased by 33%, 30%, and 34%, respectively. For beams with (c/d) ratio equal to 2.67, the maximum load of the repaired beam for (0%, 2.5%, and 5.0%) increased by 27%, 22%, and 15%, respectively.

Table 4-2 Bond strength results

		Notations	Concrete Strength f'c (MPa)	Actual mass loss (%)	Measured Ultimate load P_{max} (kN)	Steel Stress f_s (MPa)	Bond stress U_t (MPa)
Corrosion	Un-Wrapped	N-1.5	41	0	119	257	4.28
		L-1.5		1.92	89	193	3.21
		M-1.5		3.31	75	162	2.49
		N-2.0		0	102	322	4.02
		L-2.0		2.12	82	257	3.21
		M-2.0		3.21	64	200	2.69
		N-2.67		0	104	341	4.26
		L-2.67		2.07	89	293	3.66
		M-2.67		3.26	81	264	3.30
	Wrapped	NW-1.5	41	0	154	333	5.55
		LW-1.5		1.8	115	249	4.15
		MW-1.5		3.42	79	171	2.85
		NW-2.0		0	152	479	5.98
		LW-2.0		2.23	116	365	4.56
		MW-2.0		3.53	112	353	4.40
		NW-2.67		0	142	465	5.81
		LW-2.67		1.96	115	377	4.71
		MW-2.67		3.32	95	310	3.87

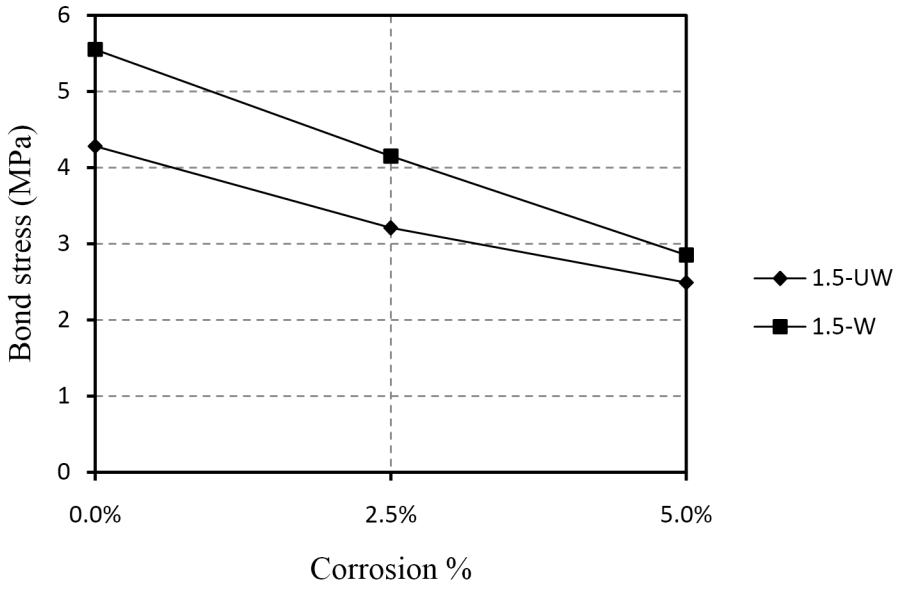

Figure 4-45 The effect of CFRP laminate on bond stress for beams with (c/d) =1.5

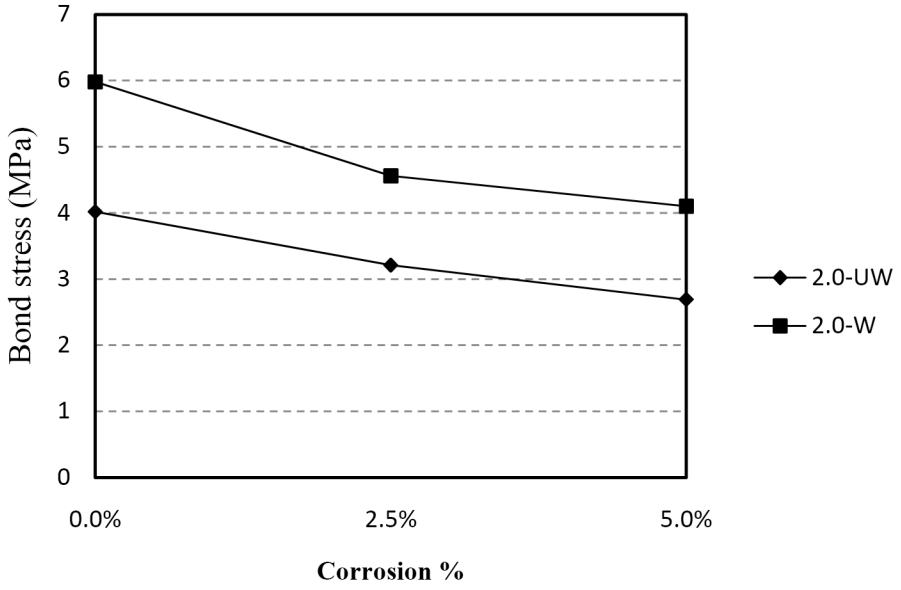

Figure 4-46 The effect of CFRP laminate on bond stress for beams with (c/d) = 2.0

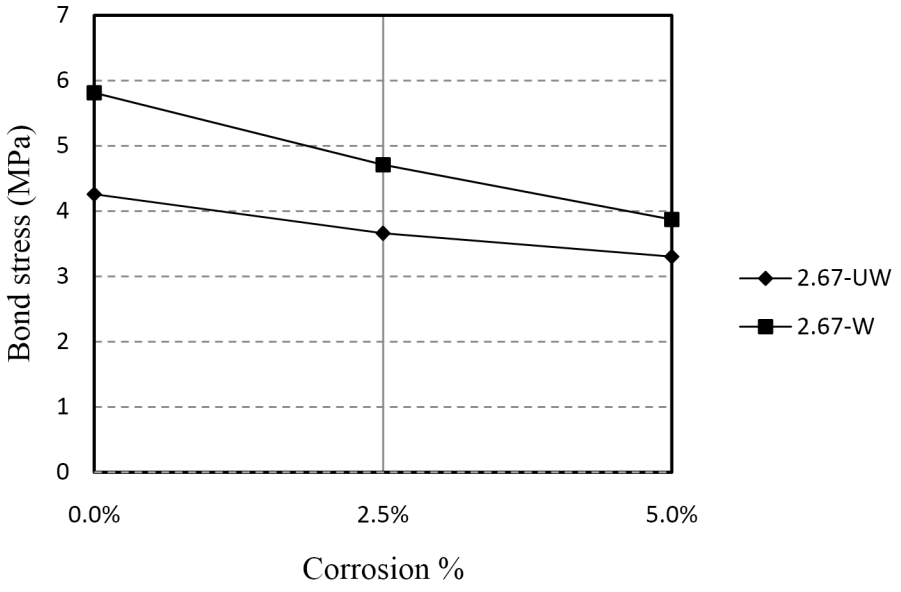

Figure 4-47 The effect of CFRP laminate on bond stress for beams with(c/d) =2.67

Chapter 5

Prediction of bond strength

5.1 Bond strength of reinforced concrete beam

The bond strength of a reinforcing bar in concrete is influenced by the diameter of the steel reinforcing bar, the thickness of the concrete cover, the concrete strength, and the amount of transverse reinforcement (stirrups) as given by Equation 5.1.

$$U_t = U_c + U_s \tag{5.1}$$

Where:

U_t: Total bond strength of the reinforcing bar in concrete (Psi).

U_c: The concrete contribution to the bond strength (Psi).

U_s: The stirrups contribution to the bond strength (Psi).

In the current work, there was no transverse reinforcement (stirrups) confining the lap spliced bars in the constant moment region (section 3.2); hence the contribution of transverse reinforcement (stirrups) to the bond strength is neglected. Therefore, the bond strength of a steel bar in concrete without transverse reinforcement can be given by Equation 5.2

$$U_t = U_c \tag{5.2}$$

ACI Committee 408 (2003) proposed Equation (5.4) based on extensive experimental data to estimate the maximum bond strength of a deformed steel bar in concrete beam

$$U_c = \frac{T_c}{\pi d_b l_s} \tag{5.3}$$

$$\frac{T_c}{f'_c{}^{1/4}} = [59.9 l_d (c_{min} + 0.5 d_b) + 2400 A_b] \tag{5.4}$$

Where

T_c : The concrete contribution to the bond force (K)

f'_c: The concrete compressive strength (psi)

l_d: Development length/ Splice length (in)

c_{min} : Minimum concrete cover (in)

d_b : Bar diameter (in)

A_b : Bar Area (in^2)

5.2 Bond strength of CFRP wrapped beams

The bond strength of lap-spliced bars in concrete confined with FRP wraps (U_t) can be expressed as the sum of the bond strength of an unconfined spliced beam (U_c) and the bond strength contribution of the FRP wraps ($U_{tr,f}$) as given in Equation 5.4:

$$U_t = U_c + U_f \tag{5.5}$$

Where

U_t: The total bond strength of reinforcing bar in concrete (Psi).

U_c: The concrete contribution to the bond strength (Psi).

U_f: The contribution of FRP to the bond strength (Psi).

Hamad, Rteil, and Soudki (2002) proposed Equation (5.5) based on their experimental work to estimate the contribution of FRP wrapping the bond strength of a lap spliced bar in FRP wrapped concrete.

$$U_{tr,f} = K_{tr,f}\sqrt{f'_c} \tag{5.6}$$

The FRP confinement index, Ktr,f is given by Equation (5.6):

$$K_{tr,f} = \frac{C_1 * A_{tf} * f_{fe}}{s_f * d_b * n_b} \quad (5.7)$$

The effective stress in the FRP laminate, f_{fe}, is given by Equation (5.7):

$$f_{fe} = \frac{k_1 * k_2 * l_e}{468 * \varepsilon_{fu}} f_{fu} \quad (5.8)$$

The active bond length of the FRP strips, l_e, is given by Equation (5.8) :

$$l_e = \frac{250}{(t_f * E_f)^{0.58}} \quad (5.9)$$

The bond reduction factor depends on two modification factors, K_1 and K_2, that account for the concrete strength and the wrapping scheme used, respectively. The K_1 and K_2 reduction factor can be given by Equation (5.9) and (5.10), respectively.

$$k_1 = (\frac{f'_c}{27.6})^{\frac{2}{3}} \quad (5.10)$$

$$k_2 = \frac{d_f - l_e}{L_f} \quad (5.11)$$

Where:

$U_{tr,f}$: The contribution of FRP wrapping to the bond strength (Psi)

A_{tf}: The area of the transverse FRP strip (in^2)

s_f : The center to centre spacing between FRP strips. For a continuous strip, it is taken as the width of the FRP strip (in)

f_{fu} : The ultimate strength of the transverse FRP sheets (Psi)

f'_c: The concrete compressive strength (Psi)

t_f : The thickness of the transverse FRP sheet (in)

E_f : The Young's modulus of the transverse FRP laminate (Psi)

ε_{fu} : The ultimate strain of the transverse FRP laminate, and

L_f : The total bonded length of the FRP sheet (in)

The model proposed by Rteil (2003) does not account for the effect of the variation of (c/d) ratio on the effectiveness of the confinement with FRP sheets.

5.2.1 Effect of the (c/d) ratio on the FRP confinement

The FRP is the passive reinforcement. The effect of the FRP depends on the dilation of the confined concrete resulting from bond/splitting stress; for the beams with constant concrete cover and different bar diameter, greater dilation means greater confinement. For a beam with (c/d) ratio equals to 2.0 (concrete cover = 30 mm), the dilation area is greater and hence more affected by the resultant force of the FRP confinement than a beam with (c/d) ratio equal to 2.67(concrete cover = 40 mm).

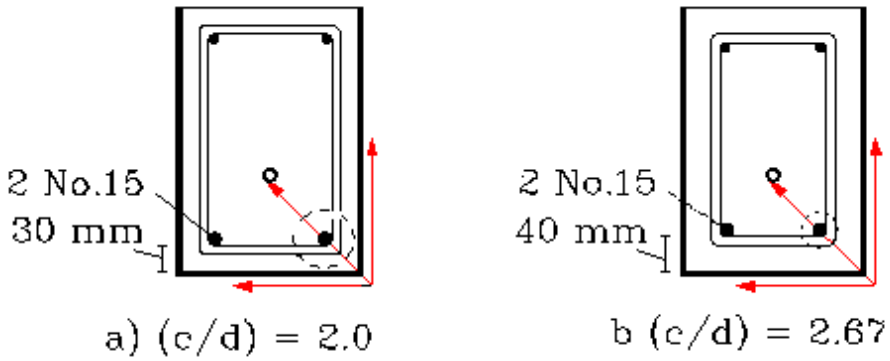

Figure 5-1 The effect of different (c/d) ratios on confinement using FRP sheet

To formulate the effect of the (c/d) ratio on the FRP confinement index($K_{tr,f}$), the measured bond stresses due to the CFRP confinement ($U_{tr,f}$) were plotted versus different (c/d) ratios (Figure 5.2). Utr,f was calculated as the difference between the measured total bond stress (Ut) and the measured bond stress due to concrete (Uc).Bond stresses in from beams reinforced with No.15 bars at two different c/d ratios (2.0 and 2.67) were only used; bond data from beams reinforced with No.20 bars at c/d of 1.5 were not included in plotting these curves because of their larger bar diameter. The bond stress (Uf) vs. (c/d) causes followed a linear function.

Figure 5.2 show that the bond stress (U_f) decreased as the (c/d) ratio increased for all corrosion levels. For confined beams with 0%, 2.5%, and 5.0% corrosion, the bond stress due to CFRP confinement decreased by 21 %, 22% and 35%, respectively, as the (c/d) ratio increased from 2.0 to 2.67. It was assumed that the maximum bond stress contribution from the FRP wrap occurs at a c/d ratio equal to 1.0

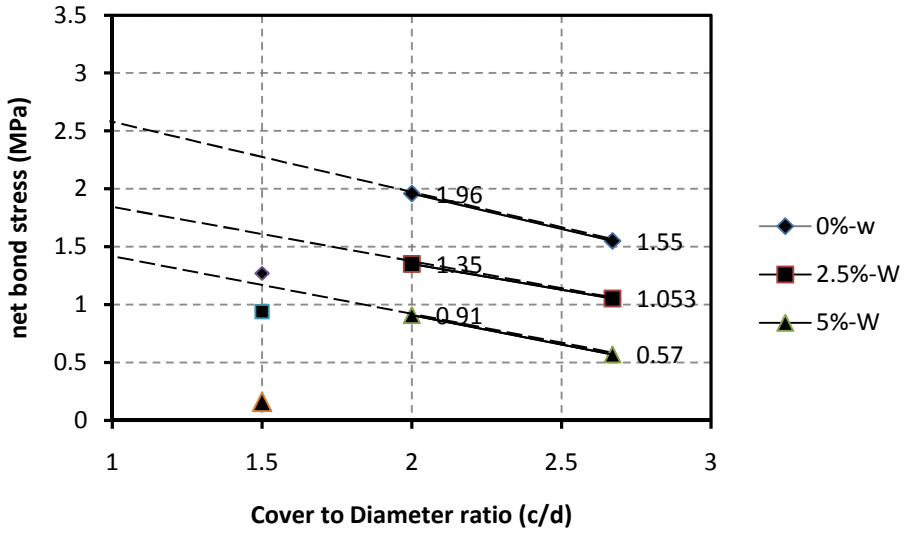

Figure 5-2 The bond stress (Utr,f) versus different (c/d) ratios

The reduction factor due to the effect of the (c/d) ratio on the FRP confinement ($K_{tr,f}$) can be expressed by Equation 5.11:

$$R_1 = 1 - \alpha \left(\frac{c_c}{d_b} - 1\right) \quad (5.12)$$

Where:

R_1: Reduction factor due to the effect of (c/d)

α : Slope of the best fit line (α =0.52)

c_c : Clear concrete cover (in)

d_b : The bar diameter (in)

Applying the reduction factor R_1 to the basic $K_{tr,f}$ (Equation 5.6), the modified $K_{tr,f}$ can be expressed by Equation 5.12.

$$K_{tr,f} = \frac{U_{tr,f}}{\sqrt{f'_c}} = \frac{C_1 * A_{tf} * f_{fe}}{s_f * d_b * n_b} \times R_1 \quad (5.13)$$

A_{tf} : The area of the transverse FRP strip (in^2)

C_1: calibration factor that accounts for effect of FRP properties and beam configuration, (to be determined). C1 is needed to account for FRP effect vs. Steel.

s_f : The center to centre spacing between FRP strips but for a continuous laminate it is taken as the width of the FRP laminate (in)

f_{fe} :The effective stress in the FRP laminate (Psi)

d_b :The steel reinforcing rebar diameter (in)

n_b : The number of steel reinforcing bars

To determine the constant C_1, $\frac{U_f}{\sqrt{f'_c}}$ values are plotted versus $K_{tr,f}$ values as shown in Figure 5.3. Using a lower bound best fit straight line for all the test data, the slope (C_1), is determined as 0.035.

After combining Equations 5.3, 5.5, 4.6 and 5.12, the maximum bond strength of FRP repaired beam is expressed by Equation 5.13:

$$U_t = \frac{T_c}{\pi d_b l_s} + \left(\frac{C_1 * A_{tf} * f_{fe}}{s_f * d_b * n_b} \times \left[1 - \alpha \left(\frac{c_c}{d_b} - 1\right)\right]\right)\sqrt{f'_c} \quad (5.14)$$

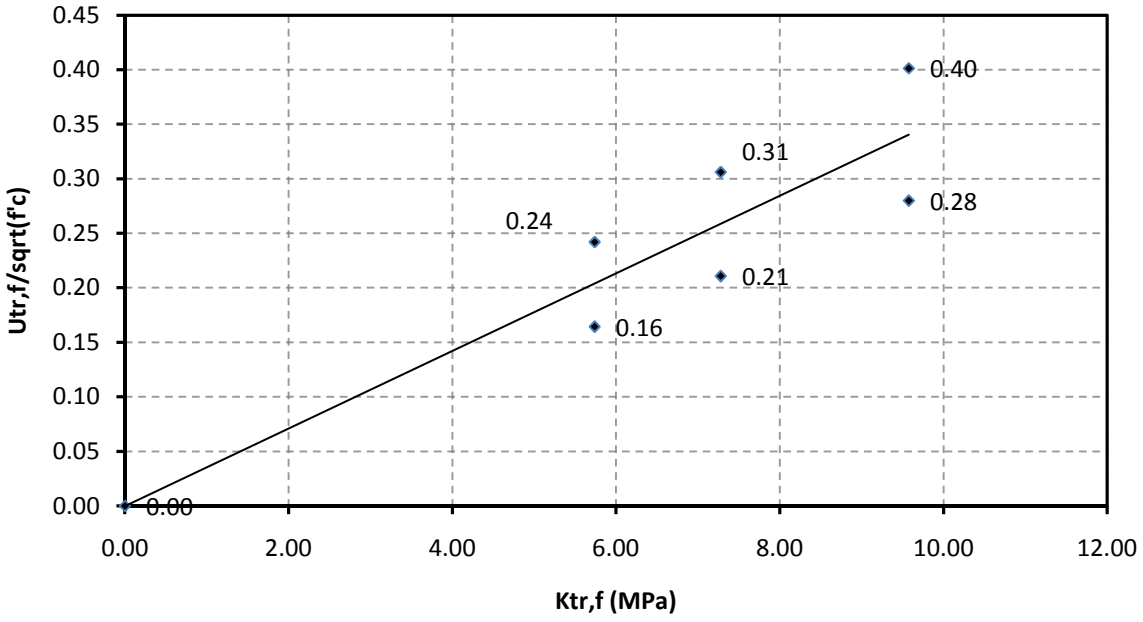

Figure 5-3 Variation of normalized FRP bond strength with Ktr,f

5.3 The effect of corrosion on bond strength

As mentioned in Section 4.7, the maximum bond stress for specimens with low and medium corrosion levels decreased more than the uncorroded control specimens. To determine the reduction factor due to corrosion, the bond stresses due to concrete and the bond stresses due to CFRP confinement are plotted versus the different (c/d) ratios as shown in Figures 5.4 and 5.5 therefore the reduction factor due to corrosion can be expressed as:

$$R_2 = (1 - 10 * m\%) \tag{5.15}$$

Where:

R_2: The reduction factor due to corrosion

m% : Percentage of theoretical mass loss

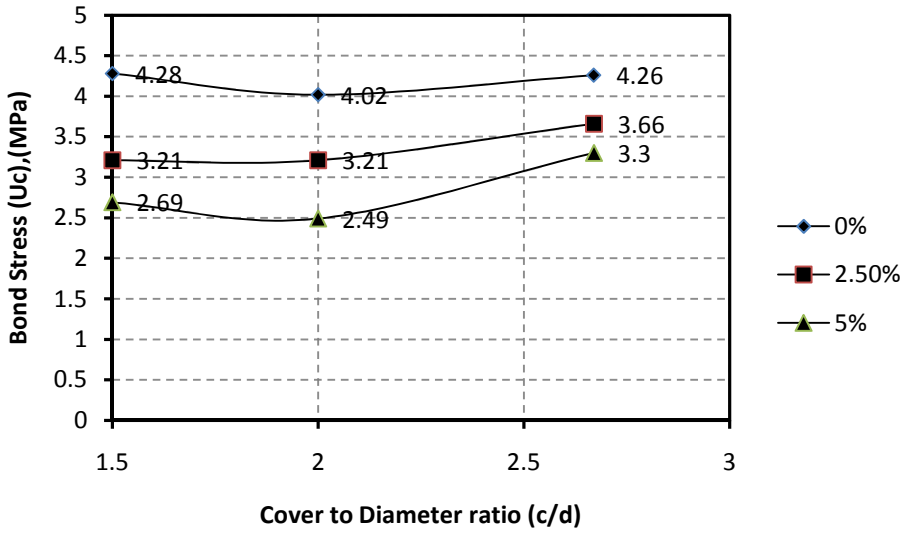

Figure 5-4 Effect of corrosion on the bond stress due to concrete

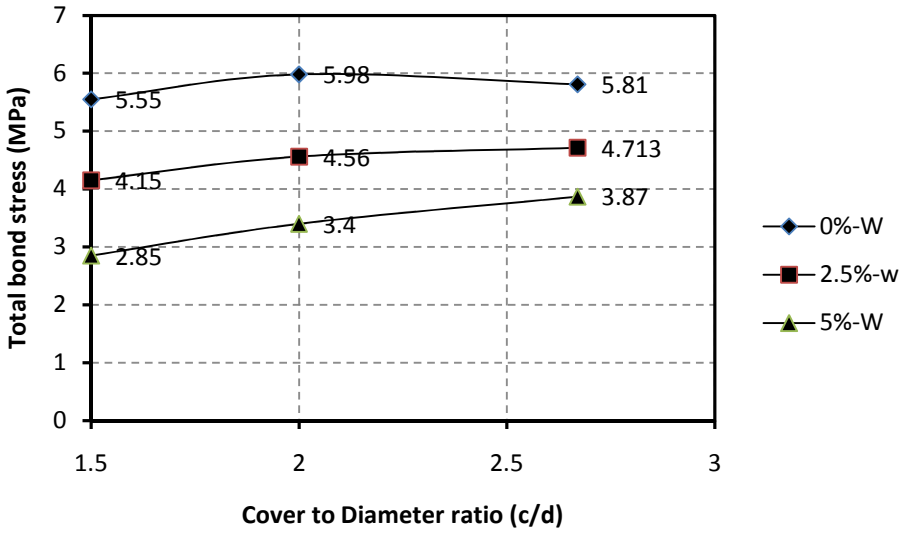

Figure 5-5 Effect of corrosion on the bond stress due to CFRP confinement

The effect of the corrosion on the total bond strength can be, expressed as follows:

$$U_t = R_2(U_c + U_f) \tag{5.16}$$

5.4 Maximum bond strength of FRP repaired and corroded beam

The bond strength of a repaired and corroded beam can be expressed by combining Equations 5.14, and 5.16 in Equation 5.18:

$$U_t = R_2 \times \left[\frac{T_c}{\pi d_b l_s} + \left(\frac{C_1 * A_{tf} * f_{fe}}{s_f * d_b * n_b} \times \left[1 - \alpha \left(\frac{c_c}{d_b} - 1\right)\right]\right)\sqrt{f'_c}\right] \quad (5.17)$$

The measured and computed values of the maximum bond stress for all beams are shown in Table 5.1. In general, the model predictions were conservative in predicting the bond strength of corroded lap-spliced bars. The ratio of calculated to measure bond stress for the corroded unwrapped beams ranged from 0.85 to 1.33, and for the corroded wrapped beams it ranged from 0.72 to 1.06.

Table 5-1Measured and predicted maximum bond stress

		Notations	U_t (model) (Psi)	U_t (model) (Mpa)	U_t (experimental) (Mpa)	Ratio (model/experimental)
Corrosion	Un-Wrapped	N-1.5	667	4.6	4.28	1.07
		L-1.5	500	3.45	3.21	1.07
		M-1.5	333	2.3	2.49	0.85
		N-2.0	713	4.91	4.02	1.22
		L-2.0	534	3.68	3.21	1.14
		M-2.0	355	2.45	2.69	0.98
		N-2.67	824	5.68	4.26	1.33
		L-2.67	618	4.26	3.66	1.16
		M-2.67	410	2.83	3.30	0.86
	Wrapped	NW-1.5	N/A	N/A	5.55	N/A
		LW-1.5	N/A	N/A	4.15	N/A
		MW-1.5	N/A	N/A	2.85	N/A
		NW-2.0	925	6.38	5.98	1.06
		LW-2.0	690	4.76	4.56	1.04
		MW-2.0	463	3.19	4.40	0.72
		NW-2.67	880	6.07	5.81	1.04
		LW-2.67	660	4.55	4.71	0.96
		MW-2.67	439	3.03	3.87	0.78

Chapter 6

Conclusions

6.1 General

The main objective of this research was to assess the effect of CFRP wraps on corroded tension lap-spliced reinforced beams. What makes this study significant is the lack of research reported in the literature on the effects of corrosion on the bond strength of the lap-spliced beams and the effect of the CFRP wraps on the bond strength of a corroded tension lap splice.

The study consisted of experimental and analytical phase. In the experimental phase, a total of 18 full-scale lap spliced beam specimens were tested. The test variables were: (1) the (c/d) ratio (1.5, 2.0, and 2.67), (2) corrosion levels (0%, 2.5%, and 5.0%), and (3) CFRP repair (wrapped vs. unwrapped beams). The beams were tested in four point bending. Analysis of the test results was based on evaluating and comparing the mode of failure, load-deflection curves, and average bond strength. A model was proposed to predict the bond strength of corroded and FRP repaired tension lap-splices.

6.2 Conclusions

- For beams with corroded lap-splices, failure occurred just after longitudinal splitting cracks formed in the bottom and side covers adjacent to the location of the bars. The final mode of failure was a face- and side splitting of the concrete cover. The failure was sudden, brittle, and noisy.
- The measured strain profile along the lap splice was almost identical for all the beams. The strain reading increased gradually until the middle of the lap splice and more rapidly between the middle and the loaded end of the lap splice. The maximum strain was concentrated at the loaded end of the spliced steel bars- end was lower than the yield strain of the steel bars. For the beam with (c/d) ratio of 1.5, the maximum strain ranged between 1980 με and 2450 με.

- The corrosion level had a significant effect on the corrosion crack width. Beams with (c/d) =1.5 had maximum crack widths of 0.5 mm and 0.8 mm for the 2.5% and 5.0% corrosion levels at the conclusion of corrosion exposure. Beams with c/d = 2.0 and 2.67 had a maximum crack widths of 0.4 mm and 0.6 mm for the 2.5% and 5.0% corrosion level.
    - Increasing the bar diameter for a given concrete cover results in higher crack width. For beams with c/d =1.5, the maximum crack width was 0.8 mm and for beams with c/d =2.0, it was 0.6 mm.
    - Increasing the concrete cover for the same bar diameter decreased the crack width. The maximum crack width for the 30 mm concrete cover was 0.6 mm and for the 40 mm concrete cover was 0.5 mm for bar diameter of 15 mm.
- Corrosion of the un-wrapped lap-splice beam led to a reduction in ultimate bond strength.
    - The reduction in the ultimate bond strength due to a 2.5% corrosion level ranged between 16% and 25% depending on the c/d ratio. The highest reduction was for c/d = 1.5.
    - The reduction in the ultimate bond strength due to a 5.0% corrosion level ranged between 20% and 45% depending on the c/d ratio. The highest reduction was for c/d = 1.5.
- FRP wraps were effective in confining the tension splice region. The mode of failure was more ductile and more gradual although the final mode of failure was splitting of the concrete cover.
    - For the CFRP wrapped beams with (c/d) ratio of 1.5, the maximum load at 0%, 2.5%, and 5.0% corrosion level increased by 22%, 24%, and 10%, respectively in comparison with the corresponding un-wrapped specimens.
    - For the CFRP wrapped beams with (c/d) ratio of 2.0, The maximum load for the CFRP wrapped beams at 0%, 2.5%, and 5.0% corrosion level increased by 33%, 30%, and 46%, respectively in comparison with the corresponding un-wrapped specimens.
    - For the CFRP wrapped beams with (c/d) ratio of 2.67, The maximum load for CFRP wrapped beams at 0% , 2.5% , and 5.0% corrosion level increased by 27% , 21%, and 12% , respectively in comparison with the un-wrapped specimens.

- FRP is the passive reinforcement. The effect of the FRP repair depends on the dilation of the confined concrete resulting from bond/splitting stress; greater dilation means greater confinement.
- A new confinement index, Ktr,f, was proposed to account for the presence and amount of CFRP confining tension lap splices. This parameter is recommended to be used in determining the bond strength contribution due to FRP. The new confinement index depends on a total cross sectional area of FRP reinforcement normal to the plane of splitting in the splice zone, effective stress in the FRP laminates, spacing between the FRP sheets, diameter of the main reinforcement, concrete cover, and the number of anchored or spliced bars.
- The ultimate bond stresses of the corroded tension lap-splice were predicted using the proposed models. The predicted results from these models had reasonable correlation in comparison to experimental results.
- The conclusions, and model calibration are only valid for the specimens' conditions and variables considered in this study, and should not be applied to general conditions without further investigation.
- Proposed factor that account for effect of corrosion on ($U_c + U_t$).

6.3 Recommendations for future work

- Research is needed to examine the behavior of the corroded tension lap splice with different splice length.

- To validate the proposed models, a wide range of experimental data is needed, including the effect of different c/d ratios and corrosion levels.

- In this study, FRP repair of corroded beams was investigated using U-wraps. It is recommended for future studies add a flexural CFRP sheet to move the failure from bond to a flexural failure.

Appendix A

Experimental calculations

A.1 Impressed Current Calculations

The time required to corrode the reinforcing steel bars, using accelerated corrosion technique, was calculated based on Faraday's law. Faraday's law along with sample induced current calculations is presented in the following:

$$m_t = \frac{MIT}{zF}$$

Where:

m_i : Weight of steel consumed (g).

M : The atomic weight of metal (56 g for *fe*)

I: Current (Ampares)

T : Time (second)

z ionic charge = 2

F: Faraday's constant = 96500 Ampares.second

For practical purposes, the current density, i, is used instead of I

$$m_t = \frac{M.i.S_a.T}{zF}$$

Where S_a is the surface area of corroded steel and i is the current density level.

Example:

Calculate the time required to obtain 2.5% mass loss in 15M bar of 900 mm length using Faraday's law. The current density to be used is 150μA/cm^2

Solution:

Mass loss of the steel reinforcement:

$$m_t = \frac{M.i.S_a.T}{zF}$$

$M = 56\ g$

$i = 150\mu A/cm^2$

$T = time\ required\ in\ second$

Z= 2

F = 96500 Ampares. Second

$S_a = \pi \; x \; d \; x \; l$

Diameter of 15M bar = 16 mm = 1.6 cm

Area of 15M bar = 200 mm² = 2 cm²

$S_a = \pi \; x \; d \; x \; l = \pi \; x \; 1.6 \; x \; 90 = 453 \; cm^2$

Also we know that

$$\% \; mass \; loss = \frac{mass \; loss \; (g)}{Original \; mass \; (g)}$$

$$mass \; loss \; (g) = \%mass \; loss \; x \; original \; mass$$

$$\% \; mass \; loss = \frac{2.5}{100} = 2.5\%$$

$$initial \; mass = density \; of \; steel \; x \; volume = 7.85 \; x \; 2 \; x \; 90 = 1413 \; g$$

$$mass \; loss \; (g) = \% \; mass \; loss \; x \; initial \; mass = 0.025 \; x \; 1413 = 35 \; g$$

$$T = \frac{m_t . zF}{M \; . \; i . s_a}$$

$$T = \frac{34 \; x \; 2 \; x \; 96500}{5 \quad x \; 150^{-6} \; x \; 453}$$

$$T = 21 \; days$$

Bibliography

1- ACI Committee 408, (2003) “Bond and Development of Straight Reinforcing Bars in Tension”, ACI 408R-03, American Concrete Institute, U.S.A.

2- ACI Committee 222, (1996) “Corrosion of Metal in Concrete”, ACI 222R-96, ACI Manual of \Concrete Practice, American Concrete Institute, Michigan, U.S.A.

3- ACI Committee 440, (2006) “State-of-the Art Report on Fiber Reinforced Polymers Reinforcement for Concrete Structure”, ACI 440R-06, American Concrete Institute, Michigan, U.S.A.

4- ACI Committee 318, (2008) “Building code requirements for structural concrete” ACI 318M-08,American Concrete Institute, Farmington Hills, MI., U.S.A.

5- ASTM G1. (1990) “Standard practice for preparing, cleaning and evaluating test specimens ”ASTM International, West Conshohocken, Pa.

6- Federation Internation du Beton (fib), (2000) “Bond of Reinforcement in Concrete, State-of-Art Report” International Federation for Structural Concrete, Switzerland.

7- ISIS Canada, (2007) “Reinforced concrete structures with fiber reinforced polymers” Design Manual No. 4.

8- Al-Hammoud, R., (2006) “ Fatigue flexural behavior of corroded reinforced concrete beams repaired with CFRP sheets” MASc Thesis, University of Waterloo, Waterloo, Ontario, Canada.

9- Al-musallam, A. A.; Al-Gahtani, A. S.; Aziz, A. R.; and Rasheeduzzafar, (1996) "Effect of reinforcement corrosion on bond strength" Construction and Building Materials, 10(2), 123-129.

10- Al-Sulaimani, G. J.; Kaleemullah, M.; Basunbul, I. A.; and Rasheeduzzafar,(1990) "Influence of corrosion and cracking on bond behavior and strength of reinforced concrete members" ACI Structural Journal, 87(2), 220-231.

11- Soudki, K. A., and Sherwood, T. G. (2000). \Behavior of reinforced concrete beams strengthened with carbon Fiber reinforced polymer laminates subjected to corrosion damage," *Canadian Journal of Civil Engineering*, Vol. 27, No. 5, pp. 1005{1010.

12- Bentur, S., Diamond, S., and Berke, N. S. (1997). *Steel Corrosion in Concrete: Fundamentals and Civil Engineering Practice*, E & FN Spon, London, UK.

13- Liu, Y., and Weyers, R. (1998). \Modeling the time-to-corrosion cracking in chloride contaminated reinforced concrete structures," *ACI Materials Journal*, Vol. 95, No. 6, pp. 675-681.

14- Raupach, M. (1996). \Chloride-induced macrocell corrosion of steel in concrete-theoretical background and practical consequences," *Construction and Building Materials*, Vol. 11, No.4, pp. 239{248.

15- El Maaddawy, T. A., and Soudki, K. A. (2003). \Effectiveness of impressed current technique to simulate corrosion of steel reinforcement in concrete," *ASCE Journal of Materials in Civil Engineering*, Vol. 15, No. 1, pp. 41-47.

16- Stanish, K., Hooton, R. D., and Pantazopoulou, S. J. (1999). \Corrosion effects on bond strength in reinforced concrete," *ACI Structural Journal*, Vol. 96, No. 6, pp. 915-921.

17- Hamad, B. S., and Soudki, K.A. (2001). \GFRP wraps for confinement of bond critical regions in beams," *International Conference on Composites in Construction*, Portugal.

18- Hamad, B., Rteil, A., Salwan, B., and Soudki, A. (2003). \Behavior of bond critical regions wrapped with FRP sheets in normal and high strength concrete," *ASCE Journal of Composites for Construction*, in press.

19- Sherwood, E. G. (2000). *Behaviour of Corroded Reinforced Concrete Beams Strengthened with CFRP Laminates,* MASc. thesis, University of Waterloo, Waterloo, ON, Canada.

20- Craig, B. C. (2002). *Confining Effects of FRP Laminates on Corroded Concrete Members,* MASc. thesis, University of Waterloo, Waterloo, ON, Canada.

21- Orangun,O.C., Jirsa, J.O.,ans Breen, J. E., " the strength of Anchored Bars: A Reevaluation of Test Data on Development Length and Splices" , ACI Journal, (March 1977):114-122

22- Badawi, M. A. (2003). Flexural Response of Uniform And Shear-span Corroded RC Beams Repaired With CFRP Laminates, MASc. thesis, Universty of Waterloo, Waterloo, ON, Canada